

# FUNCTIONAL MATERIALS FROM SUPRAMOLECULAR XEROGELS AND POLYMERS

---

Inaugural Dissertation  
to obtain the academic degree of  
Doctor rerum naturalis / Dr. rer. nat.

submitted to  
the Department of Biology, Chemistry, Pharmacy of  
Freie Universität Berlin

by

PIN-WEI LEE

Berlin, 2024



1<sup>st</sup> reviewer: Prof. Dr. Christoph A. Schalley

2<sup>nd</sup> reviewer: Prof. Dr. Rainer Haag

Date of defence: 2024.08.07





## Acknowledgment

First of all, I would like to thank Prof. Dr. Christoph A. Schalley for the opportunity to join the group. He's provided me with knowledge and insightful suggestions for this rollercoaster project. There have been many twists in the development of this work and I am very grateful for his full support with freedom and resources all along.

Secondly, I want to thank Prof. Dr. Rainer Haag for taking time out of his schedule and being the second reviewer of this thesis.

I thank Silke Benndorf for her help with all the administrative works.

I am very grateful to Dr. Adrian Saura-Sanmartin for his massive help in the later stages of the work, and for proofreading the thesis while he's got a handful of his own. I thank Yizhe Pan greatly for his help in the extensive screening and the early characterisations of the supramolecular-polymer co-assemblies. Without these two, this work might not be finished in time. I would also like to thank Dr. Tuğrul Kaynak for his help in the early stages of the work and the training for SEM operation. Thank you to the people in and out of the group, who kept the workplace pleasant and comfortable.

I thank Asst. Prof. Dr. Ching-Feng Liu for the polishing of the Kurzzusammenfassung. For Peng Tang and Guoxin Ma, I owe the appreciation of proofreading the thesis in a very short notice.

I would like to thank SFB 1349 for funding the research.

I can't be thankful enough to my family and friends. Their full support and constant encouragement get me to where I am.



# **Declaration of independence**

Herewith I certify that I have prepared and written my thesis independently and that I have not used any sources and aids other than those indicated by me.

May 28, 2024, Berlin

Pin-Wei Lee



## Abstract

This work aims to develop superhydrophobic surfaces from supramolecular xerogels with low molecular weight gelators (LMWGs). LMWGs are small organic compounds that have a strong preference to form gels in a suitable solvent. To achieve a xerogel coating, one can drop-cast the gel onto substrates such as glass cover slips, allowing it to dry under ambient condition. The LMWGs used in this work are based on a *trans*-1,2-diamidocyclohexane core, equipped with two equilateral perfluorinated side chains (**CF $n$** , where  $n$  represents the number of the carbon atoms on each chain). The amide groups on the core facilitate strong intermolecular hydrogen bondings and lead the way to supramolecular self-assembly, while the perfluorinated side chains contribute to the intrinsic low surface energy of the materials. Both parts are essential for the formation of the superhydrophobic xerogel coating.

The first part of this work focuses on investigating the effect of the side-chain length on the resulting xerogel coating. Eight LMWGs, from **CF3** to **CF10**, are included in the investigation. The xerogel coatings were examined from three different scales. In the nanoscale, surface x-ray diffraction (sXRD) reveals the difference in the structural properties of the resulting supramolecular aggregates. Scanning electron microscopy (SEM) and optical microscopy were used to reveal the morphologies of the aggregates in the microscale. As for the macroscopic scale, the coatings were tested for their hydrophobicity and durability towards water flushing. In addition to the standard contact angle measurements and gravimetric studies, an image processing script coined Morphology evolution analysis (MEA) was devised to investigate the change of the coating after intensive flushing. This method evaluates the durability by assessing the change in the relative thickness of the coating through pixel intensity. The first part of this work concludes that the length of the perfluorinated side chains has a significant impact on the resulting xerogel, as certain LMWGs provide xerogel coatings with better properties in terms of both hydrophobicity and durability.

To broaden the applicability of the xerogel coating, it is crucial to overcome the intrinsic mechanical fragility of the xerogels. Therefore, the second part of this work focuses on the preparation of the more mechanically-durable hydrophobic coatings from the combination of supramolecular xerogels and polymers. **CF7** was selected as the concept LMWG, while two monomers, methyl methacrylate (MMA) and trifluoroethyl methacrylate (TFEMA), were cho-

sen as the candidates for the polymer component. Extensive screening was done to find the optimised fabrication condition for a robust hydrophobic supramolecular-polymer co-assembly. The co-assemblies were investigated with SEM and Time-of-Flight Secondary Ion Mass Spectrometry (ToF-SIMS) for the structure of the aggregates and the uniformity of the coating, respectively. The iterability and durability of the co-assemblies are again tested with water flushing. A sclerometer was employed in addition to test the scratch resistance of the co-assemblies. Practical implementations including metal corrosion protection and oil-repellency were also carried out. In conclusion, xerogel-based hydrophobic and oleophobic coatings with significantly improved scratch-resistance are achieved by fixating the supramolecular network with a polymer matrix.

## Kurzzusammenfassung

Dieser Arbeit geht es um die Entwicklung der superhydrophoben Oberflächen aus der supramolekularen Xerogelen mit der niedermolekularen Gelatoren (LMWGs). Die LMWGs gehören zu kleine organische Verbindungen, die eine starke Vorliebe für die Gelbildung in einem geeigneten Lösungsmittel vorliegen. Daher könnte man das Gel auf dem Deckglaser als das Substrat unter allgemeiner Umgebungsbedingungen heraustropfen, wenn man eine Xerogelbeschichtung erhalten will. Das heißt, dass die verwendeten LMWGs in dieser Arbeit auf einem *trans*-1,2-Diamidocyclohexan-Kern basieren, der mit zwei gleichseitigen perfluorierten Seitenketten (**CF<sub>n</sub>**, wobei *n* für die Anzahl der Kohlenstoffatome an jeder Kette steht) ausstattet. Eine weitergehende Erklärung dafür ist, dass die Amidgruppen am Kern starke intermolekulare Wasserstoffbrückenbindungen erleichtern, zugleich muss man Beitrag zur perfluorierten Seitenketten zur niedrigen Oberflächenenergie der Materialien berücksichtigen. Nur wenn beides vorhanden ist, ebnet den Weg zur supramolekularen selbst Zusammenstellen.

Zuerst diskutiert der erste Teil der Arbeit über Auswirkung der Seitenkettenlänge auf die resultierende Xerogel-Beschichtung, nämlich wird die Untersuchung einschließlich Acht LMWGs, von **CF<sub>3</sub>** bis **CF<sub>10</sub>**, dargestellt. Insoweit wird die Xerogelbeschichtungen durch drei verschiedene Maßstäben erforscht. Das heißt, dass im Nanomaßstab die Oberflächenröntgenbeugung (sXRD) die Unterschiede in den strukturellen Eigenschaften der entstehenden supramolekularen Aggregate zeigt. Mit Hilfe der Rasterelektronenmikroskopie (REM) und der Lichtmikroskopie werden durch die Morphologien der Aggregate auf der Mikroskala sichtbar erfüllt. Demgemäß wird die Prüfung der Beschichtungen auf ihre Hydrophobie und Beständigkeit gegenüber Wasserspülungen im makroskopischen Bereich dargestellt.

Zusätzlich zu der üblichen Kontaktwinkelmessung und Gravimetrie wird Verwendung des neuen Bildverarbeitungsskripts, das als Morphologie-Evolutions-Analyse (MEA) gilt, vorgehen, um die Veränderung der Beschichtung nach der intensiven Spülung zu prüfen. Mit dieser MEA-Methode wird die Haltbarkeit abwärts, indem die Veränderung über die relative Dicke der Beschichtung anhand der Pixelintensität beurteilt wird. Deshalb kommt der erste Teil zum Schluss, dass die Länge der perfluorierten Seitenketten einen erheblichen Einfluss auf das resultierende Xerogel hat, da manche LMWGs Xerogelbeschichtungen mit besseren Eigenschaften in Bezug auf Hydrophobie und Haltbarkeit anbieten.

Des Weiteren stellt der zweite Teil der Arbeit auf die Herstellung von mechanisch beständigeren hydrophoben Beschichtungen aus der Kombination von supramolekularen Xerogelen und Polymeren. Mit anderen Worten ist es entscheidend, dass man für die Überwindung des Xerogels innewohnende mechanische Zerbrechlichkeit hält, um die Anwendbarkeit der Xerogelbeschichtung zu erweitern. Insofern wählt dieser Teil das **CF7** von LMWG-Konzept als erste vorläufige Vorüberlegung der Prüfung aus, die mit zwei Monomere, Methylmethacrylat (MMA) und Trifluorethylmethacrylat (TFEMA), die Kandidaten für die Polymerkomponente zusammen austestet. Deswegen führt dieser Teil ausführliche Prüfung durch, um die optimalen Herstellungsbedingungen für eine robuste hydrophobe supramolekulare Polymer Co-Assemblee zu finden. Auf der anderen Seite werden REM und Time-of-Flight Secondary Ion Mass Spectrometry (ToF-SIMS) durch die Struktur der Aggregate bzw. die Einheitlichkeit der Beschichtung auch geprüft. Zugleich werden die Wiederholbarkeit und Haltbarkeit von Co-Assembleen durch die Wasserspülung getestet und ein Sklerometer wurde zusätzlich eingesetzt, um die Kratzfestigkeit von Co-Assembleen zu prüfen. Weiterhin führt dieser Teil auch praktische Anwendung von Maßnahmen durch, Metallkorrosionsschutz und Ölabweisung zu enthalten.

Schließlich sei hervorgehoben, dass xerogel-basierte hydrophobe und oleophobe Beschichtungen mit deutlich verbesserter Kratzfestigkeit durch die Fixierung des supramolekularen Netzwerks mit einer Polymermatrix erreicht werden.



## Abbreviations

BSE	Backscattered electron(s)
CAH	Contact angle hysteresis(e)s
CF3	(±)- <i>N,N'</i> -( <i>trans</i> -cyclohexane-1,2-diyl)-bis(perfluorobutanamide)
CF5	(±)- <i>N,N'</i> -( <i>trans</i> -cyclohexane-1,2-diyl)-bis(perfluorohexanamide)
CF7	(±)- <i>N,N'</i> -( <i>trans</i> -cyclohexane-1,2-diyl)-bis(perfluorooctanamide)
CF9	(±)- <i>N,N'</i> -( <i>trans</i> -cyclohexane-1,2-diyl)-bis(perfluorodecanamide)
CF10	(±)- <i>N,N'</i> -( <i>trans</i> -cyclohexane-1,2-diyl)-bis(perfluoroundecanamide)
DMPA	2,2-Dimethoxy-2-phenylacetophenone
FWHM	Full width at half maximum
LMWG	Low molecular weight gelator
MEA	Morphology evolution analysis
MMA	Methyl methacrylate
SE	Secondary electron(s)
SEM	Scanning electron microscopy
sXRD	Surface x-ray diffraction
TFEMA	Trifluoroethyl methacrylate
ToF-SIMS	Time-of-flight secondary ion mass spectrometry
UHV	Ultra-high vacuum
Upy	Ureidopyrimidinone
WCA	Water contact angle
XPS	X-ray photoelectron spectroscopy



# Contents

<b>1</b>	<b>Introduction</b>	<b>1</b>
<b>2</b>	<b>Theoretical backgrounds</b>	<b>3</b>
2.1	Supramolecular chemistry . . . . .	3
2.1.1	Intermolecular non-covalent interactions . . . . .	5
2.1.2	Self-assembly and self-organisation . . . . .	8
2.1.3	Low molecular weight gelator with alkyl amide moiety . . . . .	8
2.1.4	Xerogel, aerogel, and cryogel . . . . .	10
2.1.5	Supramolecular polymers . . . . .	11
2.2	Polymer chemistry . . . . .	12
2.2.1	Photopolymerisation of acrylate monomers . . . . .	13
2.2.2	Acrylic polymers embedded with supramolecular gels . . . . .	14
2.3	Superhydrophobicity . . . . .	15
2.3.1	Surface tension . . . . .	16
2.3.2	Contact angle . . . . .	17
2.3.3	Surface roughness: Wenzel state and Cassie-Baxter state . . . . .	20
2.3.4	Contact angle hysteresis . . . . .	22
2.3.5	Hydrophobicity and oleophobicity from fluorine . . . . .	24
2.4	Analytical methods . . . . .	25
2.4.1	Scanning electron microscopy . . . . .	25

2.4.2	Surface x-ray diffraction . . . . .	28
2.4.3	Time-of-flight secondary ion mass spectroscopy . . . . .	30
<b>3</b>	<b>List of publications</b>	<b>33</b>
<b>4</b>	<b>Summarised results</b>	<b>35</b>
	<b>References</b>	<b>37</b>
	<b>Appendix</b>	<b>47</b>

# 1 Introduction

Nature constantly fascinates us with exciting properties like superhydrophobicity and self-cleaning. We've seen ducks coming out of the lake but managed to stay dry with their feathers, and water droplets beading up and sliding off from a lotus leaf. With the development of scanning electron microscopy (SEM), we can examine the grounds of these phenomena, which are complex multi-scale or hierarchical structures coated with wax or oil (**Figure 1**).<sup>[1-4]</sup> The wax and oil provide the fundamental water-repellency. The design found in the hierarchical structures minimises the contact surface between the water droplet and the solid surface. The spaces left between the densely packed nano-protrusions act as air cushions for the water droplet. This means the droplet is sitting on top and barely touching the surface, which allows it to roll off easily and is often described as the Lotus effect.<sup>[5-15]</sup>

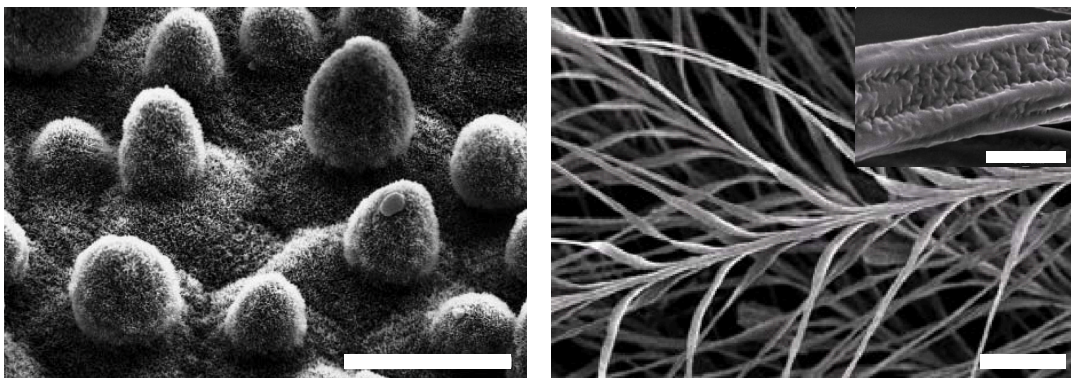


**Figure 1:** SEM images of a lotus *Nelumbo nucifera* leaf (left) and duck feathers (right, close-up image shown in inset). Hierarchical structures are seen on both surfaces. The scale bars for the lotus leaf image, the duck feather image, and the close-up image for the duck feather are 20  $\mu\text{m}$ , 40  $\mu\text{m}$ , and 1  $\mu\text{m}$ , respectively. The SEM image of the lotus leaf is reproduced with permission of Springer Nature, from Wilhelm Barthlott and Christoph Neinhuis, Purity of the sacred lotus, or escape from contamination in biological surfaces, *Planta*, **1997**, 202, 1–8, <https://doi.org/10.1007/s004250050096>.<sup>[5]</sup> The SEM image of the duck feathers is reproduced with permission of IOP Publishing, Ltd, from Y. Liu, X. Chen and J. Xin, Hydrophobic duck feathers and their simulation on textile substrates for water repellent treatment, *Bioinsp. Biomim.*, **2008**, 3, 046007, <https://doi.org/10.1088/1748-3182/3/4/046007>.<sup>[16]</sup> The permissions are conveyed through Copyright Clearance Center, Inc.

To realise the Lotus effect artificially, one has to create a surface with appropriate roughness and intrinsic hydrophobicity.<sup>[17-22]</sup> One possibility is to manufacture textures on bulk hydrophobic materials, or the "top-down" method. Various approaches are developed for this purpose,

including lithography,<sup>[23–26]</sup> chemical etching,<sup>[27–29]</sup> and plasma treatments.<sup>[30–32]</sup> However, most of them involve elaborate protocols or have strict requirements for the fabrication environment. The other way is to obtain the surface-textured bulk material by assembling hydrophobic materials of smaller scales, or the "bottom-up" method.<sup>[33–38]</sup> One of the simplest ways reported is the use of supramolecular xerogels by Wei et al.<sup>[38]</sup> A xerogel coating can be acquired within minutes by simply drop-casting a gel solution and allowing it to dry. A LMWG with a bis-amide scaffold and two perfluorinated side-chains is presented. The strong and directional intermolecular hydrogen bonds formed with the amide groups self-assembled the molecules into a hierarchical supramolecular network.<sup>[39–43]</sup> Together with the inherent low surface energies from the fluorines,<sup>[44–47]</sup> a superhydrophobic xerogel coating can be obtained. It was observed that by changing the length of the perfluorinated side chains, the xerogel coating will change accordingly in multiple aspects, including the structure of the self-assembled aggregates, the hydrophobicity, and the coating durability. These interesting findings thus inspired the first project of this thesis. A systematic comparison between eight LMWGs was carried out. From the structural characteristics in the nanoscale to the macroscopic coating properties, the xerogels are inspected.

When it comes to surface coating manufacturing, one always has to assess iterability and durability critically. Mechanical fragility is unfortunately one major drawback of xerogel coatings. Hence, a material with equivalent water-repellency as the fluorinated xerogel but elevated scratch-proofness is targeted. Commonly seen attempts to overcome this disadvantage include adding polymerisable functional groups to LWMG,<sup>[48–52]</sup> incorporating metal-coordination,<sup>[53–55]</sup> or mixing the gel with polymers.<sup>[56,57]</sup> Given the importance of maintaining the simplicity of the manufacturing process, a supramolecular-polymer co-assembly for drop-casting is presented in the second project of this thesis. Short-chain polymers are introduced to the gel network to create a new drop-cast mixture. The miscibility allows the polymer chains to move in between the gel scaffolds, followed by the UV-light curing to fixate the gel networks in the polymer matrix. The xerogel network is reinforced by the addition of the polymer matrix while the water-repellency is preserved. The iterability, durability, and applicability of the co-assembly are evaluated.

## 2 Theoretical backgrounds

### 2.1 Supramolecular chemistry

Supramolecular chemistry is a specific field that focuses on the chemistry between two or more molecules, especially structure-sensitive intermolecular interactions. The early developments of supramolecular chemistry mostly surround the *host-guest complex* system, with the philosophical root originating from the well-known selective enzyme recognition, or the "lock and key" system, proposed by Emil Fisher (**Figure 2**).<sup>[58]</sup> The host molecule is the "lock", usually a macrocyclic compound possessing a hole or a cavity; the guest molecule, just like the "key", should be smaller in size to fit into the host molecule. The *lock-key* theory was later modified by Koshland to become the *induced fit* theory, as he found out that the conformation of an enzyme could change in the presence of a ligand, which is incompatible with the rigid lock-key system.<sup>[59,60]</sup> The *induced fit* theory, or "hand in glove", incorporates the idea of structure complementarity from the lock-key theory with the additional concept of flexibility to better explain the observation regarding unusual enzymatic reactivities. Nevertheless, it is established that both components in the host-guest complex should have complementary binding sites that induce non-covalent interactions to hold them together, with flexible scaffolds for the complex to reach optimal conformation.<sup>[61,62]</sup>

The term *supramolecular chemistry* and its central concept were integrated by Jean-Marie Lehn, for that he is often regarded as the "father of supramolecular chemistry".<sup>[63]</sup> The first Nobel Chemistry Prize awarded to the field was shared by him, Donald J. Cram, and Charles J. Pedersen in 1987. Charles J. Pedersen synthesised the crown ether, the first artificial host capable of molecular recognition (**Figure 3**).<sup>[64]</sup> Jean-Marie Lehn further developed a wide range of organic hosts like the cryptands, and Donald J. Cram extended the idea of the hosts into three-dimensional molecules like cavitands and carcerands.<sup>[65–67]</sup> Nowadays, the field has grown into a more complex system, with various topics involving multiple components with encoded information or emergent properties. This includes the 2016-Nobel-awarded molecular machines,<sup>[68–70]</sup> self-organised supramolecular polymers,<sup>[71–73]</sup> sol-gel transition,<sup>[74–76]</sup> and many more (**Figure 4**).

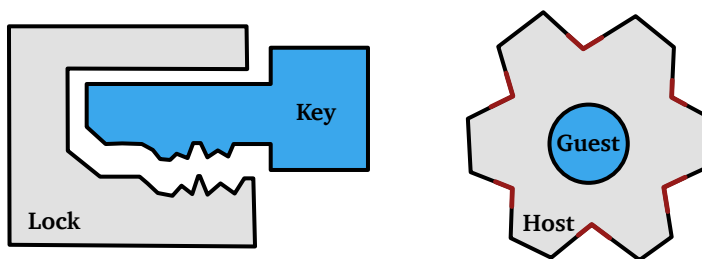


**Figure 2:** Molecular recognition of a host-guest complex is primarily accomplished through structure complementarity, similar to a pair of lock and key, but with the additional flexibility. The structure and the size of the host cavity determines which guest is available for binding.

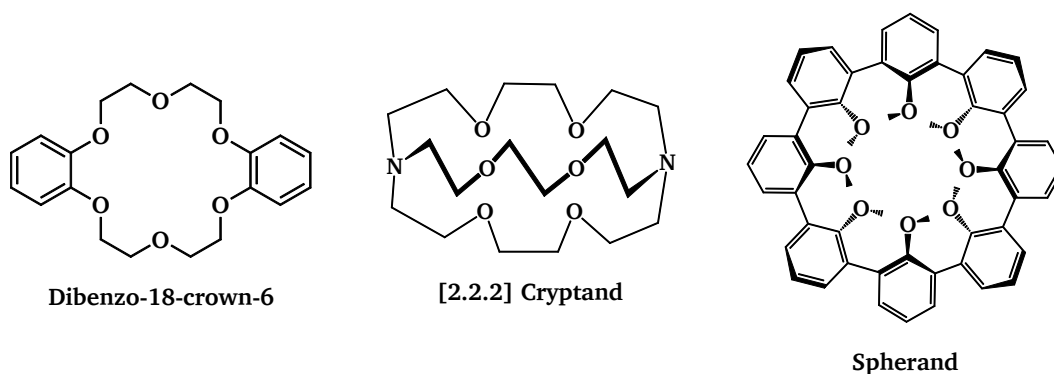


**Figure 3:** Examples of organic host molecules developed by the 1987 Nobel Chemistry Prize laureates. The dibenzo-18-crown-6 was developed by Charles J. Pedersen, Jean-Marie Lehn and co-workers developed the [2.2.2] cryptand, and the spherand was the work of Donald J. Cram and co-workers.<sup>[64-66]</sup>

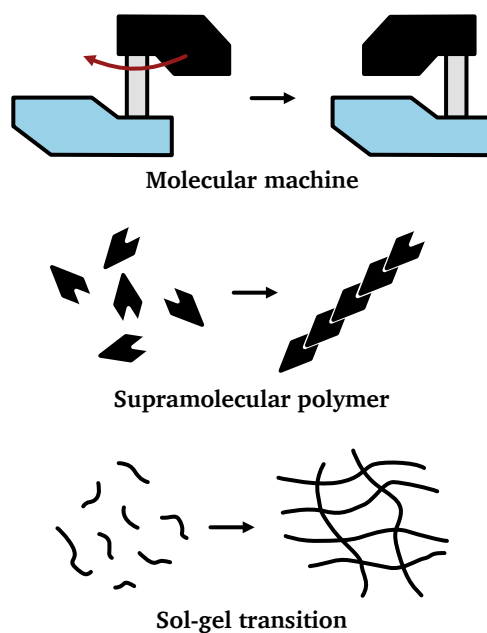


**Figure 4:** Examples of dynamic supramolecular systems involving multiple components with emergent properties.<sup>[70,72,74]</sup>



### 2.1.1 Intermolecular non-covalent interactions

As "the chemistry beyond molecules",<sup>[63]</sup> supramolecular chemistry circulates intermolecular non-covalent interactions. The function of molecules and intermolecular non-covalent interactions in supermolecules is analogous to atoms and covalent bonds in molecules. These interactions are weaker in strength, longer in range, and less directional than covalent bonds. Nevertheless, they play a crucial role in the structure, function and behaviour of the supramolecular system. This includes hydrogen bonding, van der Waals interaction, ionic pairing,  $\pi$ -acid to  $\pi$ -base interaction, metal-ligand binding, and more.<sup>[61,62]</sup> Roughly from small to large, supramolecular chemistry can be reviewed in three categories: molecular recognition, self-assembly of several molecules, and molecular assembly from numerous molecules.<sup>[77]</sup> Molecular recognition focuses on the interactions between a few molecules equipped with tailor-made receptor-substrate binding sites to accomplish structure complementarity. The ability of a host molecule to distinguish the corresponding guest results from the design of the binding sites and the interactions they may induce. Meanwhile, these spontaneous and manipulative interactions direct the structural relationship between the molecules, leading the components to approach the otherwise difficult constructions, for instance, the mechanically interlocked molecules.<sup>[41,77–81]</sup> Furthermore, numerous molecules can associate together to form a supermolecule. The construction of such architecture is a dynamic process that includes structural arrangements, binding, de-binding, and re-binding. This means in addition to the inducing of the association, the ability to adapt and rebuild should be considered when designing such molecules. It is important to balance between rigidity and flexibility for a stable but strong and comprehensive binding.<sup>[63]</sup>

One of the most important non-covalent interactions is the hydrogen bond. It is the key interaction during molecular recognition in many cases since it is highly directional.<sup>[39,82–84]</sup> Pauling delivered one of the first definitions for the hydrogen bond, which states that under certain conditions a hydrogen atom is attracted to two atoms instead of just one by rather strong forces, and may be considered to be acting as a bond between them.<sup>[85]</sup> These conditions include the atoms being highly electronegative and the coordination number being restricted to two. The hydrogen atom generally interacts stronger with one atom than the other, the former interaction behaves like a typical covalent bond while the latter is mostly electrostatic.<sup>[86]</sup> The stronger interaction of the two, usually constituted of a positively polarised hydrogen atom covalently bonded to a highly electronegative atom like nitrogen, oxygen, or fluorine, is considered as the *hydrogen*

*bond donor* (D–H). The weaker interaction connects the donor with the *hydrogen bond acceptor* (A) which is a nearby electron-rich atom, often bearing lone pair electrons, to interact with the polarised hydrogen. The term *hydrogen bonding* generally refers to this weaker interaction, which can be regarded as a type of dipole-dipole interaction. The bond energy of a typical hydrogen bond lies in a wide range of approximately  $1 \text{ kJ mol}^{-1}$  to  $160 \text{ kJ mol}^{-1}$ , and the bond length between  $1 \text{ \AA}$  to  $4 \text{ \AA}$ .<sup>[87–95]</sup> Hydrogen bondings with bond energies over  $100 \text{ kJ mol}^{-1}$  are considered *very strong hydrogen bondings*, these can be either homonuclear bonds (X–H–X) or heteronuclear bonds (X–H–X'), and the hydrogen atom is equally attracted to both electronegative atoms.<sup>[88]</sup> Difluoride anion  $\text{F}^- \cdots \text{H}-\text{F}$  has arguably one of the strongest hydrogen bonds, with characteristics usually corresponding to a single covalent bond. It is a linear, symmetric ion with the hydrogen as the inversion centre, the  $\text{F} \cdots \text{F}$  distance (226 pm) is significantly less than the sum of the van der Waals radii (280 pm),<sup>[96]</sup> and the estimated bond energy lies between  $155 \text{ kJ mol}^{-1}$  to  $252 \text{ kJ mol}^{-1}$ . Other very strong hydrogen bondings include the diquohydrogen ion  $[\text{H}_2\text{O}-\text{H} \cdots \text{OH}_2]^+$  ( $150 \text{ kJ mol}^{-1}$ ),<sup>[97]</sup> and the hydrogen bond between water and a fluoride ion  $\text{H}_2\text{O} \cdots \text{F}^-$  ( $101 \text{ kJ mol}^{-1}$ ).<sup>[98]</sup> On the other hand, unconventional donors like C–H group can sometimes form weak hydrogen bondings with bond energies lower than  $30 \text{ kJ mol}^{-1}$ .<sup>[90,91]</sup> The earliest indication of the existence of C–H group hydrogen bonding is possibly by Kumler, who pointed out that hydrogen cyanide shows a similarly abnormal dielectric constant as the compounds known to form hydrogen bondings.<sup>[99]</sup> In 1937, Glasstone discovered that there might be directional electrostatic interactions between acetone, ether, and quinoline that causes unexpected changes in the dielectric constant of the mixture.<sup>[100]</sup> He suggested that the chemical linkages within the mixture were attributed to the lone pair electrons of nitrogens and oxygens, and are not fundamentally different from the end-on dipole associations. In 1982, the crystallographic studies of Taylor and Kennard concluded the existence of C–H  $\cdots$  O hydrogen bonds and their electrostatic nature.<sup>[101,102]</sup>

Hydrogen bonding is highly directional and the geometry of the bond has a strong influence on the bond strength (**Figure 5**). Generally speaking, a linear configuration between the donor and the acceptor (D–H $\cdots$ A) gives the strongest hydrogen bond.<sup>[93]</sup> Other factors like charged components, strong resonance structure, and the neighbouring groups indubitably affect the strength of a hydrogen bond.<sup>[62,95]</sup> Hydrogen bonding is in particular important to the molecular recognition in the field of biochemistry, with the constructions of various complicated biological structures like protein and DNA rely strongly on it.<sup>[103–105]</sup>

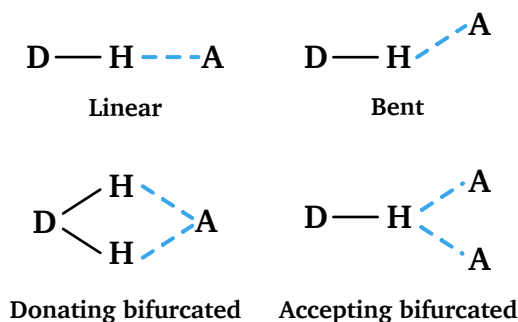


**Figure 5:** Different types of hydrogen bonding geometries. D and A refers to the electronegative atom on the bond donor and the acceptor, respectively. Blue dashed lined are suggested hydrogen bondings. Adapted with permission of John Wiley & Sons, Ltd, from J. W. Steed and J. L. Atwood, Concept, in *Supramolecular Chemistry*, John Wiley & Sons, **2009**.<sup>[62]</sup>

Another undoubtedly important interaction is the van der Waals interaction. Although it is weak and less specific, it applies to all kinds of molecules. Van der Waals interaction is a weak electrostatic attraction originated from the interaction of the electron clouds of the adjacent molecules.<sup>[62]</sup> They are non-directional, long-ranged, and decrease rapidly with increasing distance between the molecules. The individual interactions may be negligible, but the collective force contributes significantly to molecular recognition, especially when the interacting molecules are complementary in structure.<sup>[77]</sup> Van der Waals interaction can be seen as a combined force of three sources: the London dispersion energy, the Keesom orientation energy, and the Debye induction energy.<sup>[106]</sup> The London dispersion energy is the most important contribution to the total van der Waals interaction, since it acts between all atoms and molecules, even fully neutral ones with no net charge and no permanent dipole.<sup>[107,108]</sup> At any given moment, the electron distribution in an atom fluctuates and generates a finite dipole moment. This fluctuating dipole then polarises a nearby atom and induces a dipole moment in it. The interaction between the two dipole moments leads to a correlation that is in time average an attraction. The potential of this attraction is the London dispersion energy.<sup>[108–113]</sup> On the other hand, both the orientation and the induction energies are only present in molecules with permanent dipole moments. These molecules undergo Brownian rotation and induce dipole moments in other nearby molecules. Between two rotating dipoles there's the correlation energy, and since this energy is not strong enough to mutually align the participating molecules, the resulting net energy is an angle-averaged interaction free energy which is known as the Keesom orientation energy.<sup>[106,108,114–117]</sup> The Debye induction energy refers to the general attraction between a

permanent dipole and its induced dipole. All of the three forces decay with the inverse sixth power of the centre-to-centre distance between the participating atoms, and so is the combined van der Waals interaction.

### **2.1.2 Self-assembly and self-organisation**

As stated above, self-assembly in supramolecular chemistry is the concept where the interactions between two or more molecules with "well-designed" moieties are eligible to passively direct those molecules to build into a complex assembly that is otherwise difficult to approach. A self-assembly process includes three main stages. The first step is the molecular recognition to decide the type of interactions and binding sites. Then starts the sequential growth, where the components start to bind into a hierarchical structure. The final step is the automatic termination when all the possible components are engaged in the superstructure. The system reaches global equilibrium, there's no energy dissipation, and the energetically-favoured structures are stable once they are formed.<sup>[72,118]</sup> On the other hand, self-organisation is an out-of-equilibrium system that requires constant energy input to form and such superstructures, and the structures will disintegrate once the energy input is removed.<sup>[119,120]</sup> As a spontaneous but information-guided process, self-organisation is the ultimate driving force of the evolution of the biological world.<sup>[42,121,122]</sup> Self-assembly of numerous molecules may be seen as a simple collective process of the components, and self-organisation is the "dynamic, non-equilibrium" self-assembly. Since both processes require the components to be mobile, they usually take place in fluid phases.

### **2.1.3 Low molecular weight gelator with alkyl amide moiety**

Supramolecular organogels and fibres are examples of the emerging fields of supramolecular chemistry. These organogels are thermally reversible viscoelastic materials formed by small organic molecules dispersed in a suitable solvent.<sup>[123,124]</sup> They exhibit a permanent three-dimensional network structure and have solid-like mechanical and rheological properties, even though they contain a significant amount of liquid.<sup>[125]</sup> The gel can be prepared by dissolving the solid gelator in an organic solvent then cooling the solution down to below gelation transition temperature, a critical parameter where the solution undergoes a phase transition to a gel

state. Gelation happens when the gelator molecules self-assembled into a "skeleton" network to trap and immobilise the solvent molecules.<sup>[126,127]</sup>

Commonly seen are the alkyl amide and urea-derived LMWGs, which can be seen as a subcategory under the amino acid derivatives (**Figure 6**). Their remarkable gelating ability results primarily from strong intermolecular hydrogen bondings.<sup>[128–134]</sup> The initial assemblies are typically fibrous and one-dimensional.<sup>[135–137]</sup> These assemblies then go through interfacial aggregation induced by other interactions like the van der Waals interaction to form thicker bundles, and finally grow into a highly entangled network (**Figure 7**).

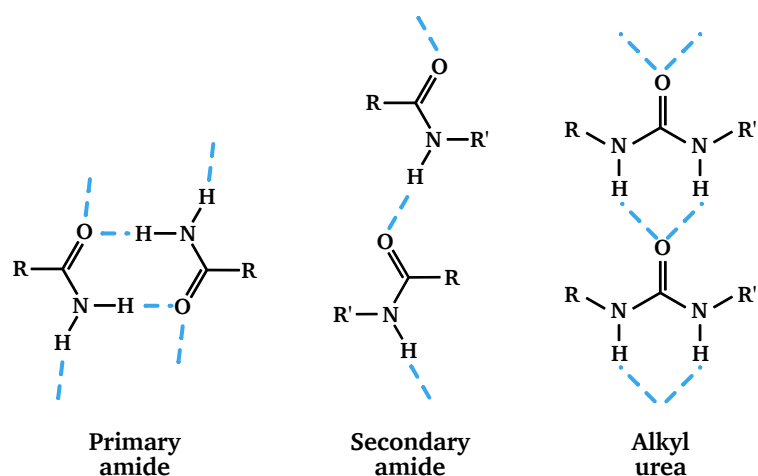


**Figure 6:** General structures and possible assembly patterns of amide and urea derived LMWGs.<sup>[129]</sup> Blue dashed lines are suggested hydrogen bondings.

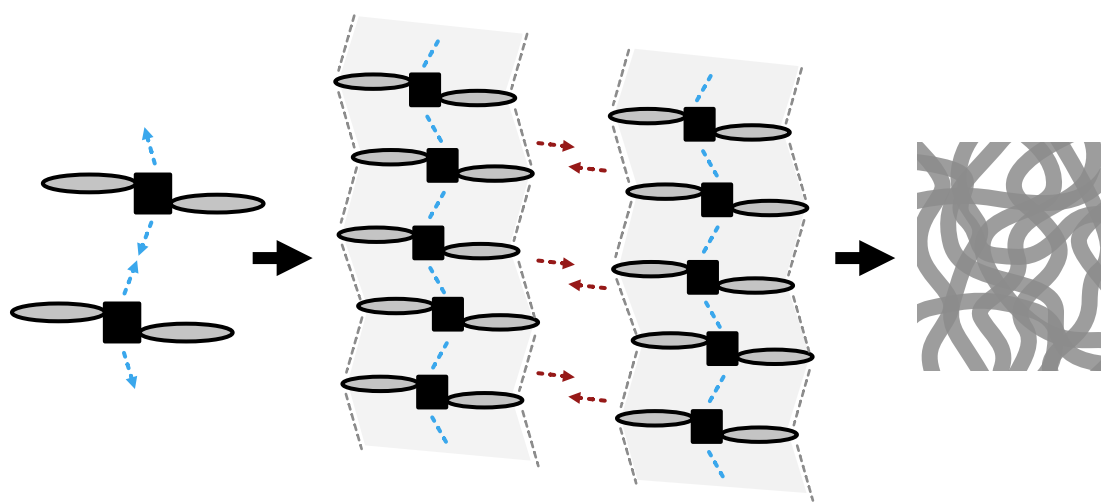


**Figure 7:** Suggested growing pattern of amide-based LMWGs. The initial assembly is primarily guided through intermolecular hydrogen bondings (blue), then the fibers aggregate interfacially through van der Waals interaction (red) to form thick bundles and entangling network.

Cyclohexane-based bisamide and bisurea compounds are reported with efficient gelation ability of various solvents.<sup>[138–141]</sup> The two amide/urea groups at the core of the gelator form strong intermolecular hydrogen bondings that induce highly directional self-assembly, and the gelators often aggregate into one-dimensional fibres. To reduce the probability of crystallisation of the gel, it is favoured to add aliphatic side chains on the compounds. Typical designs for these side chains are long hydrocarbon chains or fluorinated alkyl chains, as they are also responsible for inducing the interfacial interactions between the neighbouring molecules without interfering with the cores. The *trans*-1*R*,2*R*-cyclohexane derivative with long alkyl side chains reported by Hanabusa and co-workers exhibits the expected gelling effect in tetrahydrofuran in the presence of triethylamine.<sup>[138]</sup> It is also reported that the *cis* isomer failed to form alike macromolecular aggregates since the amide at the axial position is unavailable to form hydrogen bonding with the adjacent molecule. The chirality of the diamidocyclohexane moiety and the length of the side chains, either alkyl or fluorinated, were reported to have significant influences on the stacking pattern of the gelators.<sup>[142–145]</sup>

#### 2.1.4 Xerogel, aerogel, and cryogel

Organogels are often dried to provide solid materials for functionality. The drying methods have shown great influence on the structural properties of the dried material.<sup>[146–148]</sup> Depending on the drying method, the obtained material is named either xerogel, aerogel, or cryogel. As mentioned, a xerogel is a dried gel with the solvent being evaporated at room temperature or slightly higher under atmospheric pressure. The resulting solid is a porous material with some extent of shrinkage.<sup>[149]</sup> Aerogels are obtained with supercritical drying, where the solvent is removed under conditions above its critical point. They retain most of the original gel architecture and are highly porous since the collapsing capillary forces didn't come into play.<sup>[147,150]</sup> Cryogels are acquired through freeze drying; the gel is first frozen before the removal of solvent through sublimation. Similar to aerogels, cryogels also retain most of the pristine gel structure.<sup>[151]</sup>

Applications of xerogels reported include catalytic support,<sup>[149,152,153]</sup> target molecule segregation,<sup>[154–157]</sup> low dielectric constant material fabrication,<sup>[158]</sup> and surface modification.<sup>[159]</sup> Most of the reported preparation however includes a lengthy curing time of around 24 h, and thus needs to be in a contained and stable environment. The drop-cast method reported by Wei et. al offers rapid film formation within minutes and can be done in a standard fume hood,

expanding the potential applicability.<sup>[38]</sup>

### 2.1.5 Supramolecular polymers

Supramolecular polymers are a class of polymers with the main chains consisting of low molecular weight compounds linked with non-covalent interactions. This sole feature contributes to the one distinct difference between supramolecular polymers and conventional polymers: the former system is dynamic.<sup>[160]</sup> One of the early introductions of this concept was from Fréchet and co-workers in 1989, who published a work regarding the mesophase stabilisation with intermolecular hydrogen bondings between the mesogens.<sup>[161]</sup> Around similar times, the groups of Inoue,<sup>[162]</sup> Wuest,<sup>[163]</sup> and Whitesides<sup>[164]</sup> have published one-dimensional aggregates of amphiphilic or crystalline materials. However, these discoveries are not yet connected to supramolecular polymers but are discussed in the field of amphiphiles.<sup>[165]</sup> In 1990, Lehn and co-workers presented self-assembled fibres via hydrogen bondings with two types of structure-complementary components, and this work is commonly recognised as the first example of true supramolecular polymers (**Figure 8**).<sup>[166]</sup> Griffin and co-workers also reported supramolecular assemblies driven by molecular-recognising building units,<sup>[167]</sup> while the group of Percec reported a hydrogen-bonded tubular supramolecular architecture with only one type of monomer (**Figure 9**).<sup>[168]</sup> It is shown that acquiring supramolecular polymers with either one or multiple types of building blocks are all possible, provided that the building units have structure-complementarity.

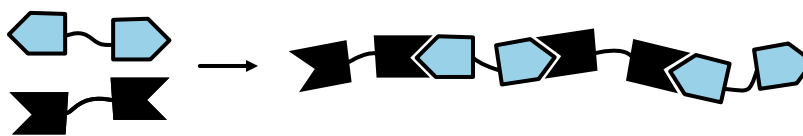


**Figure 8:** Schematic representation of the molecular recognition-driven self-assembled supramolecular polymer developed by Lehn and co-workers. Adapted with permission of John Wiley & Sons, Ltd, from C. Fouquey, J.-M. Lehn, A.-M. Levelut, *Adv. Mater.*, **1990**, **2**, 254–257, <https://doi.org/10.1002/adma.19900020506>.<sup>[166]</sup>

Despite the main chains holding together through non-covalent interactions, the mechanical properties of supramolecular polymers can still be comparable to the conventional polymers. In 1997, Meijer and co-workers presented the famous self-complementary quadruple hydrogen bonding ureidopyrimidinone (Upy) motif.<sup>[169]</sup> The Upy unit can be used to prepare fibres and

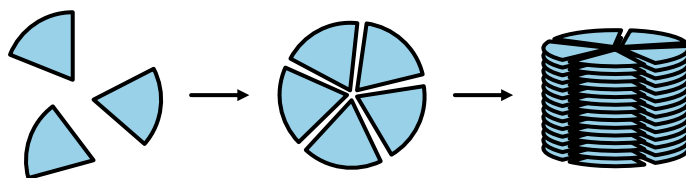


**Figure 9:** Schematic representation of the tubular supramolecular polymer developed by Percec and co-workers. Adapted with permission of Taylor & Francis Group, from V. Percec, J. Heck, G. Johansson, D. Tomazos, M. Kawasumi, G. Ungar, *J. Macro. Sci. Pure Appl. Chem.*, **1994**, *31*, 1031–1070, <https://doi.org/10.1080/10601329409349776>.<sup>[168]</sup>

films, even bioactive materials, with similar bulk properties to conventional polymers.<sup>[170,171]</sup> More recently, Schrettl and co-workers reported a series of robust metallosupramolecular copolymer with tensile strengths similar to low-density polyethylene.<sup>[55]</sup> Scherman and co-workers developed a glass-like yet compressible supramolecular polymer network.<sup>[172]</sup> Furthermore, the flexibility and reversibility of the materials offer alternate solutions that might be difficult to achieve with conventional polymers, like the brilliant self-disintegrating gastric retention devices reported by Langer and co-workers.<sup>[173]</sup>

## 2.2 Polymer chemistry

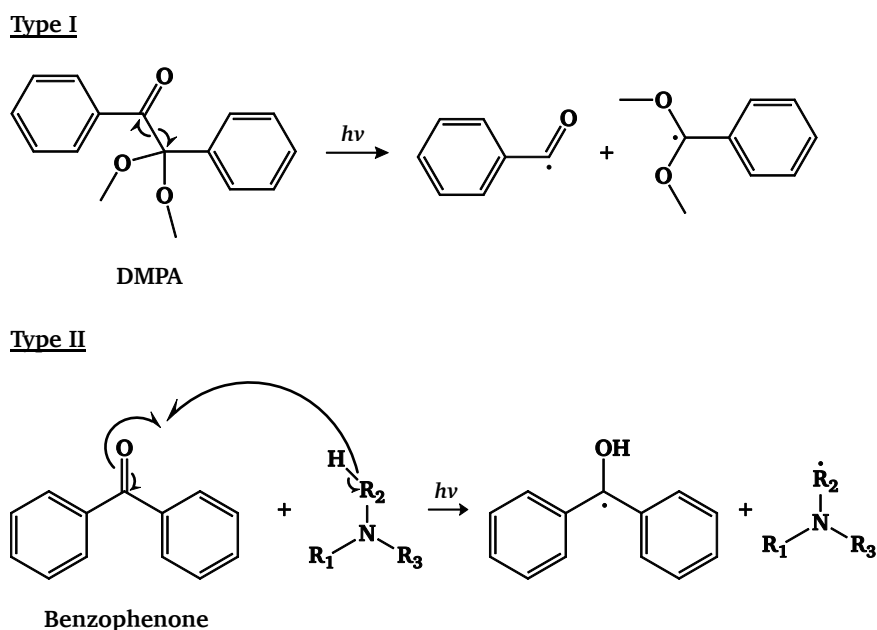
Polymers are macromolecules consisting of numerous repeating units called monomers that are linked together exclusively through covalent bonds. This feature provides polymers with distinct physical properties like high mechanical strength, high viscosity and long-range elasticity.<sup>[174–177]</sup> There are two main categories of polymers: naturally-occurred polymers like cellulose and protein, and synthetic ones like polyolefin and acrylic polymers. Various mechanisms like step-growth, chain-grow, and controlled polymerisation are available for obtaining synthetic polymers with different characteristics and functions. Step-growth polymerisation is when the polymer chain grows gradually through repeating reactions between functional groups of monomers. For example, polyesters are synthesised through step-wise condensation between a hydroxyl group in a diol and a carboxylic acid group in a dicarboxylic acid. Chain-growth polymerisation, like free radical polymerisation, allows the polymer chain to grow rapidly but without precise control over the reaction kinetic. Thus, controlled polymerisations such as living radical polymerisation and coordination polymerisation are developed to overcome the disadvantages. The properties of a synthesised polymer depend highly on the design of the repeating unit, the synthetic approach and the additives during the processing.



## 2.2.1 Photopolymerisation of acrylate monomers

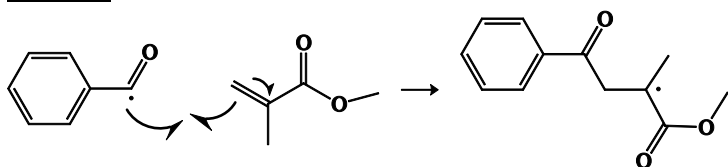
Acrylate monomers are widely used in synthetic polymers for their reactivity, versatility and desired properties. The acrylate functional group can be easily polymerised through various mechanisms including radical polymerisation and anionic polymerisation.<sup>[178–181]</sup> Using light to induce the radical polymerisation of acrylate monomers is especially appealing for the dental material and coating industry due to the advantages like the high reaction rate, the ease of management, and the possibility of a solvent-free synthesis in ambient conditions.<sup>[182–187]</sup>

Like most polymerisation mechanisms, photopolymerisation includes three reaction steps: initiation, propagation, and termination. The initiation step requires a photoinitiator absorbing UV light and generating active species by photochemical reaction. Photoinitiators in general can be categorised as either Norrish type I or type II.<sup>[188,189]</sup> Type I initiators are single molecules that undergo homolytic cleavage upon light exposure and each initiator generates two free radicals (**Scheme 1**).<sup>[190]</sup> Common examples are benzoin ether derivatives. Meanwhile, a type II initiator will abstract hydrogen from a co-initiator, typically a tertiary amine, to generate two active species. The active species then undergo chain propagation by reacting with the monomers sequentially. This continues until all of the monomers are consumed or other terminations like recombination or disproportionation occur (**Scheme 2**). In addition to propagation, it is also likely that the propagating chain cross-link with another polymer chain or even itself.

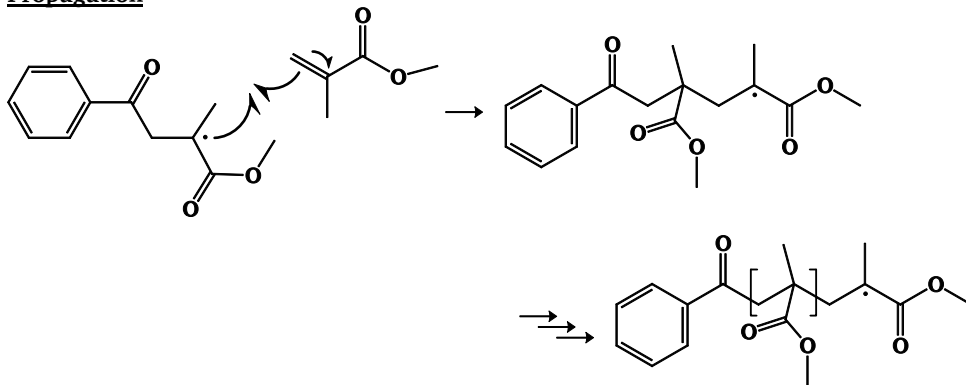


**Scheme 1:** Initiation mechanism of type I and type II photoinitiators with 2,2-Dimethoxy-2-phenylacetophenone (DMPA) and benzophenone shown as examples, respectively.

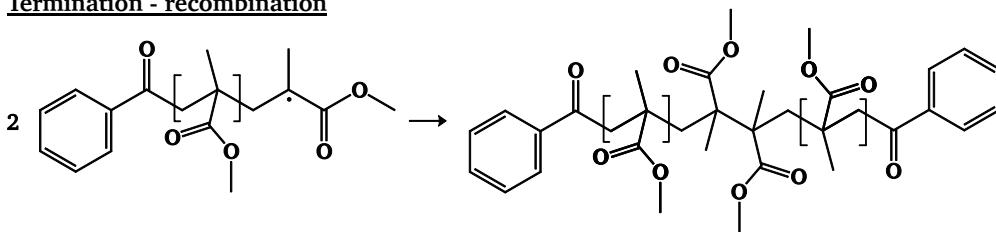
### Initiation



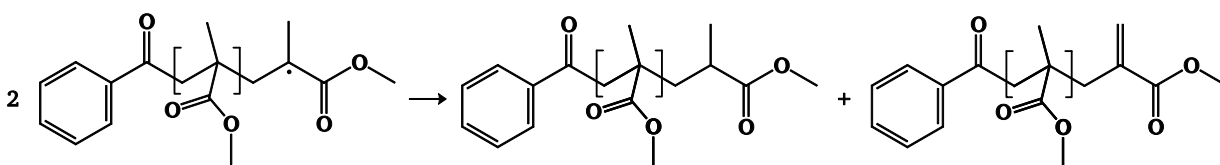
### Propagation



### Termination - recombination



### Termination - disproportionation



**Scheme 2:** General mechanism of radical polymerisation of MMA with DMPA as the initiator.

## 2.2.2 Acrylic polymers embedded with supramolecular gels

Early applications of embedding supramolecular assemblies in polymer matrixes are mainly for the preparation of porous polymer membranes. The first example was reported by Möller and co-workers, where a crystalline gel is included in and later removed from a UV-cured methyl acrylate resin.<sup>[191,192]</sup> More examples of gel template leaching with acrylate resins are reported.<sup>[193–197]</sup> On the other hand, reserving the gel inside the polymer can be beneficial for functionality. Kim and Chang have reported the fabrication of a polymer film with reversible thermochromism, which originates from the structural change of the embedded gelator assemblies.<sup>[198]</sup> Ohsedo and co-workers presented a thixotropic mixture consisting of a water-soluble

electronically conductive polymer with a polymer hydrogel, where the thixotropic property is only presented in the mixture and not in the individual components.<sup>[199]</sup> In addition, combining gelator and polymer to improve the physical and mechanical properties of dental materials has captured a great amount of interest.<sup>[200,201]</sup>

## 2.3 Superhydrophobicity

Superhydrophobicity refers to the extraordinary water-repellency exhibited on surfaces. Water droplets are seen to bead up on the surface and would either stay pinned to the surface or roll off subsequently. This phenomenon is commonly seen in nature, such as on the lotus leaf, the rose petal, the feathers of ducks, and more. Although there's no official definition, a generally accepted one is that, to be classified as superhydrophobic, a surface should exhibit a static water contact angle of  $150^\circ$  or above.<sup>[8,202,203]</sup> Nowadays it is commonly known that the contact angle on a smooth hydrophobic surface rarely exceeds  $120^\circ$ , but the proper amount of surface roughness effectively enhances that.<sup>[8,21,204–206]</sup> Early discussion of surface roughness affecting wetting regimes was carried out by Wenzel in 1936 and was extended by Cassie and Baxter in 1944.<sup>[207,208]</sup> It was in 1964 that Dettre and Johnson first proposed the direct relationship between surface roughness and superhydrophobicity, as they studied the drastic change of contact angle hysteresis on rough hydrophobic surfaces.<sup>[209]</sup> In 1977, with the development of scanning electron microscopy, Barthlott and Ehler investigated the superhydrophobic and self-cleaning lotus leaf, on which they discovered hierarchical-structured protrusions with densely distributed wax crystals.<sup>[1]</sup> This discovery thus established the importance of the synergy of surface roughness and intrinsic low surface tension for superhydrophobicity.

### 2.3.1 Surface tension

Surface tension is the attractive anisotropic force experienced by the liquid molecules at the fluid surface, or the liquid-vapour interface ( $\gamma_{LV}$ ).<sup>[210-214]</sup> The earliest direct recognition of surface tension is probably by Galileo in his published work *Discourse on Bodies that Stay Atop Water, or Move in It* in 1612, although the concept was not available to him at the time.<sup>[215]</sup> The source of this force is the uneven interactions between the molecules. Molecules in a fluid are normally attracted to each other by a variety of intermolecular forces, including the van der Waals interactions which exist in all matters, and the more distinct ones like hydrogen bonding or metallic bonds. Inside the bulk fluid, molecules experience these forces from all directions and the cohesive energy is balanced. However, molecules at the surface have fewer molecules surrounding them and no neighbour molecules above them, hence facing an unbalanced attractive force that is the surface tension. This "inward" force, however, is not normal to the fluid surface, but parallel.<sup>[214]</sup>

According to the Lennard-Jones potential, a single particle either attracts or repels another particle, depending on the distance.<sup>[216,217]</sup> In a bulk fluid, some particles attract while others repel, so attraction and repulsion both exist. A particle away from the surface experiences balanced attraction and repulsion both symmetrically (**Figure 10**); a particle at the surface experiences reduced upward repulsion due to the absence of the downward attraction. Since repulsion is a short-range force, the particle experiences the same magnitude of repulsion from all available directions.<sup>[211,218-220]</sup> In spite of that, the attraction parallel to the surface remains intact since it is still balanced by symmetry. The long-range nature of attraction makes them sensitive to the structure of the liquid and thus can be anisotropic. Marchand and co-workers provide a brilliant explanation by imagining the existence of subsystems within a bulk fluid (**Figure 11**).<sup>[214]</sup> The attraction experienced by the lower subsystem (yellow) is reduced with the size of the attracting region which is the upper subsystem (green), since the system is moving from the liquid phase towards the vapour phase and the density of the upper subsystem decreases.<sup>[214,221]</sup> Seeing the system is in equilibrium, attraction and repulsion must balance. In other words, repulsion decreases when approaching the liquid-vapour interface. However, in the region close to the interface, the anisotropic attractive force stays nearly constant, and that results in a net attractive force (**Figure 12**).<sup>[214]</sup>

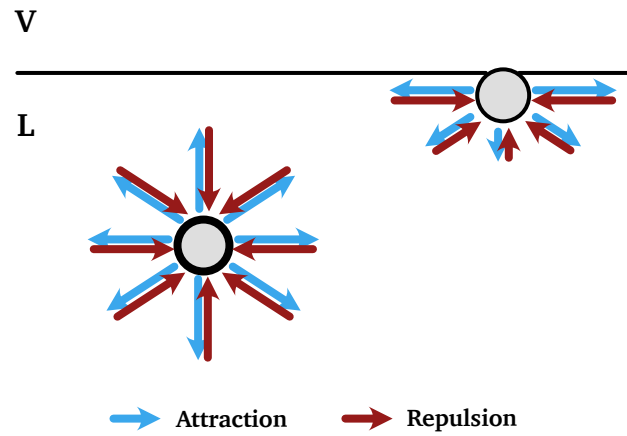


**Figure 10:** A particle in the bulk fluid experiences the same magnitude of both attraction and repulsion from all directions (left), while a particle at the surface encounters reduced upward repulsion since the lack of downward attraction (right). The magnitude of the forces parallel to the interface remains since they are still symmetrical and balanced. Adapted with the permission of the American Association of Physics Teachers, from A. Marchand, J. H. Weijs, J. H. Snoeijer, B. Andreotti, Why is surface tension a force parallel to the interface?, *Am. J. Phys.*, **2011**, 79, 999–1008, doi.org/10.1119/1.3619866.<sup>[214]</sup>

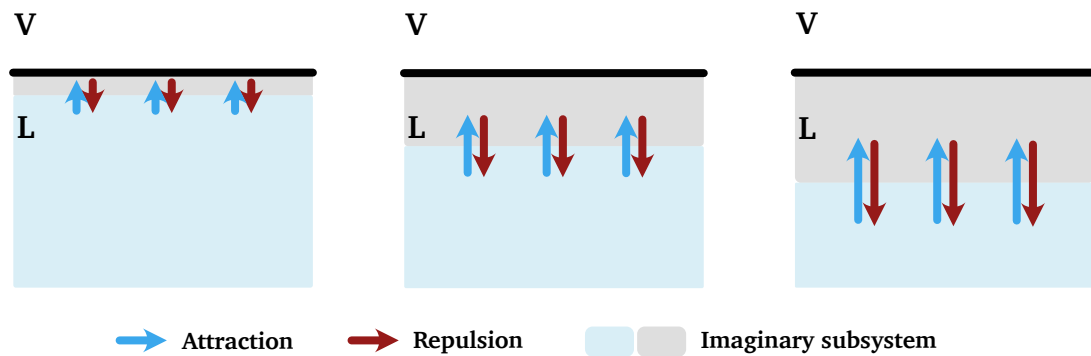


**Figure 11:** A bulk fluid is divide into two imaginary subsystems. The attraction experienced by the lower subsystem (yellow) will increase along with the size of the attracting region (green). The repulsion is increased accordingly to balance the forces. Adapted with the permission of the American Association of Physics Teachers, from A. Marchand, J. H. Weijs, J. H. Snoeijer, B. Andreotti, Why is surface tension a force parallel to the interface?, *Am. J. Phys.*, **2011**, 79, 999–1008, doi.org/10.1119/1.3619866.<sup>[214]</sup>

### 2.3.2 Contact angle

When there is contact between the three phases of solid, liquid, and vapour, the phenomenon observed is called wetting.<sup>[11]</sup> There are two wetting regimes: complete and partial wetting, which can be distinguished by the spreading parameter  $S$ :

$$S = \gamma_{SV} - (\gamma_{SL} + \gamma_{LV}). \quad (1)$$

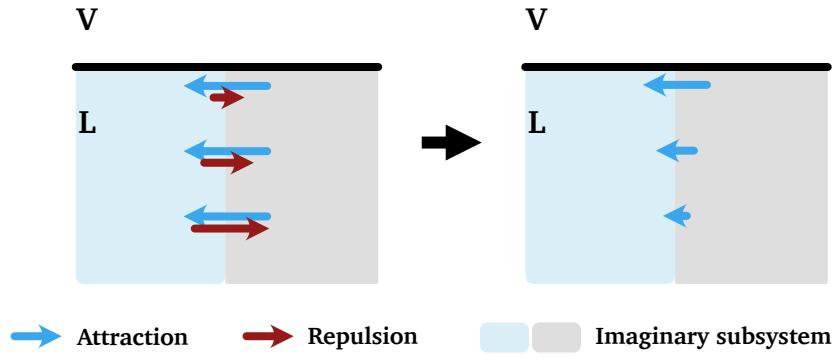


**Figure 12:** In a region very close to the liquid-vapour interface, the short-ranged repulsion decreases when approaching the interface, while the long-ranged attraction is nearly constant as the size of the attracting region remains (left). Therefore, there is a net attractive force near the interface (right). Adapted with the permission of the American Association of Physics Teachers, from A. Marchand, J. H. Weijs, J. H. Snoeijer, B. Andreotti, Why is surface tension a force parallel to the interface?, *Am. J. Phys.*, **2011**, 79, 999–1008, doi.org/10.1119/1.3619866.<sup>[214]</sup>

where  $\gamma_{SV}$ ,  $\gamma_{SL}$ , and  $\gamma_{LV}$  refer to the interfacial free energy of the solid-vapour interface, the solid-liquid interface, and the liquid-vapour interface, respectively. When

$$S \geq 0,$$

the liquid flattens, spreads and wets the surface completely to reach the minimum surface energy possible; if

$$S < 0,$$

the liquid stays in place and forms a spherical sessile drop, and the case is referred to as partial wetting.<sup>[222,223]</sup> In other words,  $S$  measures the difference in the surface energy of the substrate when it's dry or wet. When the substrate is dry, there is no liquid phase involved, and the surface energy is simply the interfacial free energy of the solid-air interface ( $\gamma_{SV}$ ). On the other hand, when the liquid phase is included, the surface energy is the sum of the interfacial free energy of the solid-liquid interface and the liquid-vapour interface ( $\gamma_{SL} + \gamma_{LV}$ ).<sup>[11]</sup>

In any partial wetting regime, there is a contact angle between the liquid resting on the substrate. In 1805, Young proposed a concept that there is a characteristic contact angle between any combination of a liquid and a solid, and this contact angle can be expressed as the equilibrium of the surface tensions of the solid ( $\gamma_S$ ), the liquid ( $\gamma_L$ ), and the solid-liquid interface ( $\gamma_{SL}$ ):<sup>[224]</sup>

$$\gamma_S - \gamma_{SL} = \gamma_L \cos \theta. \quad (2)$$

It was pointed out by Bangham and Razouk that Eq. 2 should be written as:<sup>[225]</sup>

$$\gamma_{SV} - \gamma_{SL} = \gamma_{LV} \cos \theta, \quad (3)$$

since both the liquid and the solid are actually in equilibrium with the vapour of the liquid (**Figure 13**).

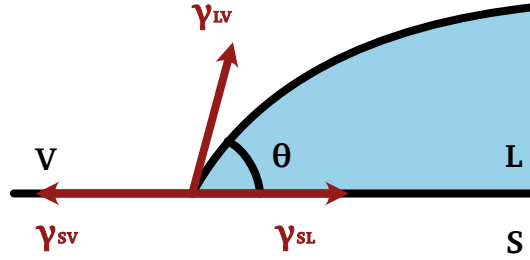


**Figure 13:** Illustration of Young's contact angle in the equilibrium of the three interfacial tensions.<sup>[224]</sup>

The first extreme case of Young's equation happens when

$$\gamma_{SV} = \gamma_{SL} + \gamma_{LV}.$$

Here,

$$S \geq 0,$$

$$\cos \theta = 1,$$

which leads to the complete wetting scenario (**Figure 14**).<sup>[226–228]</sup> In the other extreme case,

$$\gamma_{SL} = \gamma_{SV} + \gamma_{LV},$$

$$S = -2\gamma_{LV},$$

$$\cos \theta = -1,$$

which corresponds to complete nonwetting. Thus, it is obtained that

$$|\gamma_{SV} - \gamma_{SL}| < \gamma_{LV}, \quad (4)$$

and the contact angle  $\theta$  between any combination of a solid and a liquid will be between  $0^\circ$  and  $180^\circ$ .<sup>[226]</sup> When the liquid is water, and  $\theta$  is between  $0^\circ$  and  $90^\circ$ , the solid surface is categorised as hydrophilic. When  $90^\circ < \theta < 180^\circ$ , the solid surface is hydrophobic. For superhydrophobicity,  $\theta$  has to be over  $150^\circ$ .<sup>[8,202,229]</sup>

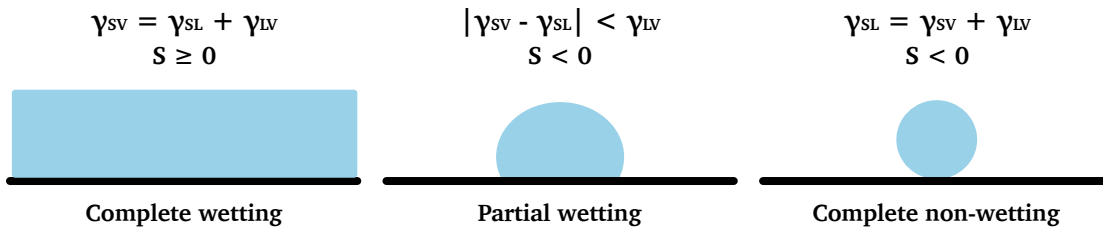


**Figure 14:** Different wetting regimes based on Young's equation and the spreading parameter  $S$ .<sup>[11,226–228]</sup>

There are several approaches to measuring contact angles. For relatively large contact angles ( $\theta > 45^\circ$ ), one can apply the projection method.<sup>[11]</sup> An intense light source from one side of the droplet will project the contour of the droplet to a converging lens that is on the other side of the drop. To determine the contact angle based on the projected contour, Bashforth and Adams have first developed a precise drop shape method, where the experimentally measured drop contour is fitted to the theoretically derived ones to calculate the interfacial tensions.<sup>[230–232]</sup> However, these calculations are strongly subjective and time-consuming. To enhance accuracy and simplification, computational curve-fitting methods like ellipse fitting and Laplace-Young fitting are developed.<sup>[231,233–235]</sup> Ellipse fitting is often referred to as the geometric fit and tends to provide different values for the left and right corners of a sessile drop.<sup>[236,237]</sup> Laplace-Young fitting applies the Laplace-Young equation to find the perfect Laplacian curve for the drop contour.<sup>[224,238–240]</sup> It is found that the Laplace-Young fitting is more reliable when the contact angle is above  $150^\circ$ , but not suitable for contact angles lower than  $90^\circ$ .<sup>[231,241]</sup> As for small contact angles ( $1^\circ < \theta < 45^\circ$ ), the mirror method based on optical reflectometry is preferred for the higher accuracy.<sup>[11]</sup>

### 2.3.3 Surface roughness: Wenzel state and Cassie-Baxter state

Although Young's equation is generally accepted, it is reported that the equation is not capable of representing all simulated results of the contact angles in a liquid-solid-vapour system.<sup>[218,242]</sup> One probable reason is that the hypothesis requires the system to be homogeneous, especially towards the interfaces.<sup>[243]</sup> Nonetheless, in real systems, there will be entropy changes due to molecular rearrangements in the subsystems. Further studies also show that the wetting property is very sensitive to the surface structure, even just at molecular levels.<sup>[227,244,245]</sup> For a smooth surface made from a material with very low intrinsic surface energy like poly(tetrafluoroethylene) (Teflon<sup>TM</sup>), the highest WCA measured is around  $120^\circ$  but



can go beyond  $160^\circ$  when it is structured.<sup>[8,246]</sup> The influence of surface roughness on liquid wetting has therefore been established. The first explanation is proposed by Wenzel.<sup>[207,247]</sup> It is suggested that a roughened surface will magnify the wetting properties of the solid since there is more surface and a greater intensity of surface energy involved in the wetting process (**Figure 15**). The magnification ratio is the ratio of the actual surface area in contact with the liquid to the geometric surface area of a given unit surface, or the roughness factor  $r$ :

$$r = \frac{\text{actual area}}{\text{geometric area}} \quad (5)$$

$$\cos \theta_W = r \cos \theta = r \frac{(\gamma_{SV} - \gamma_{SL})}{\gamma_{LV}}. \quad (6)$$

Wenzel's equation predicts that when

$$\theta < 90^\circ,$$

$$\theta_W < \theta;$$

while

$$\theta_W > \theta$$

when

$$\theta > 90^\circ.$$

This may not always be the case since  $r$  could vary from location to location on a real inhomogeneous surface.<sup>[248]</sup>

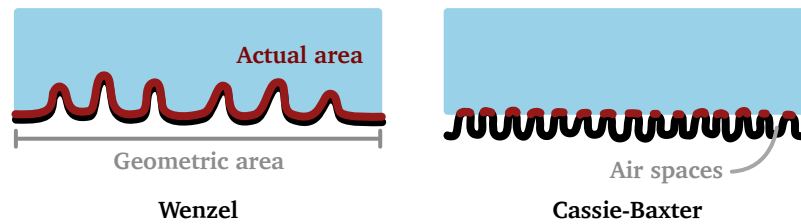


**Figure 15:** Wetting regimes on rough surfaces proposed by Wenzel (left) and Cassie and Baxter (right).

In both cases the suggested surface area in contact with the liquid is marked in red, which corresponds to the *actual area* in Eq. 5 and  $\sigma_1$  in Eq. 8, respectively.

The analysis of the contact angle on a rough surface is also discussed by Cassie and Baxter.<sup>[208]</sup> Here, a rough surface is treated as a combination of two homogeneous surfaces. The two homogeneous surface each have a fraction of the surface area of  $\sigma_1$  and  $\sigma_2$ , and the corresponding Young's contact angle  $\theta_1$  and  $\theta_2$ , respectively. Cassie's equation can therefore be written as:

$$\cos \theta_{CB} = \sigma_1 \cos \theta_1 + \sigma_2 \cos \theta_2. \quad (7)$$

To be noted is the consideration of the heterogeneous surface as the porous surface.<sup>[249]</sup> Therefore, the first homogeneous surface is the solid substrate, and the second homogeneous surface is actually the air spaces (**Figure 15**). With

$$\sigma_2 = 1 - \sigma_1,$$

$$\cos \theta_2 = -1,$$

Cassie's equation can be simplified as:

$$\cos \theta_{CB} = \sigma_1(1 + \cos \theta) - 1 \quad (8)$$

This means when

$$\sigma_1 \rightarrow 1,$$

the surface is nearly smooth and ideal, and

$$\cos \theta_{CB} \cong \cos \theta.$$

On the other hand, if

$$\sigma_1 \rightarrow 0,$$

the liquid is barely in contact with the substrate but "sitting" on the air spaces. Herein,

$$\cos \theta_{CB} \rightarrow -1,$$

$$\theta_{CB} \rightarrow 180^\circ,$$

the substrate approaches the superhydrophobic state.

### 2.3.4 Contact angle hysteresis

Contact angles can also be dynamic if the solid-liquid-vapour interfaces are moving during the measurement.<sup>[250]</sup> Experimentally, there are two ways a droplet can move on the surface: tilting the substrate so the droplet slides down, or adding/removing liquid to a pre-existing droplet to change its volume (**Figure 16**). For the first method, the contact angle measured at the advancing side right before the sliding is called the advancing contact angle ( $\theta_A$ ), and the one behind the receding contact angle ( $\theta_R$ ). For the second method, while the droplet is increasing/decreasing in volume, its contact area with the substrate remains temporarily the

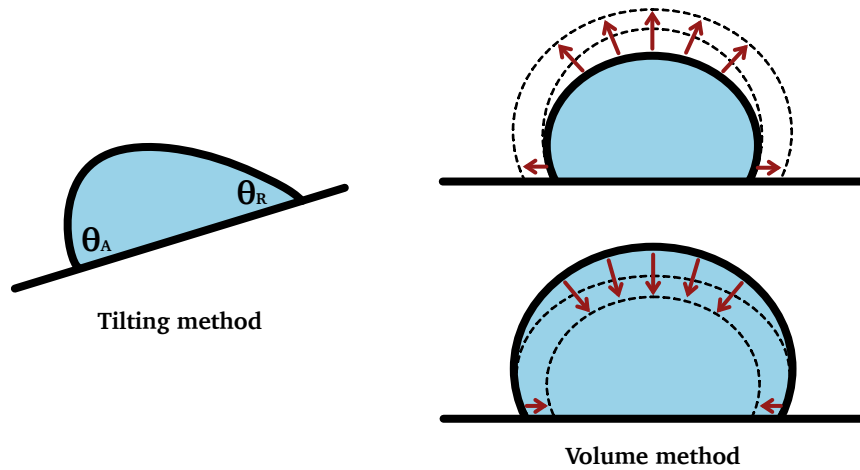


**Figure 16:** Methods for measuring the advancing ( $\theta_A$ ) and receding contact angles ( $\theta_R$ ).

same until it begins to advance/recede, and the angles measured at this metastable state are the advancing contact angle and the receding contact angle. The difference between the advancing contact angle and the receding contact angle is termed the contact angle hysteresis (CAH).

The source of CAH is a series of metastable states of the droplet that result from surface heterogeneity.<sup>[251–254]</sup> Every metastable state has a characteristic contact angle, and all of these contact angles should be observable between a maximum and a minimum, which are the advancing contact angle and the receding contact angle, respectively.<sup>[255]</sup> The existence of the metastable states and the two extremes can be explained with the concept of the *work of adhesion*, which is derived from Young's concept,<sup>[224]</sup> extended by Duprè,<sup>[256]</sup> and interpreted by Adam and Jessop, Bangham and Razouk, and Harkins and Livingston.<sup>[225,257,258]</sup> The work of adhesion, despite the name, refers to the work required to separate the liquid drop from the solid substrate, but leave behind an adlayer of the vapour on the solid.<sup>[259]</sup> The work of adhesion is therefore highly dependent on the configuration of the surface. Pease suggested that since most hydrophobic solids are distributed with polar and non-polar groups, the droplet front can end up in any position and displays the minimum work of adhesion corresponding to the configuration of the landed region.<sup>[251]</sup> When the droplet front advances, the contact line passes through a variety of configurations and requires work that can overcome the resistance. This resistance is the greatest when the work of adhesion is minimal. As for receding the droplet front, it is like weeping a wet surface dry, and work to overcome the maximum work of adhesion is needed. Good proposed that if the surface is chemically homogeneous but irregular, for the droplet front to move along the ridges, either advance or recede, the liquid-vapour interface has to contort and there will be an increase in the free energy.<sup>[252]</sup> Likewise, if the surface is smooth but chemically

inhomogeneous, the equilibrium that gives the measured contact angle will no longer fit once the droplet moves to a region with different surface energy due to a change of polar/non-polar group configuration, and the liquid-vapour interface will contort to match the varied work of adhesion. Thus, the metastable states occur since the liquid-vapour interface is passing through a variety of regions with different work of adhesion due to surface heterogeneity. The advancing contact angle is dependent upon the minimum value of the work of adhesion, and the receding contact angle the maximum.<sup>[251]</sup>

### 2.3.5 Hydrophobicity and oleophobicity from fluorine

The term *fluorous* was introduced with the idea of being used analogously to *aqueous*, as the uniqueness of highly fluorinated compounds can be, like water, classified as its own category.<sup>[260]</sup> The specific characteristics of these compounds are largely contributed from a list of physical and chemical properties of the fluorine.<sup>[44–47,261]</sup> To begin with, the fluorine atom has a larger van der Waals radius than the hydrogen atom.<sup>[262]</sup> This means a fluoroalkyl chain is bulkier and stiffer than a hydrocarbon chain for the same length,<sup>[263,264]</sup> A helical conformation is often observed in a long fluoroalkyl chain to minimise the steric limitations from the large atom size and the repulsion between the fluorine atoms.<sup>[265]</sup> Secondly, fluorine has high electronegativity that leads to the formation of a dense electron cloud around the molecule, which acts as a shield against other reagents and makes fluorocarbons behave inertly.<sup>[266]</sup> Furthermore, fluorine has low polarisability, hence the low cohesive energy densities in the condensed state of fluorocarbons. It also reflects in weak intermolecular van der Waals interactions, which results in low surface tension.<sup>[267]</sup> The large surface area and the low surface tension of the fluoroalkyl chains are the main contributors to the intrinsic hydrophobicity. Moreover, the very different cohesive energy density of fluorocarbons and hydrocarbons also makes them unlikely to mix. The fluorocarbons are therefore considered to be oleophobic as well as hydrophobic.

## 2.4 Analytical methods

### 2.4.1 Scanning electron microscopy

The development of SEM is undoubtedly an important milestone for scientific research in numerous disciplines. The powerful imaging technique allows the observation and analysis of sample morphologies at higher resolution and magnification than optical microscopy. It is how one can examine the hierarchical structures of many water-repellent plant surfaces in the first place.<sup>[1-3]</sup> Moreover, SEM is more versatile when it comes to sample preparation, as it doesn't require the sample to be coated on a special grid like in transmission electron microscopy, or on particularly flat surfaces like in atomic force microscopy.

The essential components of SEM include an electron gun, an anode, a lens system, a scan coil, and one or multiple electron detectors in an ultra-high vacuum (UHV) chamber (**Figure 17**).<sup>[268]</sup> The working principle of SEM is to scan through a designated area of the sample with an intense electron beam (1 keV to 40 keV).<sup>[269,270]</sup> The electron beam interacts with the sample through a variety of scattering effects and generates several different signals, including secondary electrons (SE), backscattered electrons (BSE), and characteristic x-rays. These signals convey information like the topography of the surface, the composition of the sample, and its elemental distribution. SE are low energy electrons generated from the sample due to high energy irradiation. After the electron beam, here as primary electrons, bombards the sample, some of the energy is transferred to the sample. If this energy is sufficient to overcome the binding energy, the electrons from the sample can emit and get extracted by the electron fields.<sup>[271]</sup> BSE are the electrons that got reflected from the sample due to elastic scattering. They originate deeper from the sample and are higher in energy than SE.<sup>[272]</sup> Characteristic x-rays originate from the ionisation of the inner shell of the atom and are especially helpful for compositional analysis. When the energy transferred from the source beam is high enough to promote the electron of the inner shell to escape, there will be a vacancy left in the inner shell which can be filled by the transition of an electron from the outer shell. Since the energies of the atomic shells are highly defined, this transition energy is characteristic of the atoms and therefore the sample.<sup>[269]</sup>

The development of SEM started in 1926 when Busch studied the trajectories of charged particles in the axial symmetric electromagnetic field and found that such a field can be used as

particle lenses.<sup>[270,273]</sup> Around similar times, de Broglie introduced the concept of *material waves*, which states that particles like electrons can also be described as waves.<sup>[274,275]</sup> The de Broglie wavelength  $\lambda$  is defined as follows:

$$\lambda = \frac{\lambda_0}{N}, \quad (9)$$

where  $\lambda_0$  and  $N$  are the wavelength and average number of constituent photons, respectively. With the de Broglie wavelength, Ruska and Knoll estimated the resolution limit of electron microscopy to be approximately 2.2 Å, which turned out to be quite accurate.<sup>[276]</sup> Later on, Ruska dedicated his research to electron optics and the development of electron microscopy, for which he was awarded half of the 1986 Nobel Physics Prize. The first true SEM was believed to have been developed by Zworykin in 1942,<sup>[277]</sup> several improvements were carried out later by Oatley,<sup>[278]</sup> Everhart and Thornley,<sup>[279]</sup> and combined by Pease and Nixon to provide the first prototype of commercial SEM.<sup>[280]</sup>

The high resolution of SEM is achievable due to the short wavelength of electrons used as the imaging source. To optimise resolution, a small electron source size is essential, therefore it is necessary to have a condenser lens system to focus the beam precisely. Additionally, a high-energy with a narrow energy distribution provides images with a better signal-to-noise ratio and minimises chromatic aberration. In case the samples are non-conductive, it is necessary to coat a layer of conductive material, typically gold, gold-palladium alloy, carbon, and aluminium, onto the surface before scanning. This layer serves to prevent charge accumulation from the limited migration due to high resistivity, which can cause issues in the imaging like low signal-to-noise ratio, low resolution, and discontinuous images.<sup>[268]</sup>

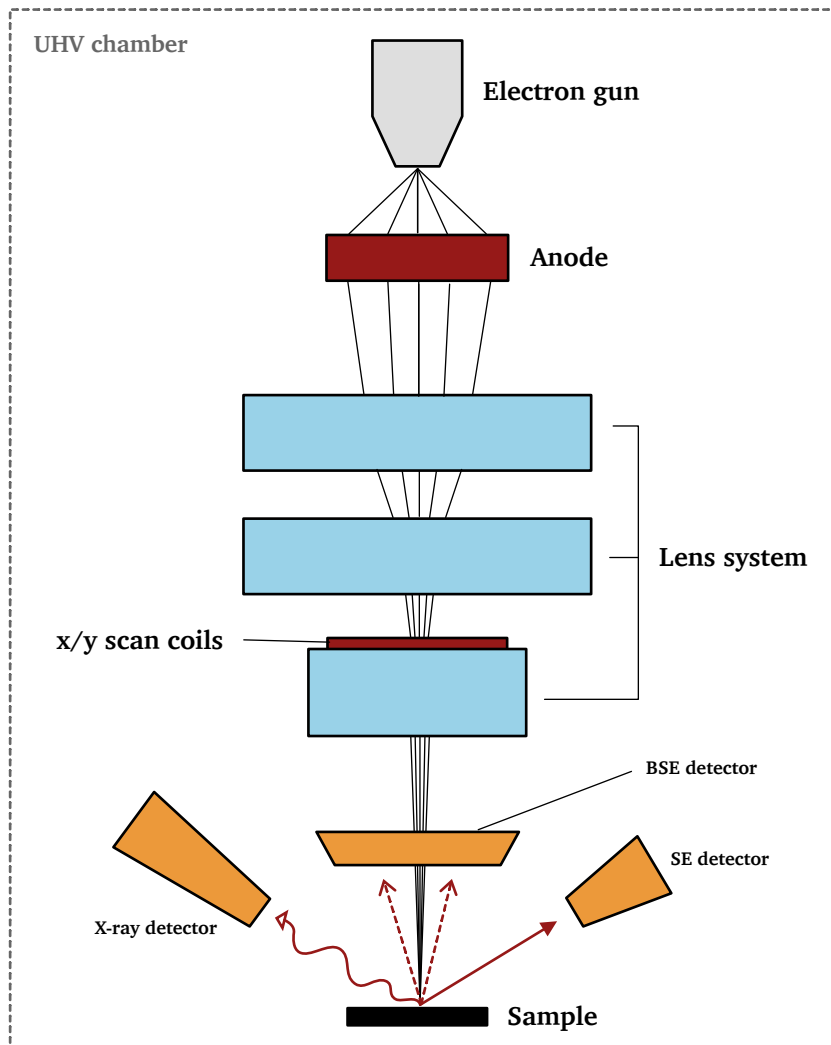


**Figure 17:** Illustration of the common components of SEM. <sup>[281]</sup>

## 2.4.2 Surface x-ray diffraction

XRD is a common technique for the investigation of the structural properties of crystalline and amorphous materials.<sup>[282]</sup> The diffraction of x-ray was observed by von Laue in 1912,<sup>[283]</sup> and soon after, the field of crystallography developed rapidly with the lead from the Braggs.<sup>[284]</sup> They were awarded the 1914 and 1915 Nobel Physics Prize, respectively. The major advantage of the method is the short wavelength of the x-ray which is comparable to the interatomic spacing, therefore it is useful for the study of atomic arrangement in crystalline structures, the interplanar distances, the particle sizes, etc.<sup>[285,286]</sup> Another advantage of using x-ray as the inspection source is the weak interaction it has with the sample, which makes it simple to analyse.<sup>[287]</sup> Diffraction patterns usually require monochromatic x-rays made with  $K_{\alpha_1\alpha_2}$  doublet as the source. Here,  $K_{\alpha}$  is the characteristic x-ray emitted from an atom, when its  $K$  shell (the innermost electron shell of an atom) vacancy is filled by an electron from the  $L$  shell (the second electron shell), and  $\alpha_1$  and  $\alpha_2$  are distinguished since the splitting of the orbitals of the  $L$  shell causes differences in the energy levels.<sup>[285]</sup> Commonly used sources include  $K_{\alpha}$  doublets of Mo, Cu, or Fe. When the x-ray strikes a crystalline material, the atomic planes act as a series of reflectors that cause the x-ray to reflect but also scatter. The diffractions are combined results of two phenomena: scattering by individual atoms and interferences between the scattered waves.<sup>[288]</sup> These scatterings as well as the reflections are produced when the conditions satisfy the Bragg's law:

$$n\lambda = 2d \sin \theta, \quad (10)$$

where  $n$  is the diffraction order,  $\lambda$  is the wavelength of the incident x-ray,  $d$  is the interplanar spacing, and  $\theta$  is the reflection angle. Since the analysis is focused on the surface of the sample, the incidence of the beam is at a shallow angle, and so are the diffracted waves. Basic components of XRD include an x-ray source, a rotatable sample stage, and a rotatable detector (**Figure 18**). The angular acceptance of the detector in the scattering plane should be wide enough to detect all scattered photons.<sup>[287]</sup> Often, the scanning speed of the goniometer is synchronised with the moving speed of the detector, therefore a diffractogram is plotted as the signal intensity against  $2\theta$ . The diffractogram provides information about the crystallographic properties of the sample. For example, amorphous materials will have broad peaks with low amplitude, while crystalline materials have more distinct sharp peaks with high intensities. According to the Eq. 10, the location of the peaks in terms of  $2\theta$  relates to the  $d$  spacing of the crystal planes. Peaks at higher  $2\theta$  regions indicate a smaller spacing of the crystal planes. In



addition, the width of the peak is related to the size of the crystallites  $L$ , the wider the peak, the smaller the size of the particles. This is described with the Scherrer's equation:<sup>[289]</sup>

$$L = \frac{K\lambda}{B \cos \theta}, \quad (11)$$

$K$  is the Scherrer constant,  $\lambda$  is the wavelength of the x-ray,  $B$  is the full width at half maximum (FWHM) of the peak, and  $\theta$  is the Bragg's angle corresponding to the peak. For a material with both crystalline and amorphous regions, there will be sharp peaks on the diffraction pattern given by the crystalline region, and diffused backgrounds from the amorphous region. The degree of the crystallinity of the material can be calculated as the fraction of the integrated area of the sharp peaks over the area of the whole pattern (**Figure 19**).<sup>[290,291]</sup>

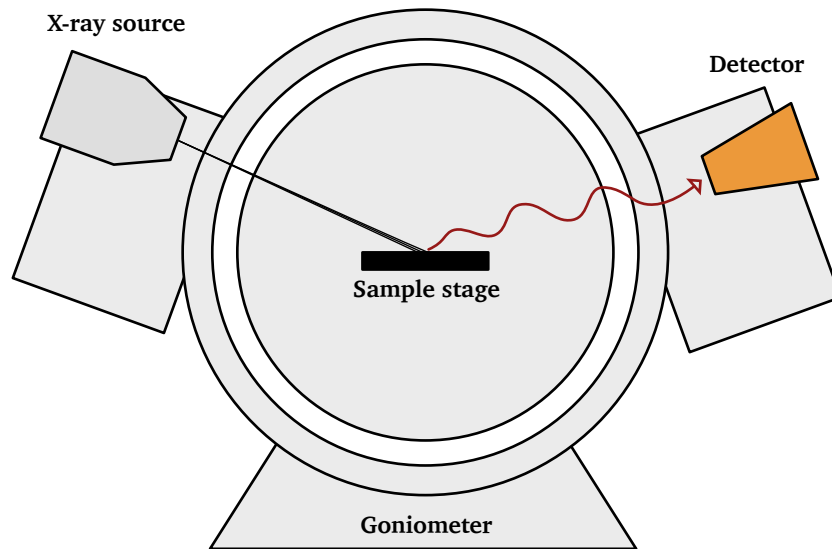
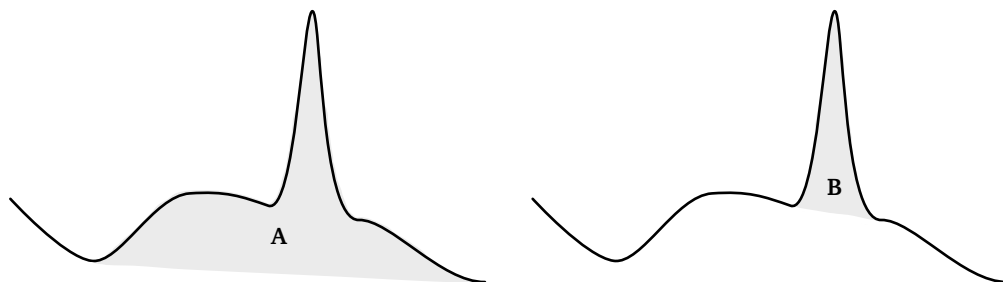


**Figure 18:** Illustration of the basic components of sXRD.<sup>[292]</sup>



$$\text{Crystallinity [\%]} = \frac{\text{Area B}}{\text{Area A}} \times 100$$

**Figure 19:** For semi-crystalline materials, the crystallinity can be calculated using the integrated area of the diffractogram of different regions.

### 2.4.3 Time-of-flight secondary ion mass spectroscopy

ToF-SIMS is a compositional surface analysis technique with high lateral resolution.<sup>[293,294]</sup> Moreover, it is capable of carrying out three-dimensional analysis, which is especially useful for samples like composite coatings and thin films. In ToF-SIMS, a high-energy ion beam, typically a liquid metal ion like bismuth, is used to bombard the sample to eject some fragments through a collision cascade (**Figure 20**). An electrostatic field will extract and accelerate these ionised fragments to a certain energy before they travel through a drift tube to arrive at the time-of-flight analyser. As all ions have the same energy, the difference in the arrival time results exclusively from the mass of the fragment. Since the interaction of the collision cascade with surface molecules is soft enough, fragments with masses up to 12 000 u can be emitted.<sup>[295]</sup> By rastering the ion beam through the surface, one can obtain a chemical composition map of the sample. As mentioned, the three-dimensional analysis, also known as depth profiling, of the sample can be achieved with the dual beam technique.<sup>[295,296]</sup> In addition to the liquid metal ion gun, a gas cluster ion source like argon with large cluster size is used for sputtering. The gas cluster ion beam sputters the sample and creates a crater while the metal ion beam analyses the bottom of the crater. By repeating this process, a depth profile of the sample is obtained. ToF-SIMS is often used in complementary with x-ray photoelectron spectroscopy (XPS) for surface chemical characteristic analysis.

The development of SIMS can be traced back to 1897 when Thomson observed the deflection of a cathode ray induced by an electric field under reduced pressure.<sup>[297]</sup> Furthermore, in 1910, he reported the discovery of secondary rays generated by striking a metal plate with a cathode ray.<sup>[298]</sup> This can be seen as the first report of the generation of secondary ions from ion bombardment. The first SIMS prototype was introduced by Herzog and Viehböck in 1949.<sup>[299]</sup> Benninghoven, Niehuis and Steffens combined the SIMS with a time-of-flight analyser to produce the first ToF-SIMS in 1985.<sup>[300]</sup> Here, a static SIMS was used, which is a SIMS with a low-current-density primary ion source.<sup>[293]</sup> This ensures low sputtering rates with secondary ions generated only from the topmost atomic layer of the specimen. In contrast, one can apply the dynamic SIMS for bulk analysis of surfaces and thin films.<sup>[301]</sup> The dynamic SIMS has a primary beam with high current density and can break several layers of the sample for analysing the vertical distribution of the components.<sup>[302]</sup> The time-of-flight analyser, as mentioned, separates the ions based on their mass-to-charge ratios ( $m/z$ ) by measuring the time it takes for

ions to arrive at the analyser.<sup>[303]</sup> Theoretically, all ions travelling through the drift tube gain the same potential energy  $E$  from the accelerating electric field with a potential difference of  $U$ :

$$E = zU. \quad (12)$$

This potential energy translates to the kinetic energy that enables the ion to travel through the drift tube:

$$E = zU = \frac{1}{2}mv^2. \quad (13)$$

The velocity of the ion  $v$  stays constant in the field-free drift tube with the travel distance of  $L$ , and the arrival time of the ion  $t$  can be calculated as:

$$v = \frac{L}{t} \quad (14)$$

$$zU = \frac{1}{2}m\left(\frac{L}{t}\right)^2 \quad (15)$$

$$t = \frac{L}{\sqrt{2U}} \sqrt{\frac{m}{z}} \quad (16)$$

In reality, there will be slight variations in the potential energies gained by the ions, and the use of a reflecting system can partially overcome this drawback.<sup>[304]</sup> The reflecting system consists of an ion mirror with a constant electric field in front. The ions travel to the end of the drift tube, penetrate the electric field, and are reflected by the ion mirror before reaching the detector. Ions with higher energy will penetrate deeper into the electric field and thus take a longer time to arrive at the detector.

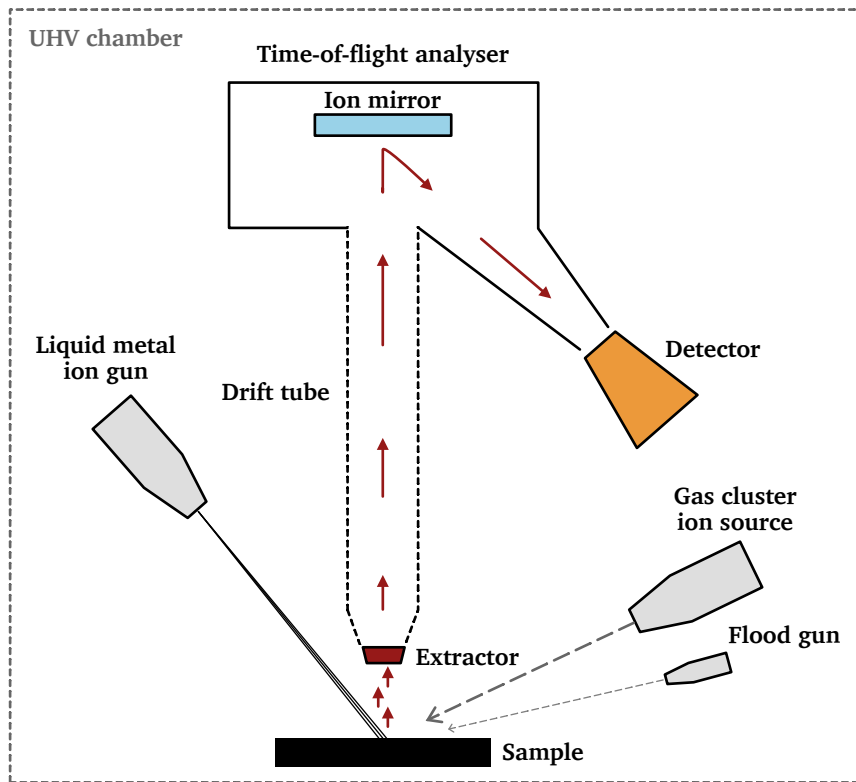


**Figure 20:** Illustration of the core components of ToF-SIMS. <sup>[295]</sup>

### **3 List of publications**

#### **Effect of Perfluorinated Side-Chain Length on the Morphology, Hydrophobicity, and Stability of Xerogel Coatings**

The project was developed by Tuğrul Kaynak with help coming from me. Tuğrul Kaynak, me, Dominik Al-Sabbagh and Christoph A. Schalley wrote the manuscript with main contributions from me. The synthetic work and the CA measurements were carried out by me with help coming from Tuğrul Kaynak. SEM micrographs were taken by Tuğrul Kaynak. Dominik Al-Sabbagh and Franziska Emmerling conducted the sXRD measurements. I assembled and programmed the MEA. All authors contributed to the final version of the manuscript.

#### **Scratch-Resistant Hydrophobic Coating with Supramolecular-Polymer Co-Assembly**

The project was developed by me. Adrian Saura-Sanmartin, me and Christoph A. Schalley wrote the manuscript with main contributions from Adrian Saura-Sanmartin and me. The sample fabrications, CA measurements, SEM micrographs, TGA measurements and the corrosion protection test were carried out by me. Adrian Saura-Sanmartin conducted and evaluated the analyses of ToF-SIMS, FT-IR, elemental analysis and XPS. The oil repellency test and sclerometer test were carried out by Adrian Saura-Sanmartin and me. All authors contributed to the final version of the manuscript.

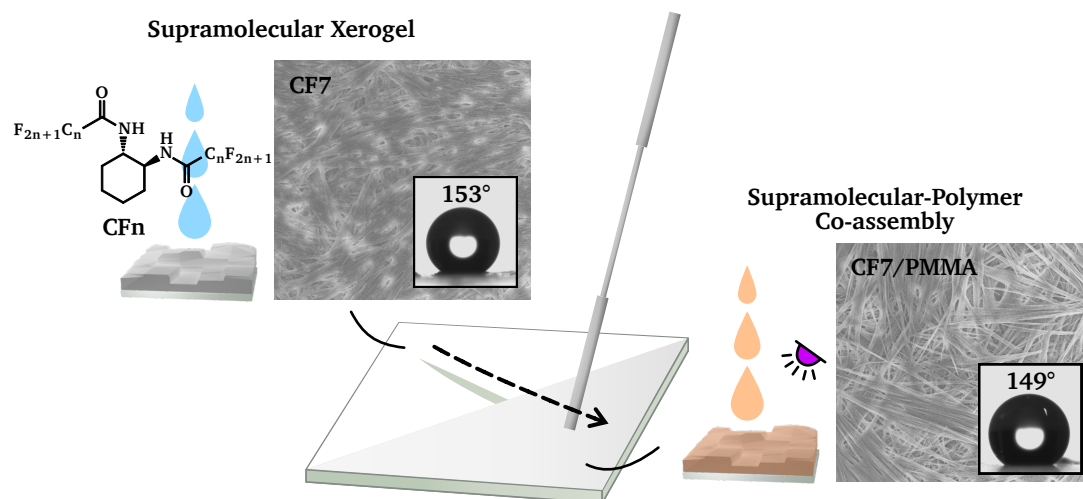


## 4 Summarised results

The overall goal of this work is to develop a simple and easily reproducible method for superhydrophobic coating fabrication by employing supramolecular assemblies. The supramolecular molecules involved in this work are a class of LMWGs with a cyclohexyl-diamide core and two perfluorinated side chains (**CF $n$** ,  $n = 3-10$ ). The first published result of this work focuses on understanding how the length of the perfluorinated side chains can affect the resulting xerogel coating. Firstly, the structural properties of the self-assembled aggregates from the LMWGs were examined with sXRD. It is shown that **CF5** and **CF7** are the least crystalline materials and have relatively smaller particle sizes than others. In SEM micrographs, **CF5** and **CF7** both form fibrous networks while the others self-assembled into scattered aggregates with various dimensions. The trend of the particle size calculated from the diffractogram corresponds to the grain size measured on the micrographs. Xerogel coatings from **CF7** to **CF10** show superhydrophobicity in their pristine state, but only **CF7**, **CF9**, and **CF10** retain high static WCA and low CAH after five rounds of intensive water flushing. In addition, gravimetric studies of the material loss and MEA both show similar conclusions. The first project reveals that the length of the perfluorinated side chains has a definite influence on the characteristics of the xerogel coating, even though a repetitious effect can not be concluded with the current results.

Despite the encouraging results from the first project, the coating mixture still has to be improved for better applicability. The second project was therefore set to explore a more durable, scratch-resistant hydrophobic coating material. A supramolecular xerogel-polymer composite is used. For the xerogel component, **CF7** was chosen as the concept molecule for its superior properties in hydrophobicity, durability and coating uniformity, according to the findings of the first project. MMA was targeted as the primary polymer candidate for its easiness in the curing process and the polymer's outstanding mechanical properties. TFEMA was included as the second candidate in the interest of the additional effect from the extra fluorine components. It is shown that in the composite material, the supramolecular aggregates preserve the fibrous structure in the presence of the polymer, and the distribution of the components is uniform. The iterability and the durability of the coating were tested with repeating water flushing. Moreover, a sclerometer was employed to evaluate the scratch-proofness. The **CF7/PMMA** and **CF7/PTFEMA** co-assemblies turn out to be 50 and 12 times more scratch-resistant than the pristine **CF7** xerogel coating, respectively. The co-assemblies also demonstrate excellent heat

tolerance, frost resistance, oil-repellency and corrosion prevention of copper plates. In conclusion, the supramolecular-polymer composite coatings show significant improvements in the mechanical properties while retaining the water- and oil-repellency, and have been presented with great potential in various applications.





## References

- [1] W. Barthlott, N. Ehler, *Raster-elektronenmikroskopie der Epidermis-oberflächen von Spermato-phyten*, Akad. Wiss. Lit. Mainz, **1977**.
- [2] W. Barthlott, E. Wollenweber, *Zur Feinstruktur; Chemie und taxonomischen Signifikanz epicutic-ularer Wachse und ähnlicher Sekrete*, Akad. Wiss. Lit. Mainz, **1981**.
- [3] W. Barthlott, *Klima-und Umweltforschung an der Universität Bonn*, Rheinische Friedrich-Wilhelms-Universität Bonn, **1992**.
- [4] W. Barthlott, M. Mail, C. Neinhuis, *Phil. Trans. R. Soc.*, **2016**, 374, 20160191.
- [5] W. Barthlott, C. Neinhuis, *Planta*, **1997**, 202, 1–8.
- [6] C. Neinhuis, W. Barthlott, *Ann. Bot.*, **1997**, 79, 667–677.
- [7] J. Bico, U. Thiele, D. Quéré, *Colloids Surf. A: Physicochem. Eng. Asp.*, **2002**, 206, 41–46.
- [8] A. Lafuma, D. Quéré, *Nat. Mater.*, **2003**, 2, 457–460.
- [9] A. Marmur, *Langmuir*, **2003**, 19, 8343–8348.
- [10] N. A. Patankar, *Langmuir*, **2003**, 19, 1249–1253.
- [11] P.-G. Gennes, F. Brochard-Wyart, D. Quéré, et al., *Capillarity and wetting phenomena: drops, bubbles, pearls, waves*, Springer, **2004**.
- [12] A. Marmur, *Soft Matter*, **2006**, 2, 12–17.
- [13] M. Nosonovsky, B. Bhushan, *Microelectron. Eng.*, **2007**, 84, 382–386.
- [14] B. Bhushan, Y. C. Jung, K. Koch, *Phil. Trans. R. Soc.*, **2009**, 367, 1631–1672.
- [15] S. F. Ahmadi, V. Umashankar, Z. Dean, B. Chang, S. Jung, J. B. Boreyko, *ACS Appl. Mater. Interfaces*, **2021**, 13, 27567–27574.
- [16] Y. Liu, X. Chen, J. H. Xin, *Bioinsp. Biomim.*, **2008**, 3, 046007.
- [17] Z. Yoshimitsu, A. Nakajima, T. Watanabe, K. Hashimoto, *Langmuir*, **2002**, 18, 5818–5822.
- [18] N. A. Patankar, *Langmuir*, **2004**, 20, 8209–8213.
- [19] A. Marmur, *Langmuir*, **2004**, 20, 3517–3519.
- [20] K. Koch, B. Bhushan, Y. C. Jung, W. Barthlott, *Soft Matter*, **2009**, 5, 1386–1393.
- [21] Y. Jung, B. Bhushan, *J. Microsc.*, **2008**, 229, 127–140.
- [22] S. S. Latthe, C. Terashima, K. Nakata, A. Fujishima, *Molecules*, **2014**, 19, 4256–4283.
- [23] J.-Y. Shiu, C.-W. Kuo, P. Chen, C.-Y. Mou, *Chem. Mater.*, **2004**, 16, 561–564.
- [24] A. Pozzato, S. Dal Zilio, G. Fois, D. Vendramin, G. Mistura, M. Belotti, Y. Chen, M. Natali, *Microelectron. Eng.*, **2006**, 83, 884–888.
- [25] T. Baldacchini, J. E. Carey, M. Zhou, E. Mazur, *Langmuir*, **2006**, 22, 4917–4919.
- [26] M. Kim, K. Kim, N. Y. Lee, K. Shin, Y. S. Kim, *Chem. Commun.*, **2007**, 2237–2239.
- [27] M. Callies, Y. Chen, F. Marty, A. Pépin, D. Quéré, *Microelectron. Eng.*, **2005**, 78, 100–105.
- [28] Y. Xiu, L. Zhu, D. W. Hess, C. Wong, *Nano Lett.*, **2007**, 7, 3388–3393.
- [29] N. Blondiaux, E. Scolan, A. Popa, J. Gavillet, R. Pugin, *Appl. Surf. Sci.*, **2009**, 256, S46–S53.
- [30] I. Woodward, W. Schofield, V. Roucoules, J. Badyal, *Langmuir*, **2003**, 19, 3432–3438.
- [31] B. Balu, V. Breedveld, D. W. Hess, *Langmuir*, **2008**, 24, 4785–4790.
- [32] A. Milella, R. Di Mundo, F. Palumbo, P. Favia, F. Fracassi, R. d’Agostino, *Plasma Process. Polym.*, **2009**, 6, 460–466.
- [33] D. Schondelmaier, S. Cramm, R. Klingeler, J. Morenzin, C. Zilkens, W. Eberhardt, *Langmuir*, **2002**, 18, 6242–6245.
- [34] E. Hosono, S. Fujihara, I. Honma, H. Zhou, *J. Am. Chem. Soc.*, **2005**, 127, 13458–13459.
- [35] M. Hikita, K. Tanaka, T. Nakamura, T. Kajiyama, A. Takahara, *Langmuir*, **2005**, 21, 7299–7302.
- [36] T. Kamegawa, Y. Shimizu, H. Yamashita, *Adv. Mater.*, **2012**, 24, 3697–3700.

- [37] H. Kim, K. Nam, D. Y. Lee, *Polymers*, **2020**, *12*, 1420.
- [38] Q. Wei, C. Schlaich, S. Prévost, A. Schulz, C. Böttcher, M. Gradzielski, Z. Qi, R. Haag, C. A. Schalley, *Adv. Mater.*, **2014**, *26*, 7358–7364.
- [39] J. Bernstein, R. E. Davis, L. Shimoni, N.-L. Chang, *Angew. Chem. Int. Ed.*, **1995**, *34*, 1555–1573.
- [40] K. Tomioka, T. Sumiyoshi, S. Narui, Y. Nagaoka, A. Iida, Y. Miwa, T. Taga, M. Nakano, T. Handa, *J. Am. Chem. Soc.*, **2001**, *123*, 11817–11818.
- [41] J.-M. Lehn, *Science*, **2002**, *295*, 2400–2403.
- [42] J.-M. Lehn, *Eur. Rev.*, **2009**, *17*, 263–280.
- [43] H.-J. Schneider, *Angew. Chem. Int. Ed.*, **2009**, *48*, 3924–3977.
- [44] T. M. Reed, *Fluorine chemistry*, Elsevier, **1964**, pages 133–236.
- [45] M. P. Krafft, J. G. Riess, *Biochimie*, **1998**, *80*, 489–514.
- [46] J. A. Gladysz, D. P. Curran, I. T. Horváth, *Handbook of fluorine chemistry*, John Wiley & Sons, **2006**.
- [47] M. P. Krafft, J. G. Riess, *Chem. Rev.*, **2009**, *109*, 1714–1792.
- [48] M. De Loos, J. van Esch, I. Stokroos, R. M. Kellogg, B. L. Feringa, *J. Am. Chem. Soc.*, **1997**, *119*, 12675–12676.
- [49] M. Masuda, T. Hanada, K. Yase, T. Shimizu, *Macromolecules*, **1998**, *31*, 9403–9405.
- [50] K. Inoue, Y. Ono, Y. Kanekiyo, K. Hanabusa, S. Shinkai, *Chem. Lett.*, **1999**, *28*, 429–430.
- [51] G. Wang, A. D. Hamilton, *Chem. Eur. J.*, **2002**, *8*, 1954–1961.
- [52] S. H. Kang, B. M. Jung, J. Y. Chang, *Adv. Mater.*, **2007**, *19*, 2780–2784.
- [53] N. Amanokura, Y. Kanekiyo, S. Shinkai, D. N. Reinhoudt, *J. Chem. Soc., Perkin Trans.*, **1999**, 1995–2000.
- [54] K. Hanabusa, Y. Maesaka, M. Suzuki, M. Kimura, H. Shirai, *Chem. Lett.*, **2000**, *29*, 1168–1169.
- [55] J. Sautaux, F. Marx, I. Gunkel, C. Weder, S. Schrettl, *Nat. Commun.*, **2022**, *13*, 356.
- [56] K. Hanabusa, A. Itoh, M. Kimura, H. Shirai, *Chem. Lett.*, **1999**, *28*, 767–768.
- [57] A. E. Way, A. B. Korpusik, T. B. Dorsey, L. E. Buerkle, H. A. Von Recum, S. J. Rowan, *Macromolecules*, **2014**, *47*, 1810–1818.
- [58] E. Fischer, *Stsch. Chem. Ges.*, **1894**, *27*, 2985–2993.
- [59] D. E. Koshland Jr, *Proc. Natl. Acad. Sci. U.S.A.*, **1958**, *44*, 98–104.
- [60] D. E. Koshland Jr, *Angew. Chem. Int. Ed.*, **1995**, *33*, 2375–2378.
- [61] D. J. Cram, *Angew. Chem. Int. Ed.*, **1988**, *27*, 1009–1020.
- [62] J. W. Steed, J. L. Atwood, *Supramolecular chemistry*, John Wiley & Sons, **2022**.
- [63] J.-M. Lehn, *Angew. Chem. Int. Ed.*, **1988**, *27*, 89–112.
- [64] C. J. Pedersen, *Science*, **1988**, *241*, 536–540.
- [65] J.-M. Lehn, *Acc. Chem. Res.*, **1978**, *11*, 49–57.
- [66] D. J. Cram, *Science*, **1983**, *219*, 1177–1183.
- [67] D. J. Cram, S. Karbach, Y. H. Kim, L. Baczynskyj, K. Marti, R. M. Sampson, G. W. Kallemeyn, *J. Am. Chem. Soc.*, **1988**, *110*, 2554–2560.
- [68] A. E. Friedman, J. C. Chambron, J. P. Sauvage, N. J. Turro, J. K. Barton, *Journal of the American Chemical Society*, **1990**, *112*, 4960–4962.
- [69] J. F. Stoddart, *Angew. Chem. Int. Ed.*, **2017**, *56*, 11094.
- [70] B. L. Feringa, *J. Org. Chem.*, **2007**, *72*, 6635–6652.
- [71] L. Brunsveld, B. J. Folmer, E. W. Meijer, R. P. Sijbesma, *Chem. Rev.*, **2001**, *101*, 4071–4098.
- [72] T. Aida, E. Meijer, S. Stupp, *Science*, **2012**, *335*, 813–817.
- [73] H. Fu, J. Huang, J. J. van der Tol, L. Su, Y. Wang, S. Dey, P. Zijlstra, G. Fytas, G. Vantomme, P. Y. Dankers, et al., *Nature*, **2024**, *626*, 1011–1018.

- [74] L. Su, J. Mosquera, M. F. Mabesoone, S. M. Schoenmakers, C. Muller, M. E. Vleugels, S. Dhiman, S. Wijker, A. R. Palmans, E. Meijer, *Science*, **2022**, 377, 213–218.
- [75] T. Ogoshi, Y. Takashima, H. Yamaguchi, A. Harada, *J. Am. Chem. Soc.*, **2007**, 129, 4878–4879.
- [76] S. Matsumoto, S. Yamaguchi, S. Ueno, H. Komatsu, M. Ikeda, K. Ishizuka, Y. Iko, K. V. Tabata, H. Aoki, S. Ito, et al., *Chem. Eur. J.*, **2008**, 14, 3977–3986.
- [77] K. Ariga, T. Kunitake, *Supramolecular chemistry—fundamentals and applications: Advanced textbook*, Springer, **2006**.
- [78] D. Philp, J. F. Stoddart, *Angew. Chem. Int. Ed.*, **1996**, 35, 1154–1196.
- [79] J.-P. Sauvage, C. Dietrich-Buchecker, *Molecular catenanes, rotaxanes and knots: a journey through the world of molecular topology*, John Wiley & Sons, **2008**.
- [80] S. Erbas-Cakmak, D. A. Leigh, C. T. McTernan, A. L. Nussbaumer, *Chem. Rev.*, **2015**, 115, 10081–10206.
- [81] M. Gaedke, H. Hupatz, F. Witte, S. M. Rupf, C. Douglas, H. V. Schröder, L. Fischer, M. Malischewski, B. Paulus, C. A. Schalley, *Organic Chemistry Frontiers*, **2022**, 9, 64–74.
- [82] G. R. Desiraju, *Angew. Chem. Int. Ed.*, **1995**, 34, 2311–2327.
- [83] G. A. Jeffrey, *An introduction to hydrogen bonding*, volume 12, Oxford University Press, **1997**.
- [84] R. P. Sijbesma, E. Meijer, *Curr. Opin. Colloid Interface Sci.*, **1999**, 4, 24–32.
- [85] L. Pauling, *The Nature of the Chemical Bond*, 3<sup>rd</sup> Ed., Cornell University Press, **1960**.
- [86] S. J. Grabowski, *Chem. Rev.*, **2011**, 111, 2597–2625.
- [87] M. Ichikawa, *J. Cryst. Mol. Struct.*, **1979**, 9, 87–105.
- [88] J. Emsley, *Chem. Soc. Rev.*, **1980**, 9, 91–124.
- [89] A. Legon, D. Millen, *Chem. Soc. Rev.*, **1987**, 16, 467–498.
- [90] Y. Gu, T. Kar, S. Scheiner, *J. Am. Chem. Soc.*, **1999**, 121, 9411–9422.
- [91] S. Scheiner, S. J. Grabowski, T. Kar, *J. Phys. Chem. A*, **2001**, 105, 10607–10612.
- [92] S. J. Grabowski, *J. Phys. Chem. A*, **2001**, 105, 10739–10746.
- [93] T. Steiner, *Angew. Chem. Int. Ed.*, **2002**, 41, 48–76.
- [94] S. J. Grabowski, *J. Mol. Struct.*, **2002**, 615, 239–245.
- [95] S. J. Grabowski, *J. Phys. Org. Chem.*, **2004**, 17, 18–31.
- [96] R. M. Bozorth, *J. Am. Chem. Soc.*, **1923**, 45, 2128–2132.
- [97] P. Kebarle, S. K. Searles, A. Zolla, J. Scarborough, M. Arshadi, *J. Am. Chem. Soc.*, **1967**, 89, 6393–6399.
- [98] G. H. Dierksen, W. P. Kraemer, *Chem. Phys. Lett.*, **1970**, 5, 570–572.
- [99] W. D. Kumler, *J. Am. Chem. Soc.*, **1935**, 57, 600–605.
- [100] S. Glasstone, *Trans. Faraday Soc.*, **1937**, 33, 200–206.
- [101] R. Taylor, O. Kennard, *J. Am. Chem. Soc.*, **1982**, 104, 5063–5070.
- [102] G. Desiraju, T. Steiner, *The Weak Hydrogen Bond in Structural Chemistry and Biology*, Oxford University Press, **1999**, pages 29–121.
- [103] E. T. Kool, *Annu. Rev. Biophys. Biomol. Struct.*, **2001**, 30, 1–22.
- [104] D. Leckband, J. N. Israelachvili, *Q. Rev. Biophys.*, **2001**, 34, 105–267.
- [105] S. Horowitz, R. C. Trievel, *J. Biol. Chem.*, **2012**, 287, 41576–41582.
- [106] M. A. Bevan, D. C. Prieve, *Langmuir*, **1999**, 15, 7925–7936.
- [107] A. Buckingham, B. Utting, *Annu. Rev. Phys. Chem.*, **1970**, 21, 287–316.
- [108] J. N. Israelachvili, *Intermolecular and Surface Forces*, Academic Press, **2011**.
- [109] F. London, *Trans. Faraday Soc.*, **1937**, 33, 8b–26.
- [110] J. O. Hirschfelder, C. F. Curtiss, R. B. Bird, *Molecular theory of gases and liquids*, Wiley New York, **1954**.

- [111] J. N. Israelachvili, D. Tabor, *Progress in surface and membrane science*, volume 7, Elsevier, **1973**, pages 1–55.
- [112] H. Margenau, N. R. Kestner, *Theory of Intermolecular Forces: International Series of Monographs in Natural Philosophy*, volume 18, Pergamon Press, **1971**.
- [113] J. Mahanty, B. W. Binham, *Dispersion Forces*, Academic Press, **1976**.
- [114] J. J. Thomson, *Lond. Edinb. Dubl. Phil. Mag. & J. Sci.*, **1914**, 27, 757–789.
- [115] W. H. Keesom, *Koninkl. Akad. van Wetensch.*, **1921**, 23, 943–948.
- [116] P. Debye, *Nobel Lectures, Chem.*, **1922**, 1941, 383–401.
- [117] P. Debye, *Physik. Zeits*, **1935**, 36, 100.
- [118] G. M. Whitesides, B. Grzybowski, *Science*, **2002**, 295, 2418–2421.
- [119] J. D. Halley, D. A. Winkler, *Complexity*, **2008**, 13, 10–15.
- [120] J. D. Halley, D. A. Winkler, *Complexity*, **2008**, 14, 10–17.
- [121] M. Eigen, *Naturwissenschaften*, **1971**, 58, 465–523.
- [122] F. E. Yates, *Self-organizing systems: The emergence of order*, Springer, **1987**.
- [123] D. J. Abdallah, R. G. Weiss, *Adv. Mater.*, **2000**, 12, 1237–1247.
- [124] P. Dastidar, *Chem. Soc. Rev.*, **2008**, 37, 2699–2715.
- [125] P. Flory, *Faraday Discuss. Chem. Soc.*, **1974**, 57, 7–18.
- [126] P. Terech, R. G. Weiss, *Chem. Rev.*, **1997**, 97, 3133–3160.
- [127] K. Hanabusa, M. Suzuki, *Polym. J.*, **2014**, 46, 776–782.
- [128] F. Ilmain, T. Tanaka, E. Kokufuta, *Nature*, **1991**, 349, 400–401.
- [129] J. C. MacDonald, G. M. Whitesides, *Chem. Rev.*, **1994**, 94, 2383–2420.
- [130] Y. Yasuda, Y. Takebe, M. Fukumoto, H. Inada, Y. Shirota, *Adv. Mater.*, **1996**, 8, 740–741.
- [131] R. J. H. Hafkamp, B. P. A. Kokke, I. M. Danke, H. P. M. Geurts, A. E. Rowan, M. C. Feiters, R. J. M. Nolte, *Chem. Commun.*, **1997**, 545–546.
- [132] J. H. van Esch, B. L. Feringa, *Angew. Chem. Int. Ed.*, **2000**, 39, 2263–2266.
- [133] M. George, G. Tan, V. T. John, R. G. Weiss, *Chem. Eur. J.*, **2005**, 11, 3243–3254.
- [134] J. W. Steed, *Chem. Commun.*, **2011**, 47, 1379–1383.
- [135] K. Yabuuchi, E. Marfo-Owusu, T. Kato, *Org. Biomol. Chem.*, **2003**, 1, 3464–3469.
- [136] T. Kato, Y. Hirai, S. Nakaso, M. Moriyama, *Chem. Soc. Rev.*, **2007**, 36, 1857–1867.
- [137] Y. Sasada, R. Ichinoi, K. Oyaizu, H. Nishide, *Chem. of Mater.*, **2017**, 29, 5942–5947.
- [138] K. Hanabusa, M. Yamada, M. Kimura, H. Shirai, *Angew. Chem. Int. Ed. Engl.*, **1996**, 35, 1949–1951.
- [139] T. Kato, T. Kutsuna, K. Hanabusa, M. Ukon, *Adv. Mater.*, **1998**, 10, 606–608.
- [140] J. H. Jung, Y. Ono, S. Shinkai, *Chem. Eur. J.*, **2000**, 6, 4552–4557.
- [141] F. Fages, F. Vögtle, M. Žinic, *Low Molecular Mass Gelator*, Springer, **2005**, pages 77–131.
- [142] N. Zweep, A. Hopkinson, A. Meetsma, W. R. Browne, B. L. Feringa, J. H. van Esch, *Langmuir*, **2009**, 25, 8802–8809.
- [143] H. Sato, T. Nakae, K. Morimoto, K. Tamura, *Org. Biomol. Chem.*, **2012**, 10, 1581–1586.
- [144] T. Yajima, E. Tabuchi, E. Nogami, A. Yamagishi, H. Sato, *RSC Adv.*, **2015**, 5, 80542–80547.
- [145] T. Sasaki, A. Egami, T. Yajima, H. Uekusa, H. Sato, *Cryst. Growth Des.*, **2018**, 18, 4200–4205.
- [146] A. C. Pierre, G. M. Pajonk, *Chem. Rev.*, **2002**, 102, 4243–4266.
- [147] N. Job, A. Théry, R. Pirard, J. Marien, L. Kocon, J.-N. Rouzaud, F. Béguin, J.-P. Pirard, *Carbon*, **2005**, 43, 2481–2494.
- [148] N. Buchtová, T. Budtova, *Cellulose*, **2016**, 23, 2585–2595.
- [149] H. Tamai, K. Shiraki, T. Shiono, H. Yasuda, *J. Colloid Interface Sci.*, **2006**, 295, 299–302.
- [150] H. Gesser, P. Goswami, *Chem. Rev.*, **1989**, 89, 765–788.

- [151] N. Kathuria, A. Tripathi, K. K. Kar, A. Kumar, *Acta Biomater.*, **2009**, *5*, 406–418.
- [152] P. V. Samant, F. Gonçalves, M. M. A. Freitas, M. F. R. Pereira, J. L. Figueiredo, *Carbon*, **2004**, *42*, 1321–1325.
- [153] N. Job, J. Marie, S. Lambert, S. Berthon-Fabry, P. Achard, *Energy Convers. Manag.*, **2008**, *49*, 2461–2470.
- [154] F. H. Dickey, *Proc. Natl. Acad. Sci. U.S.A.*, **1949**, *35*, 227–229.
- [155] R. A. Dunbar, J. D. Jordan, F. V. Bright, *Anal. Chem.*, **1996**, *68*, 604–610.
- [156] C. I. Lin, A. K. Joseph, C. K. Chang, Y. C. Wang, Y. Der Lee, *Anal. Chim. Acta*, **2003**, *481*, 175–180.
- [157] S. Marx, A. Zaltsman, I. Turyan, D. Mandler, *Anal. Chem.*, **2004**, *76*, 120–126.
- [158] J.-K. Hong, H.-S. Yang, M.-H. Jo, H.-H. Park, S.-Y. Choi, *Thin Solid Films*, **1997**, *308*, 495–500.
- [159] B. J. Privett, J. Youn, S. A. Hong, J. Lee, J. Han, J. H. Shin, M. H. Schoenfish, *Langmuir*, **2011**, *27*, 9597–9601.
- [160] T. F. A. de Greef, E. W. Meijer, *Nature*, **2008**, *453*, 171–173.
- [161] T. Kato, J. M. J. Frechet, *J. Am. Chem. Soc.*, **1989**, *111*, 8533–8534.
- [162] T. Aida, A. Takemura, M. Fuse, S. Inoue, *J. Chem. Soc., Chem. Commun.*, **1988**, 391–393.
- [163] Y. Ducharme, J. D. Wuest, *J. Org. Chem.*, **1988**, *53*, 5787–5789.
- [164] J. A. Zerkowski, C. T. Seto, D. A. Wierda, G. M. Whitesides, *J. Am. Chem. Soc.*, **1990**, *112*, 9025–9026.
- [165] T. Aida, E. W. Meijer, *Isr. J. Chem.*, **2020**, *60*, 33–47.
- [166] C. Fouquey, J.-M. Lehn, A.-M. Levelut, *Adv. Mater.*, **1990**, *2*, 254–257.
- [167] C.-M. Lee, C. P. Jariwala, A. C. Griffin, *Polymer*, **1994**, *35*, 4550–4554.
- [168] V. Percec, J. Heck, G. Johansson, D. Tomazos, M. Kawasumi, G. Ungar, *J. Macro. Sci. Pure Appl. Chem.*, **1994**, *31*, 1031–1070.
- [169] R. P. Sijbesma, F. H. Beijer, L. Brunsveld, B. J. B. Folmer, J. Hirschberg, R. F. M. Lange, J. K. L. Lowe, E. W. Meijer, *Science*, **1997**, *278*, 1601–1604.
- [170] B. J. Folmer, R. P. Sijbesma, R. M. Versteegen, J. A. J. van der Rijt, E. W. Meijer, *Adv. Mater.*, **2000**, *12*, 874–878.
- [171] P. Y. W. Dankers, M. C. Harmsen, L. A. Brouwer, M. J. A. Van Luyn, E. W. Meijer, *Nat. Mater.*, **2005**, *4*, 568–574.
- [172] Z. Huang, X. Chen, S. J. O'Neill, G. Wu, D. J. Whitaker, J. Li, J. A. McCune, O. A. Scherman, *Nat. Mater.*, **2022**, *21*, 103–109.
- [173] S. Zhang, A. M. Bellinger, D. L. Gletting, R. Barman, Y.-A. L. Lee, J. Zhu, C. Cleveland, V. A. Montgomery, L. Gu, L. D. Nash, et al., *Nat. Mater.*, **2015**, *14*, 1065–1071.
- [174] P. J. Flory, *Principles of polymer chemistry*, Cornell University Press, **1953**.
- [175] C. E. Carraher Jr, *Seymour/Carraher's polymer chemistry*, volume 16, CRC Press, **2003**.
- [176] L. H. Sperling, *Introduction to physical polymer science*, John Wiley & Sons, **2005**.
- [177] P. C. Hiemenz, T. P. Lodge, *Polymer chemistry*, CRC Press, **2007**.
- [178] N. Nugay, T. Nugay, R. Jérôme, P. Teyssié, *J. Polym. Sci., Part A: Polym. Chem.*, **1997**, *35*, 361–369.
- [179] D. Baskaran, *Prog. Polym. Sci.*, **2003**, *28*, 521–581.
- [180] J.-S. Wang, K. Matyjaszewski, *J. Am. Chem. Soc.*, **1995**, *117*, 5614–5615.
- [181] V. Coessens, T. Pintauer, K. Matyjaszewski, *Prog. Polym. Sci.*, **2001**, *26*, 337–377.
- [182] S. C. Ligon-Auer, M. Schwentenwein, C. Gorsche, J. Stampfl, R. Liska, *Polym. Chem.*, **2016**, *7*, 257–286.
- [183] W. Sweeney, G. Brauer, I. Schoonover, *J. Dent. Res.*, **1955**, *34*, 306–312.

- [184] J. E. Moore, Photocurable acrylate-acrylonitrile polymer-coated plastics, U.S. Patent 4557975, **1985**.
- [185] N. Moszner, U. Salz, *Prog. Polym. Sci.*, **2001**, *26*, 535–576.
- [186] R. Bongiovanni, F. Montefusco, A. Priola, N. Macchioni, S. Lazzeri, L. Sozzi, B. Ameduri, *Prog. Org. Coat.*, **2002**, *45*, 359–363.
- [187] J. Fouassier, X. Allonas, D. Burget, *Prog. Org. Coat.*, **2003**, *47*, 16–36.
- [188] R. Norrish, C. Bamford, *Nature*, **1937**, *140*, 195–196.
- [189] C. Decker, *Prog. Polym. Sci.*, **1996**, *21*, 593–650.
- [190] L. Angiolini, D. Caretti, C. Carlini, E. Corelli, E. Salatelli, *Polymer*, **1999**, *40*, 7197–7207.
- [191] H. Gankema, M. A. Hempenius, M. Möller, *Recl. Trav. Chim. Pays-Bas*, **1994**, *113*, 241–249.
- [192] H. Gankema, M. A. Hempenius, M. Möller, G. Johansson, V. Percec, *Macromol. Symp.*, volume 102, Wiley Online Library, pages 381–390.
- [193] W. Gu, L. Lu, G. B. Chapman, R. G. Weiss, *Chem. Commun.*, **1997**, 543–544.
- [194] R. J. Hafkamp, B. P. Kokke, I. M. Danke, H. P. Geurts, A. E. Rowan, M. C. Feiters, R. J. Nolte, *Chem. Commun.*, **1997**, 545–546.
- [195] G. Tan, M. Singh, J. He, V. T. John, G. L. McPherson, *Langmuir*, **2005**, *21*, 9322–9326.
- [196] M. I. Burguete, F. Galindo, R. Gavara, M. A. Izquierdo, J. C. Lima, S. V. Luis, A. J. Parola, F. Pina, *Langmuir*, **2008**, *24*, 9795–9803.
- [197] J. A. Foster, D. W. Johnson, M.-O. M. Pipenbrock, J. W. Steed, *New J. Chem.*, **2014**, *38*, 927–932.
- [198] H. Kim, J. Y. Chang, *Langmuir*, **2014**, *30*, 13673–13679.
- [199] Y. Ohseido, K. Saruhashi, H. Watanabe, N. Miyamoto, *New J. Chem.*, **2017**, *41*, 9602–9606.
- [200] E. A. Wilder, K. S. Wilson, J. B. Quinn, D. Skrtic, J. M. Antonucci, *Chem. Mater.*, **2005**, *17*, 2946–2952.
- [201] N. Karim, T. D. Jones, K. M. Lewandowski, B. D. Craig, S. B. Mitra, J. Yang, Dental compositions including organogelators, products, and methods, U.S. Patent 8,445,558 B2, **2013**.
- [202] A. Nakajima, K. Hashimoto, T. Watanabe, *Recent studies on super-hydrophobic films*, Springer, **2001**.
- [203] P. Roach, N. J. Shirtcliffe, M. I. Newton, *Soft matter*, **2008**, *4*, 224–240.
- [204] D. Quéré, *Annu. Rev. Mater. Res.*, **2008**, *38*, 71–99.
- [205] X.-M. Li, D. Reinhoudt, M. Crego-Calama, *Chem. Soc. Rev.*, **2007**, *36*, 1350–1368.
- [206] X. Deng, L. Mammen, H.-J. Butt, D. Vollmer, *Science*, **2012**, *335*, 67–70.
- [207] R. N. Wenzel, *Ind. Eng. Chem.*, **1936**, *28*, 988–994.
- [208] A. B. D. Cassie, S. Baxter, *Trans. Faraday Soc.*, **1944**, *40*, 546–551.
- [209] R. E. Johnson Jr, R. H. Dettre, *Contact Angle, Wettability, and Adhesion*, ACS Publications, **1964**.
- [210] F. M. Fowkes, *Ind. Eng. Chem.*, **1964**, *56*, 40–52.
- [211] M. Berry, *Phys. Educ.*, **1971**, *6*, 79–84.
- [212] J. U. Brackbill, D. B. Kothe, C. Zemach, *J. Comput. Phys.*, **1992**, *100*, 335–354.
- [213] N. J. Shirtcliffe, G. McHale, S. Atherton, M. I. Newton, *Adv. Colloid Interface Sci.*, **2010**, *161*, 124–138.
- [214] A. Marchand, J. H. Weijs, J. H. Snoeijer, B. Andreotti, *Am. J. Phys.*, **2011**, *79*, 99–1008.
- [215] G. Galilei, Discourse on Bodies that Stay Atop Water, or Move in It, **1612**.
- [216] J. E. Jones, *Proc. R. Soc. Lond. A*, **1924**, *106*, 441–718.
- [217] J. Yntema, W. Schneider, *J. Chem. Phys.*, **1950**, *18*, 646–650.
- [218] M. Nijmeijer, C. Bruin, A. Bakker, J. Van Leeuwen, *Phys. Rev. A*, **1990**, *42*, 6052.
- [219] J. Indekeu, *Physica A*, **1992**, *183*, 439–461.
- [220] J. H. Weijs, A. Marchand, B. Andreotti, D. Lohse, J. H. Snoeijer, *Phys. Fluids*, **2011**, *23*.
- [221] R. Evans, *Adv. Phys.*, **1979**, *28*, 143–200.

- [222] N. K. Adam, *Nature*, **1957**, *180*, 809–810.
- [223] W. Tyson, W. Miller, *Surf. Sci.*, **1977**, *62*, 267–276.
- [224] T. Young, *Phil. Trans. R. Soc.*, **1805**, *95*, 65–87.
- [225] D. Bangham, R. Razouk, *Trans. Faraday Soc.*, **1937**, *33*, 1459–1463.
- [226] D. Sullivan, *J. Chem. Phys.*, **1981**, *74*, 2604–2615.
- [227] L. Leger, J. Joanny, *Rep. Prog. Phys.*, **1992**, *55*, 431.
- [228] P.-G. De Gennes, *Rev. Mod. Phys.*, **1985**, *57*, 827.
- [229] A. Tuteja, W. Choi, M. Ma, J. M. Mabry, S. A. Mazzella, G. C. Rutledge, G. H. McKinley, R. E. Cohen, *Science*, **2007**, *318*, 1618–1622.
- [230] F. Bashforth, J. C. Adams, *An attempt to test the theories of capillary action by comparing the theoretical and measured forms of drops of fluid*, Cambridge University Press, **1883**.
- [231] I. Jimbo, A. W. Cramb, *ISIJ international*, **1992**, *32*, 26–35.
- [232] H. Fujii, H. Nakae, *Phil. Mag. A*, **1995**, *72*, 1505–1512.
- [233] J. N. Butler, B. H. Bloom, *Surf. Sci.*, **1966**, *4*, 1–17.
- [234] C. Maze, G. Burnet, *Surf. Sci.*, **1969**, *13*, 451–470.
- [235] Y. Rotenberg, L. Boruvka, A. Neumann, *J. Colloid Interface Sci.*, **1983**, *93*, 169–183.
- [236] W. Gander, G. H. Golub, R. Strebel, *BIT Numer. Math.*, **1994**, *34*, 558–578.
- [237] A. Fitzgibbon, M. Pilu, R. B. Fisher, *IEEE Trans. Pattern Anal. Mach. Intell.*, **1999**, *21*, 476–480.
- [238] N. K. Adam, *The physics and chemistry of surfaces*, Oxford University Press, **1930**.
- [239] P. S. Laplace, *Traité De Mécanique Céleste: Supplément au dixième livre du traité de mécanique céleste sur l'action capillaire*, volume 6, Duprat, **1808**.
- [240] L. M. Siqueland, S. M. Skjæveland, *Capillarity*, **2021**.
- [241] A. F. Stalder, T. Melchior, M. Müller, D. Sage, T. Blu, M. Unser, *Colloids Surf. A Physicochem. Eng. Asp.*, **2010**, *364*, 72–81.
- [242] G. Saville, *J. Chem. Soc. Faraday Trans. 2*, **1977**, *73*, 1122–1132.
- [243] G. Jameson, M. Del Cerro, *J. Chem. Soc. Faraday Trans. 1*, **1976**, *72*, 883–895.
- [244] R. Shuttleworth, G. Bailey, *Disc. Faraday Soc.*, **1948**, *3*, 16–22.
- [245] J. Z. Tang, J. G. Harris, *J. Chem. Phys.*, **1995**, *103*, 8201–8208.
- [246] M. Yamabe, *Organofluorine chemistry: principles and commercial applications*, Springer, **1994**, pages 397–401.
- [247] R. N. Wenzel, *J. Phys. Chem.*, **1949**, *53*, 1466–1467.
- [248] C. Huh, S. Mason, *J. Colloid Interface Sci.*, **1977**, *60*, 11–38.
- [249] A. B. D. Cassie, *Disc. Faraday Soc.*, **1948**, *3*, 11–16.
- [250] L. Gao, T. J. McCarthy, *Langmuir*, **2006**, *22*, 6234–6237.
- [251] D. C. Pease, *J. Phys. Chem.*, **1945**, *49*, 107–110.
- [252] R. J. Good, *J. Am. Chem. Soc.*, **1952**, *74*, 5041–5042.
- [253] R. E. Johnson Jr, R. H. Dettre, *Contact Angle, Wettability, and Adhesion*, ACS Publications, **1964**.
- [254] R. J. Good, *J. Adhesion Sci. Technol.*, **1992**, *6*, 1269–1302.
- [255] R. E. Johnson Jr, R. H. Dettre, D. A. Brandreth, *J. Colloid Interface Sci.*, **1977**, *62*, 205–212.
- [256] A. Dupré, P. Dupré, *Théorie mécanique de la chaleur*, Gauthier-Villars, **1869**.
- [257] N. K. Adam, G. Jessop, *J. Chem. Soc. Trans.*, **1925**, *127*, 1863–1868.
- [258] W. D. Harkins, H. Livingston, *J. Chem. Phys.*, **1942**, *10*, 342–356.
- [259] M. E. Schrader, *Langmuir*, **1995**, *11*, 3585–3589.
- [260] I. T. Horváth, J. Rábai, *Science*, **1994**, *266*, 72–75.
- [261] J. G. Riess, *Tetrahedron*, **2002**, *58*, 4113–4131.
- [262] A. Bondi, *J. Phys. Chem.*, **1964**, *68*, 441–451.

- [263] G. Tiddy, *Modern Trends of Colloid Science in Chemistry and Biology*, Birkhäuser, **1985**.
- [264] H. Hoffmann, J. Kalus, H. Thurn, *Colloid Polym. Sci.*, **1983**, *261*, 1043–1049.
- [265] C. Bunn, E. Howells, *Nature*, **1954**, *174*, 549–551.
- [266] J. G. Riess, *Colloids Surf. A: Physicochem. Eng. Asp.*, **1994**, *84*, 33–48.
- [267] H. W. Dodgen, W. Libby, *J. Chem. Phys.*, **1949**, *17*, 951–957.
- [268] J. Goldstein, *Practical scanning electron microscopy: electron and ion microprobe analysis*, Springer Science & Business Media, **2012**.
- [269] J. Goldstein, D. Newbury, J. Michael, N. Ritchie, J. Scott, D. Joy, *Scanning electron microscopy and X-ray microanalysis*, Springer, **2017**.
- [270] A. Bogner, P.-H. Jouneau, G. Thollet, D. Basset, C. Gauthier, *Micron*, **2007**, *38*, 390–401.
- [271] H. Seiler, *J. Appl. Phys.*, **1983**, *54*, R1–R18.
- [272] K. L. Scrivener, *Cem. Concr. Compos.*, **2004**, *26*, 935–945.
- [273] H. Busch, *Ann. Phys.*, **1926**, *386*, 974–993.
- [274] L. De Broglie, *Nature*, **1923**, *112*, 540–540.
- [275] L. De Broglie, *Nobel Lecture*, **1929**, *12*, 244–256.
- [276] M. Knoll, E. Ruska, *Physik. Zeits.*, **1932**, *78*, 318–339.
- [277] V. K. Zworykin, *Sci. Am.*, **1942**, *167*, 111–113.
- [278] C. W. Oatley, *J. Appl. Phys.*, **1982**, *53*, R1–R13.
- [279] T. E. Everhart, R. Thornley, *J. Sci. Instr.*, **1960**, *37*, 246.
- [280] R. Pease, W. Nixon, *J. Sci. Instr.*, **1965**, *42*, 81.
- [281] B. J. Inkson, *Materials characterization using nondestructive evaluation (NDE) methods*, Elsevier, **2016**, pages 17–43.
- [282] I. Robinson, D. Tweet, *Rep. Prog. Phys.*, **1992**, *55*, 599.
- [283] W. Friedrich, P. Knipping, M. Laue, *Ann. Phys.*, **1913**, *346*, 971–988.
- [284] W. L. Bragg, *Proc. R. Soc. Lond. A*, **1913**, *89*, 248–277.
- [285] J. A. Bearden, *Rev. Mod. Phys.*, **1967**, *39*, 78.
- [286] B. Warren, *J. Appl. Phys.*, **1941**, *12*, 375–384.
- [287] R. Feidenhans, *Surface Science Reports*, **1989**, *10*, 105–188.
- [288] A. Guinier, *X-ray diffraction in crystals, imperfect crystals, and amorphous bodies*, Courier Corporation, **1994**.
- [289] A. Patterson, *Phys. Rev.*, **1939**, *56*, 978.
- [290] İ. Uzun, *J. Polym. Res.*, **2023**, *30*, 394.
- [291] H. Kilian, E. Jenckel, *Kolloid Zeits.*, **1959**, *165*, 25–31.
- [292] X-RAY DIFFRACTION (XRD) - D8 ADVANCE, <https://www.bruker.com/en/products-and-solutions/diffractometers-and-x-ray-microscopes/x-ray-diffractometers/d8-advance-family/d8-advance.html>.
- [293] A. Benninghoven, *Phys. Stat. Sol.*, **1969**, *34*, K169–K171.
- [294] A. Benninghoven, *Angew. Chem. Int. Ed.*, **1994**, *33*, 1023–1043.
- [295] TOF-SIMS Technique, <https://www.iontof.com/tof-sims-secondary-ion-mass-spectrometry.html>.
- [296] S. Ninomiya, K. Ichiki, H. Yamada, Y. Nakata, T. Seki, T. Aoki, J. Matsuo, *Rapid Commun. Mass Spectrom.*, **2009**, *23*, 1601–1606.
- [297] J. J. Thomson, *Lond. Edinb. Dubl. Phil. Mag. & J. Sci.*, **1897**, *44*, 293–316.
- [298] J. J. Thomson, *Lond. Edinb. Dubl. Phil. Mag. & J. Sci.*, **1910**, *20*, 752–767.
- [299] R. Herzog, F. Viehböck, *Phys. Rev.*, **1949**, *76*, 855.
- [300] P. Steffens, E. Niehuis, T. Friese, D. Greifendorf, A. Benninghoven, *J. Vac. Sci. Technol. A*, **1985**, *3*, 1322–1325.
- [301] W. Huber, H. Selhofer, A. Benninghoven, *J. Vac. Sci. Technol.*, **1972**, *9*, 482–486.



- [302] R. Chûcê, T. Nishi, Y. Sumi, T. Adachi, H. Naito, H. Frenzel, *J. Polym. Sci. Polym. Lett. Ed.*, **1983**, *21*, 487–494.
- [303] I. V. Chernushevich, A. V. Loboda, B. A. Thomson, *J. Mass. Spectrom.*, **2001**, *36*, 849–865.
- [304] B. Mamyrin, V. Karataev, D. Shmikk, V. Zagulin, *Zh. Eksp. Teor. Fiz.*, **1973**, *64*, 82–89.



The article

Effect of Perfluorinated Side-Chain Length on the Morphology, Hydrophobicity, and Stability of Xerogel Coatings

Pin-Wei Lee, Tuğrul Kaynak, Dominik Al-Sabbagh, Franziska Emmerling, and Christoph A.

Schalley. *Langmuir*, **2021**, *37*, 14390–14397

<http://doi.org/10.1021/acs.langmuir.1c02341>

has been removed due to copyright and can be accessed via the DOI link provided.

The article

Scratch-Resistant Hydrophobic Coating with Supramolecular-Polymer Co-Assembly

Pin-Wei Lee, Adrian Saura-Sanmartin, Christoph A. Schalley

*Adv. Funct. Mater.*, **2024**, *34*, 2309140

<http://doi.org/10.1002/adfm.202309140>

is an open access article under the terms of the Creative Commons Attribution-NonCommercial License, which permits use, distribution and reproduction in any medium, provided the original work is properly cited and is not used for commercial purposes.



# Scratch-Resistant Hydrophobic Coating with Supramolecular-Polymer Co-Assembly

Pin-Wei Lee, Adrian Saura-Sanmartin, and Christoph A. Schalley\*

Supramolecular assembly for superhydrophobic coatings is known for its efficiency and efficacy. However, the mechanical fragility of the coatings limits their use as coating materials. Herein, the combination of ( $\pm$ )-*N,N'*-(*trans*-cyclohexane-1,2-diyl)-bis(perfluorooctanamide) CF7, a cyclohexyl diamide-based low molecular weight gelator, with acrylate polymers for the generation of semi-transparent omniphobic coatings with significantly enhanced scratch proofness is presented. CF7 has shown the ability to self-assemble in common solvents into highly entangled fibrous networks with extreme water repellency. The incorporation of covalent polymers, specifically poly(methyl methacrylate) (PMMA) and poly(trifluoroethyl methacrylate) (PTFEMA), helps to fixate the supramolecular CF7 fibers without interfering with the self-assembled structures. The resulting coatings, namely CF7/PMMA and CF7/PTFEMA, show significantly improved mechanical resistance as well as optical transparency while maintaining excellent water and oil repellency. Furthermore, the homogeneity of the coating in bulk is confirmed by depth profiling of the 3D distribution of the components using time-of-flight secondary ion mass spectrometry imaging, which turns out to be an essential technique in order to characterize such materials.

different applications in catalysis,<sup>[9–11]</sup> bioengineering,<sup>[12–16]</sup> and materials science,<sup>[17–19]</sup> among others, due to the tailorable properties and functions that can be obtained through a rational design.

The use of LMWGs as coating materials offers advantages, such as low cost, short curing time, and scalability. However, one major disadvantage of LMWGs is their mechanical fragility. Thus, applications where the coating needs to withstand mechanical stress or abrasion are limited by this drawback. To overcome this limitation, researchers have tried to change the design of the gelator and equipped it with polymerizable groups like acrylic esters, acrylic amides and diacetylene,<sup>[20–23]</sup> used metal coordination,<sup>[24,25]</sup> or added commercially available polymers.<sup>[26,27]</sup>

Polymer coatings, on the other hand, are highly resistant to abrasion. Excellent mechanical properties make them an attractive alternative to LMWG coatings, especially in applications where durability is a critical factor. One of the primary

drawbacks of polymer coatings is that they usually have moderate water repellency compared to LMWG coatings, although some exceptions of functionalized polymer coatings have been reported with high water contact angles and low sliding angles.<sup>[28,29]</sup> Creating surface roughness on the polymers is one of the most popular solutions to enhance the hydrophobicity, but often involves nanoparticles<sup>[30–32]</sup> or requires elaborate protocols like lithography, chemical etching, or plasma treatment.<sup>[33–38]</sup>


In our previous study of superhydrophobic xerogel coatings made from ( $\pm$ )-*N,N'*-(*trans*-cyclohexane-1,2-diyl)-bis(perfluorooctanamide) (CF7),<sup>[39–41]</sup> we found the coating to be quite resistant to intense water flows, since after five cycles of flushing 4 L of deionized water to the xerogel over a minute, the water contact angle (WCA) values hardly decreased (from  $153^\circ \pm 3^\circ$  to  $150^\circ \pm 6^\circ$ ). However, gravimetric analyses indicated a loss of around 13% of the deposited material after these five flushing cycles. Therefore, we decided to conduct further studies toward the preparation of more resistant materials. En route to prepare such improved coatings, the deposition of our CF7-based xerogel coatings together with a stabilizing covalent polymer should provide materials with improved iterability and longer lifespans, which is essential to waterproof materials that need

## 1. Introduction

Low molecular weight gelators (LMWGs) are materials of great interest due to their versatility and ease of fabrication.<sup>[1–8]</sup> Furthermore, these materials are postulated as ideal scaffolds for

P.-W. Lee, A. Saura-Sanmartin, C. A. Schalley  
Institut für Chemie und Biochemie  
Freie Universität Berlin  
Arnimallee 20, 14195 Berlin, Germany  
E-mail: c.schalley@fu-berlin.de

A. Saura-Sanmartin  
Departamento de Química Orgánica  
Facultad de Química  
Campus de Espinardo  
Universidad de Murcia  
Murcia 30100, Spain

 The ORCID identification number(s) for the author(s) of this article can be found under <https://doi.org/10.1002/adfm.202309140>

© 2023 The Authors. Advanced Functional Materials published by Wiley-VCH GmbH. This is an open access article under the terms of the Creative Commons Attribution-NonCommercial License, which permits use, distribution and reproduction in any medium, provided the original work is properly cited and is not used for commercial purposes.

DOI: 10.1002/adfm.202309140

to be exposed to more abrasive conditions. In 1996, Gankema et al. demonstrated the first example of embedding xerogel networks inside a polymer matrix.<sup>[42]</sup> Monomers and crosslinking reagents that are UV curable are used as solvents in the organogel system to create the aggregates-embedded resin. The aggregates can be later removed to provide nanostructured porous polymeric materials.<sup>[43–45]</sup> The groups of Stupp,<sup>[46,47]</sup> Kostopoulos,<sup>[48]</sup> and Korley<sup>[49]</sup> have reported the toughening of polymers using supramolecular polymers or gels. In addition, the composition of organogelators and polymerizable components used particularly in dental composite to reduce shrinkage and/or to improve mechanical properties have been reported.<sup>[50,51]</sup> However, to the best of our knowledge, no examples of fixating a xerogel network with polymers for a more durable hydrophobic coating have been reported.

Here, we report the combination of polymers and LMWG in superhydrophobic coatings with improved mechanical stability. Acrylate monomers are considered for their availability, variety, and the ease of curing. Simple acrylate monomers, like methyl acrylate and methyl methacrylate (MMA), are very common in industrial applications. One of the most appealing features about these monomers is that they can undergo photopolymerization without complicated setup. The fabrication can be done with low power bench-top UV chambers and can be scaled up easily. Although a decrease in the value of WCAs is expected, a significant enhancement of the mechanical resistance is envisioned due to the robustness provided by the polymeric matrix. For this work, MMA was chosen for the polymer's exceptional mechanical properties and low cost. In addition, trifluoroethyl methacrylate (TFEMA) was included in order to investigate the effect of a fluorine-containing monomer in the mixture with fluorinated gelators. The microstructure of the supramolecular-polymer co-assembly was examined with scanning electron microscopy (SEM). X-Ray photoelectron spectroscopy (XPS) was used to characterize the outer surface of the coatings. Furthermore, imaging and depth profiling with time-of-flight secondary ion mass spectrometry (ToF-SIMS) were used to investigate the uniformity of the co-assembly coating. The iterability of the coating was tested by repeating water flushing.

## 2. Results and Discussion

### 2.1. Coating Characterization

The supramolecular-polymer coatings, namely CF7/PMMA and CF7/PTFEMA, are prepared by mixing the corresponding monomer with the organogel of CF7,<sup>[39]</sup> treating the mixture with UVA for a short time, and then applying the mixture to the substrate before final curing. In order to achieve homogeneity of the coating, the irradiation time before drop casting is crucial. Insufficient time will lead to phase separation between the organogel and the monomer/polymer phase, while excessive time will cause the mixture to be overly viscous, resulting in considerably thick filaments in the co-assembly that reduce surface roughness. This irradiation time will differ between the choice of monomer, the photoinitiator, and its concentration.

The morphology of CF7/PMMA and CF7/PTFEMA coatings was examined by SEM, showing that both materials retain the fibrous network obtained from the pristine CF7 xerogels throughout the surface (Figure 1). Consequently, the presence of the monomer did not disturb the formation of the fibrous network of CF7. Moreover, the presence of fluorine on the outer surface of both co-assemblies was confirmed with XPS analysis (see Supporting Information).

The uniform distribution of CF7 and PMMA or PTFEMA throughout the surface of the coatings was confirmed by the reconstruction of the 3D distribution of CF7/PMMA and CF7/PTFEMA coating samples using ToF-SIMS. While sputtering using a 5 keV Ar<sub>2000</sub><sup>+</sup> cluster ion beam allowed to record the spectrometric data of the CF7 coating, both co-assemblies required to increase the energy of the cluster ion beam to 20 keV in order to carry out such analysis. This observation already indicates a higher coating robustness caused by the presence of a polymeric matrix in the xerogel coatings. ToF-SIMS imaging together with depth profiling suggest a thin layer of material in the pristine CF7 xerogel coating (Figure 2a), while the thickness increases in those samples having polymers (Figure 2b,c). Ions with *m/z* value of 906.04 attributed to CF7 were detected in all the samples (see Figures S1–S3, Supporting Information). Additional ions having *m/z* values of  $n * 100.05$  and  $n * 154.02$  (where  $n = 1, 2, 3, 4, 5, \dots$ ) for different fragments of PMMA and PTFEMA, respectively, were also detected throughout the CF7/PMMA and CF7/PTFEMA coatings (see Figures S2 and S3, Supporting Information), thus confirming the desired uniform distribution which would result in the envisioned hydrophobic properties and high mechanical resistance.

Fourier transform infrared (FT-IR) analyses shows shifts of several PMMA and PTFEMA bands for the CF7/PMMA and CF7/PTFEMA coatings (see Figures S4–S8, Supporting Information), highlighting those related to sp<sup>3</sup> C-H and ester C=O stretching. The amide C=O stretching band of CF7 also experiences a shifting in both co-assemblies, thus suggesting interactions between the components of the aggregates.

### 2.2. Contact Angles

The hydrophobicity of the coatings was tested by the measurement of the WCAs. As above mentioned, coatings made from CF7-based xerogels turned out to be superhydrophobic, showing a WCA of  $153^\circ \pm 3^\circ$  (Table 1, entry 1). The coatings of the co-assemblies show slight decreases in the WCA values as expected, due to the homogeneous distribution of polymer and CF7, which leads to a smaller fluorinated surface area. Thus, the WCA decreases by 2.6% (WCA  $149^\circ$ ) in the CF7/PMMA coating (Table 1, entry 2) and by 9.8% (WCA  $138^\circ$ ) in the CF7/PTFEMA coating (Table 1, entry 3). This difference between both polymer-bearing coatings can be attributed to the distinct morphology of the surfaces. Possible nanostructures are visible in the CF7/PMMA co-assembly (see Figure S9, Supporting Information), while they are not found in the CF7/PTFEMA co-assembly. These nanostructures could lead to an enhancement in the WCAs of CF7/PMMA. The obtained results show that the use of polymeric precursors in the preparation of the xerogel coatings can still well retain the hydrophobic properties of the materials. Nevertheless, both

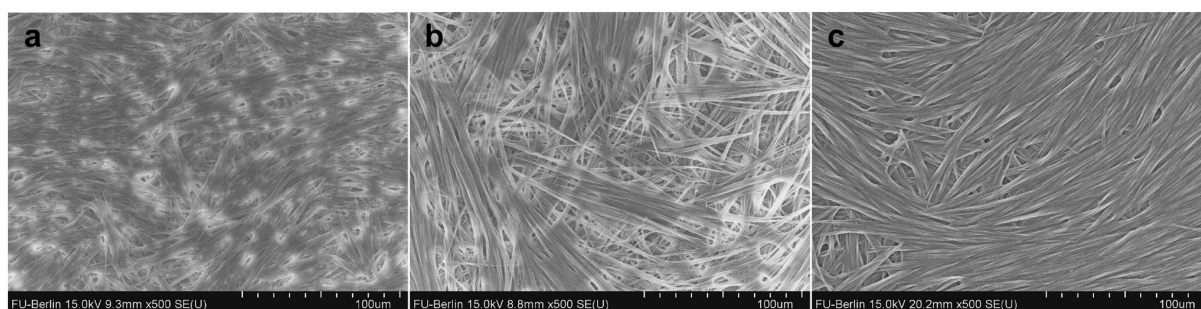


**Figure 1.** SEM images of the coatings of a) CF7 xerogel (reprinted with permission from Lee et al.<sup>[39]</sup>, Copyright 2021 American Chemical Society.), b) CF7/PMMA co-assembly, and c) CF7/PTFEMA co-assembly.

co-assemblies show drastic increases in hydrophobicity and oleophobicity compared to the polymer coatings without the fluorinated gelator (Table 1, entries 4 and 5).

Yang et al. prepared a lignin-based hydrophobic xerogel with WCA of  $146^\circ$ .<sup>[52]</sup> The xerogel film made from organosiloxanes by Shang et al. have WCAs up to  $105^\circ$ .<sup>[53]</sup> Storm et al. reported a *N*-diazoniumdiolate-modified xerogel film with WCA of  $103^\circ$ , which can be increased to  $157^\circ$  by adding nanoparticles to the coating.<sup>[54]</sup> The xerogel coatings reported in this work show similar or superior hydrophobicity and, additionally, an enhanced mechanical strength without the need for further modification.

### 2.3. Iterability and Durability

Aiming to fabricate coatings with improved mechanical properties, we evaluated the stabilities of the polymer-infused coating from several aspects. An enhanced mechanical stability of CF7/PMMA and CF7/PTFEMA coatings was obtained compared to that of pristine CF7 xerogel coatings as determined by gravimetric analyses of the material loss after five water flushing cycles (Table 1 and Table S1, Supporting Information). Indeed, the presence of polymers in the coatings turns out to be

an important factor that substantially increases the mechanical stability of the materials, while maintaining their hydrophobic properties. Although the data included in this text refer to the weight percent of the material, elemental analyses of the coatings before and after water flushings suggest that these data are analogous to those referring only to weight percent of the gelator (see Table S2, Supporting Information). Thus, while the pristine CF7 coating lost 13% of mass of the material after five water flushing cycles, these values were significantly reduced to 3.7% and 3.5% for CF7/PMMA and CF7/PTFEMA coatings, respectively (Figure 3a,b). The WCA has dropped to  $142^\circ \pm 3^\circ$  for the CF7/PMMA coating, and  $135^\circ \pm 6^\circ$  for the CF7/PTFEMA coating (Figure 3c,d). These values suggest that the mechanical stability of the coatings having polymers is enhanced to almost 400% compared to that of the CF7 xerogel coating, thus compensating for the slight decrease in WCAs when coatings having improved reusability and iterability are required.

The thermal stabilities of CF7/PMMA and CF7/PTFEMA coatings were evaluated by using thermogravimetric analysis (TGA) under nitrogen stream (see Experimental Section). Pristine CF7 and the polymers were also tested as control measurements. TGA plots show analogous thermal stabilities of

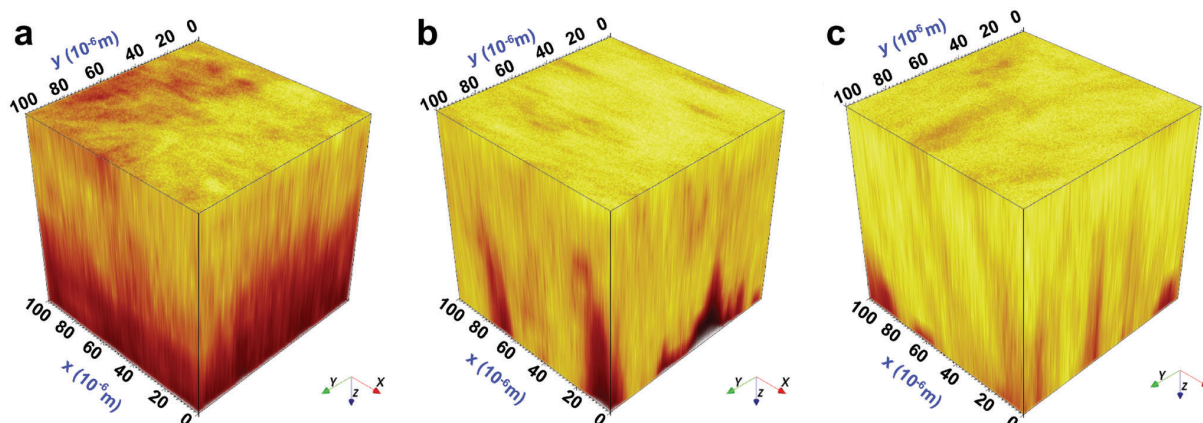


**Figure 2.** ToF-SIMS 3D imaging of a) CF7 xerogel, b) CF7/PMMA co-assembly, and c) CF7/PTFEMA co-assembly. Color key: yellow = CF7 or CF7-based co-assemblies; brown = glass support.



**Table 1.** Characterizations of the pristine and five-times-flushed coatings.

Entry	Coating	WCA	DCA	WCA (flushed)	Material removal (flushed) [wt%]
1	CF7 <sup>[39]</sup>	153° ± 3°	147° ± 3°	150° ± 6°	13
2	CF7/PMMA	149° ± 3°	85° ± 6°	142° ± 3°	3.7
3	CF7/PTFEMA	138° ± 4°	84° ± 2°	135° ± 6°	3.5
4	PMMA	50° ± 1°	25° ± 3°	–	–
5	PTFEMA	101° ± 3°	76° ± 3°	–	–

the pristine materials and the coatings made from the mixtures, revealing that all the samples exhibit a high thermostability upon heating to above 150°C (see Figure S10, Supporting Information).

In addition to high temperature resistance, the coatings also showed excellent frost resistance. After five cycles of freezing/defrosting, the WCAs of CF7/PMMA and CF7/PTFEMA coatings remain in the same range of the pristine materials (Figure 3e,f). These measurements together with the TGA reveal a high stability of the coatings against drastic changes in temperature.

For real-life applications, the coating can be damaged by unavoidable scratching during the process of transportation or usage. Therefore, we simulated the situation by performing scratches using a sclerometer. This test shows that the co-assemblies have a significantly higher scratch resistance. CF7 coating is completely removed when scratching using the sclerometer with a preset force of 0.05 N, as can be observed with the eye (Figure 4a). In stark contrast, only a residual trace of the path of the tip of the sclerometer is shown in the optical micrographs of CF7/PMMA and CF7/PTFEMA with the above-mentioned preset force. The scratching test was repeated by increasing the force in the intervals of 0.05 N, observing that CF7/PMMA coating is partially removed at 2.5 N and completely removed at 2.7 N. In the case of CF7/PTFEMA co-assembly, these numbers decrease to 0.6 N and 0.7 N, respectively (see Figures S11 and S12, Supporting Information). Consequently, the scratch resistance is improved by a factor of 50 for CF7/PMMA and a factor of 12 for CF7/PTFEMA, compared to that of CF7 coating. Thus, the preparation of the supramolecular-polymer co-assemblies turns out to be an effective strategy toward the improvement of the mechanical stability of the coatings, affording materials having scratch resistance properties.

#### 2.4. Practical Implementations

We further evaluate the strength-improved hydrophobic coatings with several applications. One of the typical applications for polymer films is to prevent corrosion of the material underneath.<sup>[55–57]</sup> The co-assemblies were coated on piranha-washed copper plates, then stored in 30 mL of deionised water for 7 days. After the time period, the sample was dried and the polymeric coating was removed to expose the copper surface underneath. An uncoated copper plate was used as a control. The uncoated copper plate shows significant color change due to corrosion, while the coated samples preserve the shiny

surface (Figure 4b), indicating that the co-assembly successfully functioned in corrosion prevention.

Moreover, the oleophobicity of the coatings was evaluated by dropping 100 µL of silicon oil colored with ≈2 wt% of green marker ink on the coated samples. On non-coated glass cover slips, the oil wetted the entire traveled surface. In contrast, the major fraction of the deposited oil rolled off the surface of CF7/PMMA and CF7/PTFEMA coatings, while the residue appears to be in a beaded shape or has left a much narrower trace than on the glass (Figure 4c).

### 3. Conclusion

While LMWGs are an easy-to-handle material for many applications, their mechanical fragility limits the potential as a coating material. The combination of LMWG with polymers can overcome this limitation and results in the development of tough and water-repellent coatings that have a broad range of applications, including industrial and biomedical applications. In our work, we have demonstrated how the formation of co-assembled coatings from CF7 xerogels and PTFEMA or PMMA can be applied to obtain enhanced mechanical stability of the coatings. These materials were characterized using different techniques, including ToF-SIMS which allow to unambiguously confirm the uniform distribution of the polymer and the gelator in the coatings.

Interestingly, the iterability of these materials has been improved to almost 400% as a means of the water flushing resistance while retaining the hydrophobicity. Additionally, the CF7/PMMA and CF7/PTFEMA co-assemblies turn out to be significantly more scratch resistant compared to the pristine CF7 coating. Properties of the resulting coating can be fine-tuned through the choice of the components. Future research should be focused on the combination of different LMWGs and polymers toward the preparation of co-assembled coatings having both superhydrophobicity and high mechanical and scratch resistance.

### 4. Experimental Section

**Materials:** All reagents were purchased from either abcr, Acros Organics, Apollo Scientific, Sigma-Aldrich/Merck, TCI, or VWR Chemicals. Reagents except the acrylate monomers were used directly without purification. The acrylate monomers were distilled under reduced pressure to remove the inhibitors. Menzel glass coverslips (22 mm × 22 mm × 13–16 mm) were purchased from VWR. Copper plates were acquired from the mechanic workshop of Institut für Chemie und Biochemie, Freie Universität Berlin. Both glass cover slips and copper plates were cleaned with freshly prepared piranha solution, followed by rinsing with Milli-Q water and acetone.

**Sample Preparation:** The organogel was prepared by dissolving 10 mg of CF7 in the corresponding amount of diethyl ether (Table 2) and sonicating for 10 min. Then the corresponding amount of monomer (with 0.5 wt% of 2,2-dimethoxy-2-phenyl-acetophenone) was added to the organogel and the mixture was sonicated for another 10 min. Afterward, 5.6 µL of triethylamine was added to the mixture, and the mixture was irradiated with UVA for 20 min while stirring vigorously. 0.40 mL of the mixture was then drop-casted on a piranha-cleaned substrate, followed by UVA irradiation until dried. The coatings were further dried in a vacuum chamber overnight before any measurements or tests.

**X-Ray Photoelectron Spectroscopy:** XPS analysis was carried out using a SPECS EnviroESCA instrument with an excitation energy of 1486.71 eV, a detector voltage of 1650 V, and a bias voltage of 100 V.



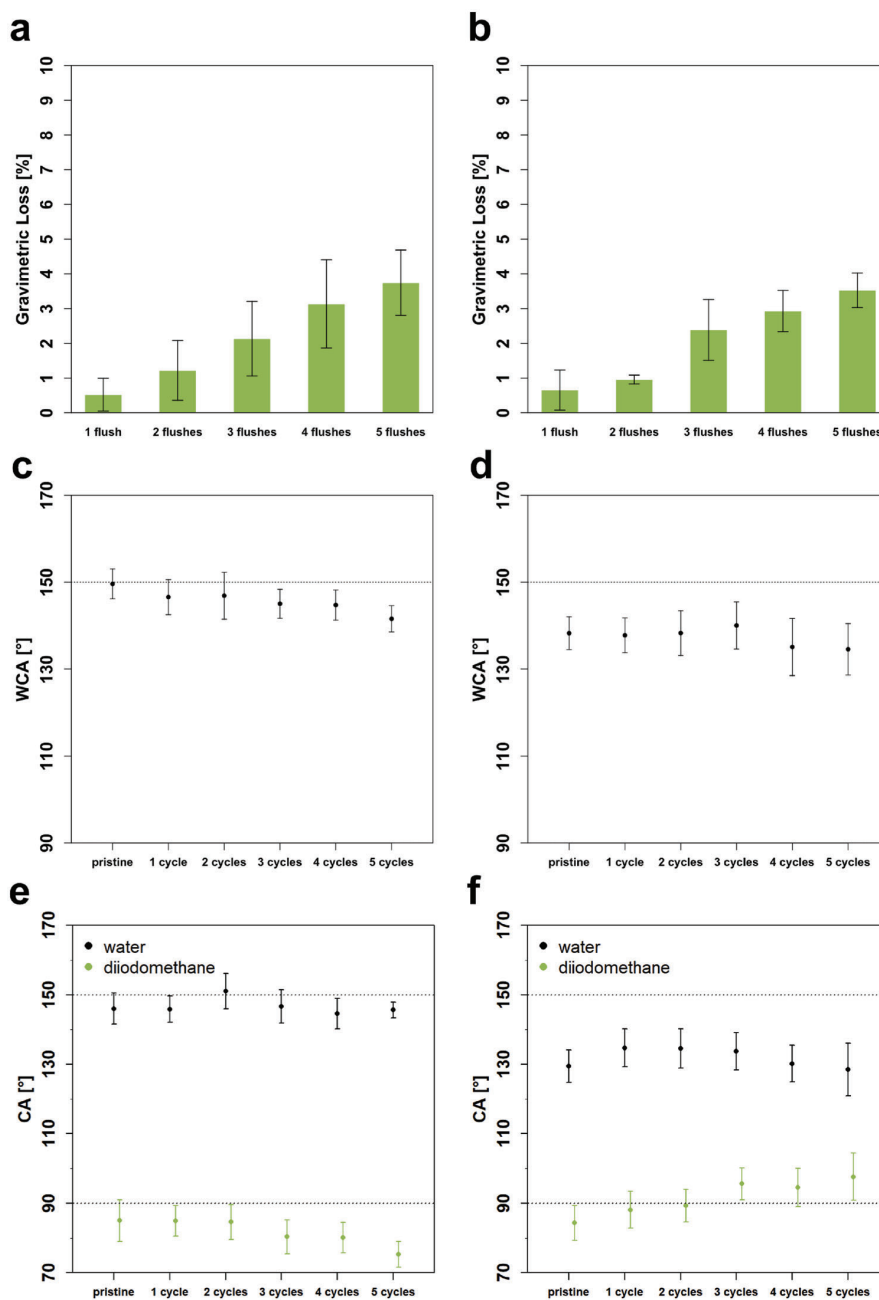


**Figure 3.** a) Gravimetric analyses of CF7/PMMA and b) CF7/PTFMEA coatings measured after flushing with water. c) WCAs of CF7/PMMA and d) CF7/PTFMEA coatings measured before and after flushing with water. e) WCAs and DCAs of CF7/PMMA and f) CF7/PTFMEA coatings measured before and after the freezing cycles.

**Time-of-Flight Secondary Ion Mass Spectrometry:** ToF-SIMS analyses were recorded using a IONTOF M6, using a Bi<sup>3+</sup> primary liquid metal ion gun (LMIG) and an argon gas cluster sputter depth profiling ion gun. Sputtering was carried out by using a 20 keV Ar<sup>+</sup> cluster ion beam. A 100 × 100 μm area was measured, repeating 30 sputtering cycles.

**Thermogravimetric Analysis:** Thermogravimetric analyses of the samples were recorded using a PerkinElmer TGA 8000. Measurements were performed under a nitrogen flow within the temperature range of 50–1000 °C with a heating rate of 40 °C min<sup>-1</sup>. All samples were held by ceramic crucibles. Sample masses were in the range of 1–4 mg. A waiting time of 5 min was given before running the analyses with nitrogen flushing and

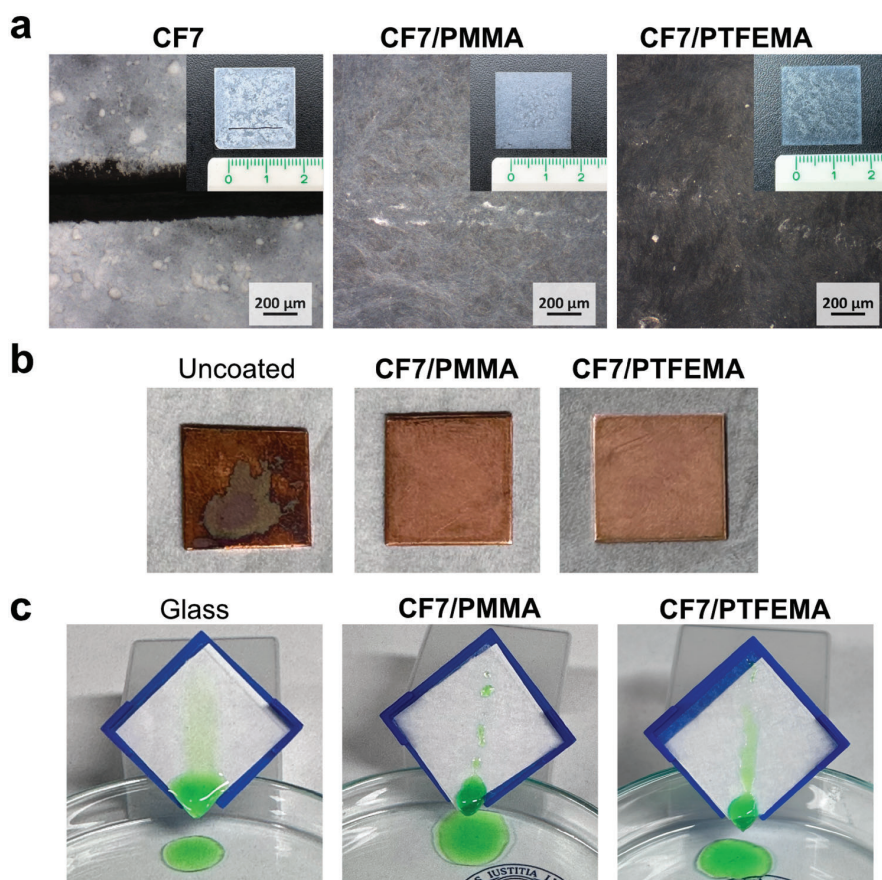


**Figure 4.** a) Optical micrographs showing the scratches performed with a constant force of 0.05 N with the sclerometer. Photographs of the full length are shown in the insets. b) Copper corrosion is successfully prevented by the polymeric coatings after storing in deionised water for 7 days. c) Observed phenomena of silicon oil sliding on different surfaces.

temperature holding at 50 °C in order to ensure stable and inert conditions for all measurements.

**Scanning Electron Microscopy:** SEM images were conducted using a scanning electron microscope from Hitachi (SU 8030). All surfaces were precoated with a 5 nm gold layer using the sputtering system SC 500 from Emscope.

**Contact Angle Measurement:** All CA measurements were performed under ambient conditions using Milli-Q water or diiodomethane on horizontally placed coated substrates. The measurements were performed with a Dataphysics Contact Angle System (OCA). The analysis of the images was carried out using the software SCA 20. Laplace–Young fitting was used to determine the CA from a digital photograph of the droplet profile for static CAs, employing 3  $\mu\text{L}$  of Milli-Q water (see Figure S13, Supporting Information). A set of three samples were measured to obtain nine mea-

surements (three measurements on each of the sample on random locations). The indicated average values and standard deviations were then calculated from these nine measurements, omitting the highest and lowest values. Due to the destructive note of most tests, a different set of samples were used for different characterizations.

**Gravimetric Analysis:** Gravimetric analyses of the coating stability were carried out on the pristine co-assembled coatings and, also, after each round of flushing on the surfaces. All rinsed surfaces were dried overnight under ambient conditions before the measurement. The indicated average values and standard deviations were calculated from three independent measurements on three different samples.

**Elemental Analysis:** Elemental analysis measurements were conducted using a Elementar Vario EL with two columns.

**Optical Microscopy:** Optical micrographs were recorded with a Zeiss Microscope Axio Scope A1 using episcopal illumination with dark-field contrasting.

**Scratch Resistance:** Scratch resistance measurements were tested using a TQC SP0010 sclerometer. Different preset pressures were used in an increasing sequence for testing to check the scratch resistance of the corresponding coating. The sclerometer is moved along the surface with a rate of  $0.43 \pm 0.2 \text{ cm s}^{-1}$  and a total distance of 1.5 cm on every tested surface.

**Frost Resistance:** Frost resistance measurements were analyzed measuring the CAs after different freezing cycles. For every freezing cycle,

**Table 2.** The corresponding amount of solvent and monomer for the co-assemblies..

Co-assembly	Diethyl ether [mL]	Monomer [mL]
CF7/PMMA	1.1	0.90
CF7/PTFEMA	1.2	0.80

samples are placed in the freezing compartment of a standard household fridge for 2 h, then defrosted on the bench for 2 h before the measurements. Condensation disturbance from air humidity during defrosting was not observed.

**Corrosion Resistance:** Corrosion tests were conducted by soaking a supramolecular-polymer coated copper plate in  $\approx$  50 mL of deionised water for 7 days. A non-coated copper plate was used as control.

## Supporting Information

Supporting Information is available from the Wiley Online Library or from the author.

## Acknowledgements

This work was supported by Gefördert durch die Deutsche Forschungsgemeinschaft (DFG)–Projekt nummer 387284271–SFB 1349 (funded by the Deutsche Forschungsgemeinschaft [DFG, German Research Foundation] project-ID 387284271–CRC 1349). The authors are grateful to the technical support from the DFG-supported instrumental core facility BioSupraMol. A.S.-S. thanks the funding by the European Union-NextGenerationEU (Margarita Salas postdoctoral grant of the Ministerio de Universidades of the Government of Spain). Although the primary affiliation of A.S.-S. is Universidad de Murcia, the author has been a Margarita Salas guest postdoctoral researcher at Freie Universität Berlin since January 2022 (until December 2023). The authors thank Yizhe Pan for his help with the screening.

Open access funding enabled and organized by Projekt DEAL.

## Conflict of Interest

The authors declare no conflict of interest.

## Data Availability Statement

The data that support the findings of this study are available from the corresponding author upon reasonable request.

## Keywords

hydrophobicity, low molecular weight gelators, oleophobicity, polymers, self-assemblies

Received: September 14, 2023  
Published online: October 6, 2023

- [1] D. J. Abdullah, R. G. Weiss, *Adv. Mater.* **2000**, *12*, 1237.
- [2] M. De Loos, B. L. Feringa, J. H. van Esch, *Eur. J. Org. Chem.* **2005**, *2005*, 3615.
- [3] S. S. Babu, V. K. Praveen, A. Ajayaghosh, *Chem. Rev.* **2014**, *114*, 1973.
- [4] E. R. Draper, D. J. Adams, *Chem* **2017**, *3*, 390.
- [5] S. Datta, S. Bhattacharya, *Chem. Soc. Rev.* **2015**, *44*, 5596.
- [6] J. Zhang, C.-Y. Su, *Coord. Chem. Rev.* **2013**, *257*, 1373.
- [7] P. R. Chivers, D. K. Smith, *Nat. Rev. Mater.* **2019**, *4*, 463.
- [8] S. Correa, A. K. Grosskopf, H. L. Hernandez, D. Chan, A. C. Yu, L. M. Stapleton, E. A. Appel, *Chem. Rev.* **2021**, *121*, 11385.
- [9] D. Díaz Díaz, D. Kühbeck, R. J. Koopmans, *Chem. Soc. Rev.* **2011**, *40*, 427.
- [10] K. Hawkins, A. K. Patterson, P. A. Clarke, D. K. Smith, *J. Am. Chem. Soc.* **2020**, *142*, 4379.
- [11] M. Albino, T. J. Burden, C. C. Piras, A. C. Whitwood, I. J. Fairlamb, D. K. Smith, *ACS Sustain. Chem. Eng.* **2023**, *11*, 1678.
- [12] I. Tomatsu, K. Peng, A. Kros, *Adv. Drug Deliv. Rev.* **2011**, *63*, 1257.
- [13] K. J. Skilling, F. Citossi, T. D. Bradshaw, M. Ashford, B. Kellam, M. Marlow, *Soft Matter* **2014**, *10*, 237.
- [14] T. Das, M. Häring, D. Haldar, D. D. Díaz, *Biomater. Sci.* **2018**, *6*, 38.
- [15] D. M. Raymond, B. L. Abraham, T. Fujita, M. J. Watrous, E. S. Toriki, T. Takano, B. L. Nilsson, *ACS Appl. Bio Mater.* **2019**, *2*, 2116.
- [16] C. C. Piras, A. G. Kay, P. G. Genever, D. K. Smith, *Chem. Sci.* **2021**, *12*, 3958.
- [17] D. J. Cornwell, D. K. Smith, *Mater. Horiz.* **2015**, *2*, 279.
- [18] M. Bielejewski, A. Rachocki, J. Kaszyńska, J. Tritt-Goc, *Phys. Chem. Chem. Phys.* **2018**, *20*, 5803.
- [19] X. Cao, A. Gao, J.-T. Hou, T. Yi, *Coord. Chem. Rev.* **2021**, *434*, 213792.
- [20] M. De Loos, J. van Esch, I. Stokroos, R. M. Kellogg, B. L. Feringa, *J. Am. Chem. Soc.* **1997**, *119*, 12675.
- [21] M. Masuda, T. Hanada, K. Yase, T. Shimizu, *Macromolecules* **1998**, *31*, 9403.
- [22] K. Inoue, Y. Ono, Y. Kanekiyo, K. Hanabusa, S. Shinkai, *Chem. Lett.* **1999**, *28*, 429.
- [23] S. Kang, B. Jung, J. Chang, *Adv. Mater.* **2007**, *19*, 2780.
- [24] K. Hanabusa, Y. Maesaka, M. Suzuki, M. Kimura, H. Shirai, *Chem. Lett.* **2000**, *29*, 1168.
- [25] J. Sautaux, F. Marx, I. Gunkel, C. Weder, S. Schrettl, *Nat. Comm.* **2022**, *13*, 356.
- [26] K. Hanabusa, A. Itoh, M. Kimura, H. Shirai, *Chem. Lett.* **1999**, *28*, 767.
- [27] A. E. Way, A. B. Korpusik, T. B. Dorsey, L. E. Buerkle, H. A. von Recum, S. J. Rowan, *Macromolecules* **2014**, *47*, 1810.
- [28] L. Feng, S. Li, Y. Li, H. Li, L. Zhang, J. Zhai, Y. Song, B. Liu, L. Jiang, D. Zhu, *Adv. Mater.* **2002**, *14*, 1857.
- [29] H. H. Ipekci, H. H. Arkaz, M. S. Onses, M. Hancer, *Surf. Coat. Technol.* **2016**, *299*, 162.
- [30] X. Huang, Y. Yuan, S. Liu, W. Wang, R. Hong, *Mater. Lett.* **2017**, *208*, 62.
- [31] J. Liu, L. Ye, Y. Sun, M. Hu, F. Chen, S. Wegner, V. Mailänder, W. Steffen, M. Kappel, H.-J. Butt, *Adv. Mater.* **2020**, *32*, 1908008.
- [32] R. S. Sutar, S. S. Gaikwad, S. S. Latthe, V. S. Kodag, S. B. Deshmukh, L. P. Saptal, S. R. Kulal, A. K. Bhosale, *Macromol. Symp.* **2020**, *393*, 2000116.
- [33] N. Vourdas, A. Tserepi, E. Gogolides, *Nanotechnology* **2007**, *18*, 125304.
- [34] M. Cardoso, V. Tribuzi, D. T. Balogh, L. Misoguti, C. R. Mendonça, *Appl. Surf. Sci.* **2011**, *257*, 3281.
- [35] E. Huovinen, L. Takkunen, T. Korpela, M. Suvanto, T. T. Pakkanen, T. A. Pakkanen, *Langmuir* **2014**, *30*, 1435.
- [36] K. K. Lau, J. Bico, K. B. Teo, M. Chhowalla, G. A. Amaratunga, W. I. Milne, G. H. McKinley, K. K. Gleason, *Nano Lett.* **2003**, *3*, 1701.
- [37] L. Mishchenko, B. Hatton, V. Bahadur, J. A. Taylor, T. Krupenkin, J. Aizenberg, *ACS Nano* **2010**, *4*, 7699.
- [38] E. K. Her, T.-J. Ko, B. Shin, H. Roh, W. Dai, W. K. Seong, H.-Y. Kim, K.-R. Lee, K. H. Oh, M.-W. Moon, *Plasma Processes Polym.* **2013**, *10*, 481.
- [39] P.-W. Lee, T. Kaynak, D. Al-Sabbagh, F. Emmerling, C. A. Schalley, *Langmuir* **2021**, *37*, 14390.
- [40] Q. Wei, C. Schlaich, S. Prévost, A. Schulz, C. Böttcher, M. Gradzielski, Z. Qi, R. Haag, C. A. Schalley, *Adv. Mater.* **2014**, *26*, 7358.
- [41] F. Junge, P.-W. Lee, A. Kumar Singh, J. Wasternack, M. P. Pachnicz, R. Haag, C. A. Schalley, *Angew. Chem. Int. Ed.* **2023**, *62*, e202213866.
- [42] H. Gankema, M. A. Hempenius, M. Möller, G. Johansson, V. Percec, *Macromol. Symp.* **1996**, *102*, 381.
- [43] U. Beginn, S. Keinath, M. Möller, *Macromol. Chem. Phys.* **1998**, *199*, 2379.

- [44] U. Beginn, S. Sheiko, M. Möller, *Macromol. Chem. Phys.* **2000**, *201*, 1008.
- [45] F.-X. Simon, N. S. Khelfallah, M. Schmutz, N. Díaz, P. J. Mésini, *J. Am. Chem. Soc.* **2007**, *129*, 3788.
- [46] J. Stendahl, L. Li, E. Zubarev, Y.-R. Chen, S. Stupp, *Adv. Mater.* **2002**, *14*, 1540.
- [47] E. Zubarev, M. Pralle, E. Sone, S. Stupp, *Adv. Mater.* **2002**, *14*, 198.
- [48] V. Kostopoulos, A. Kotrotsos, S. Tsantzas, P. Tsokanas, T. Loutas, A. Bosman, *Compos. Sci. Technol.* **2016**, *128*, 84.
- [49] D. A. Stone, L. Hsu, N. R. Wheeler, E. Wilusz, W. Zukas, G. E. Wnek, L. T. J. Korley, *Soft Matter* **2011**, *7*, 2449.
- [50] E. A. Wilder, K. S. Wilson, J. B. Quinn, D. Skrtic, J. M. Antonucci, *Chem. Mater.* **2005**, *17*, 2946.
- [51] N. Karim, T. D. Jones, K. M. Lewandowski, B. D. Craig, S. B. Mitra, J. Yang, U.S. Patent 8,445,558 B2, **2013**.
- [52] Y. Yang, Y. Deng, Z. Tong, C. Wang, *ACS Sustain. Chem. Eng.* **2014**, *2*, 1729.
- [53] D. Shang, X. Sun, X. Shen, J. Hang, L. Jin, L. Shi, *Prog. Org. Coat.* **2018**, *121*, 142.
- [54] W. L. Storm, J. Youn, K. P. Reighard, B. V. Worley, H. M. Lodaya, J. H. Shin, M. H. Schoenfisch, *Acta Biomater.* **2014**, *10*, 3442.
- [55] R. Twite, G. Bierwagen, *Prog. Org. Coat.* **1998**, *33*, 91.
- [56] S. H. Cho, S. R. White, P. V. Braun, *Adv. Mater.* **2009**, *21*, 645.
- [57] D. Iqbal, J. Rechmann, A. Sarfraz, A. Altin, G. Genchev, A. Erbe, *ACS Appl. Mater. Interfaces* **2014**, *6*, 18112.

# ADVANCED FUNCTIONAL MATERIALS

## Supporting Information

for *Adv. Funct. Mater.*, DOI 10.1002/adfm.202309140

Scratch-Resistant Hydrophobic Coating with Supramolecular-Polymer Co-Assembly

*Pin-Wei Lee, Adrian Saura-Sanmartin and Christoph A. Schalley\**

## Supporting Information

# Scratch-resistant hydrophobic coating with supramolecular-polymer co-assembly

Pin-Wei Lee,<sup>a</sup> Adrian Saura-Sanmartin,<sup>b, a</sup> and Christoph A. Schalley<sup>\*a</sup>

<sup>a</sup>Institut für Chemie und Biochemie, Freie Universität Berlin, Arnimallee 20, 14195 Berlin, Germany

<sup>b</sup>Departamento de Química Orgánica, Facultad de Química, Campus de Espinardo, Universidad de Murcia, 30100 Murcia, Spain

# Contents

<b>1 ToF-SIMS</b>	<b>S3</b>
<b>2 FT-IR</b>	<b>S6</b>
<b>3 SEM</b>	<b>S8</b>
<b>4 Gravimetric Analysis</b>	<b>S8</b>
<b>5 Elemental Analysis</b>	<b>S9</b>
<b>6 TGA</b>	<b>S9</b>
<b>7 Scratch test</b>	<b>S10</b>
<b>8 Contact Angle Measurement</b>	<b>S11</b>
<b>9 XPS</b>	<b>S12</b>
<b>10 References</b>	<b>S13</b>

# 1 ToF-SIMS

ToF-SIMS turns out to be a powerful and essential technique to analyse the homogeneity of the thick material layer. It allows the spatial resolved visualisation of the structures and component distribution within the sample. In addition to the rendered figures that include all possible fragments picked up by the time-of-flight analyser (see main text Figure 2), each figure below shows only one selected fragment from the co-assemblies. The peak at  $m/z = 906.04$  is attributed to the **CF7** gelator and is observed in all three materials (Figure S1, S2a, and S3a). The peak at  $m/z = 100.05$  is attributed to the MMA monomers (Figure S2b). 3D rendering for peaks attributed to the MMA dimers, trimers, tetramers and pentamers are also provided, showing a homogeneous distribution of the polymeric scaffold (Figure S2c–f). Likewise, peaks for TFEMA monomers to pentamers are displayed separately, confirming that the polymeric material is distributed homogeneously, and the polymerisation was carried out evenly through the coating (Figure S3).

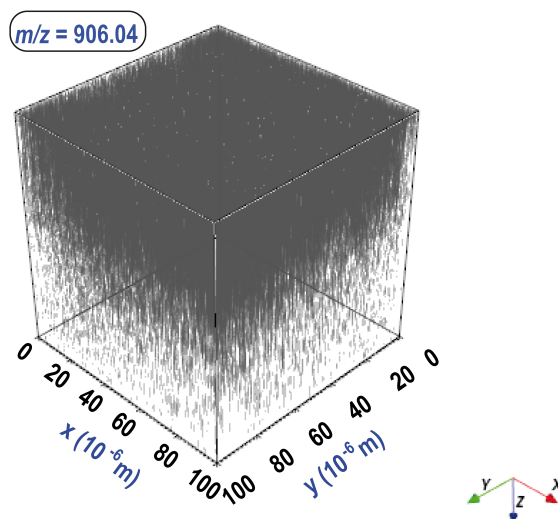


**Figure S1:** ToF-SIMS 3D imaging of **CF7** coating in the absence of any co-assembled polymer. The grey area corresponds to **CF7**, while the vacant spaces below represents the glass substrate since the coating has been removed after multiple cycles of sputtering and the substrate has been reached.



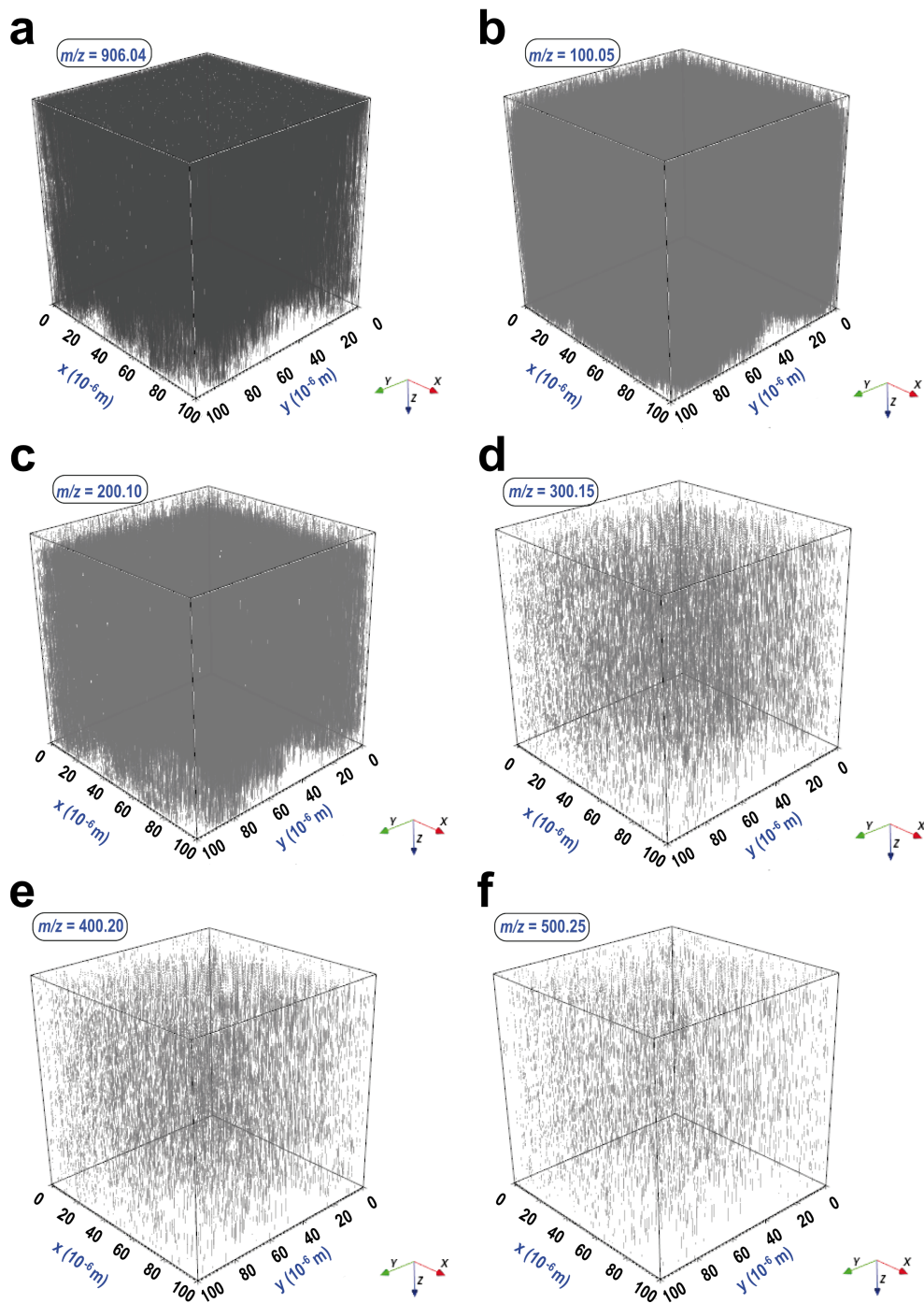


**Figure S2:** ToF-SIMS 3D imaging of CF7/PMMA coating. Each grey area represents the distribution of: (a) CF7; (b) MMA monomer; (c) MMA dimer; (d) MMA trimer; (e) MMA tetramer; and (f) MMA pentamer.

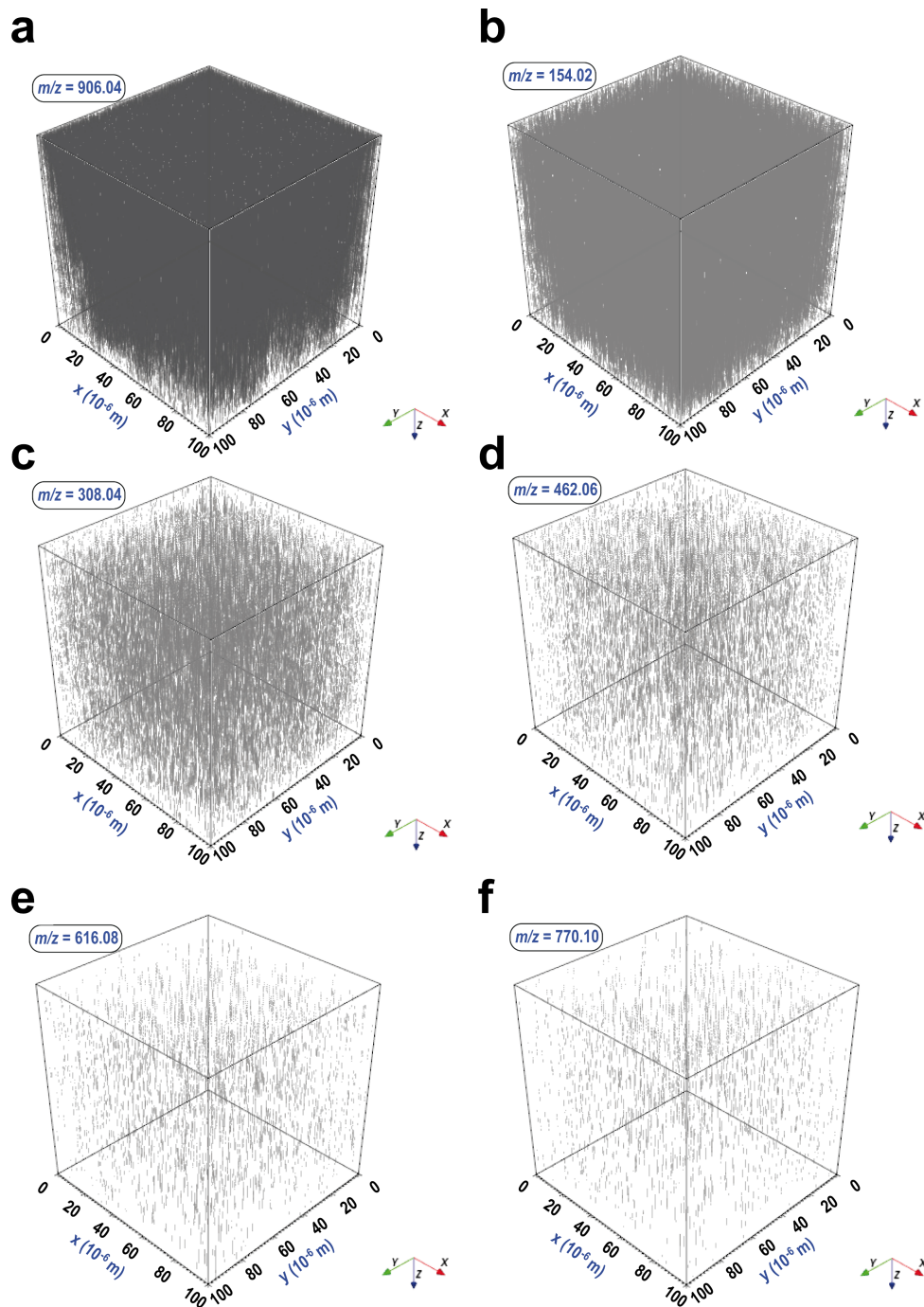


**Figure S3:** ToF-SIMS 3D imaging of CF7/PTFEMA coating. Each grey area represents the distribution of: (a) CF7; (b) TFEMA monomer; (c) TFEMA dimer; (d) TFEMA trimer; (e) TFEMA tetramer; and (f) TFEMA pentamer.

## 2 FT-IR

FT-IR spectra of the samples show the main bands of the polymers (Figures S5, S7) in both co-assemblies (Figures S6, S8), although there is a shifting of the wavelength values due to possible interactions between polymeric scaffolds and CF7. A C=O band of CF7 (Figure S4) is showed in the spectra of the co-assemblies.

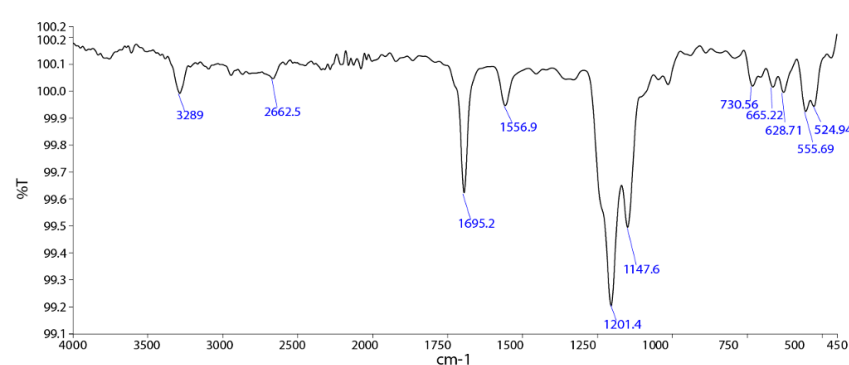


**Figure S4:** FT-IR spectrum of CF7 xerogel coating in the absence of any co-assembled polymer, showing the C=O stretching band of the amide groups at 1695.2 cm<sup>-1</sup>.

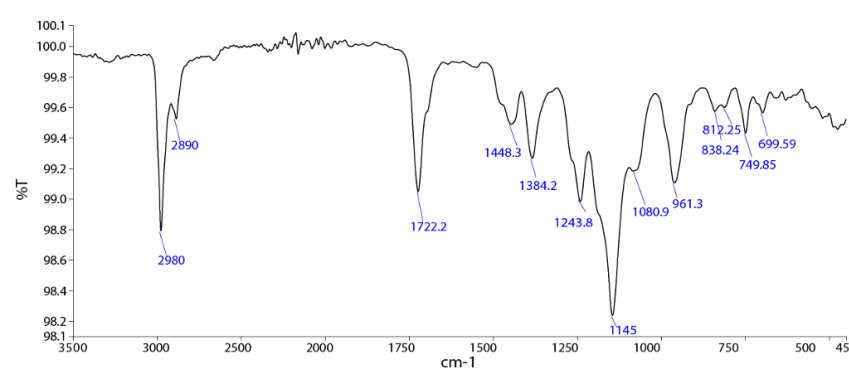


**Figure S5:** FT-IR spectrum of PMMA alone, showing the C=O stretching band of the ester groups at 1722.2 cm<sup>-1</sup>.

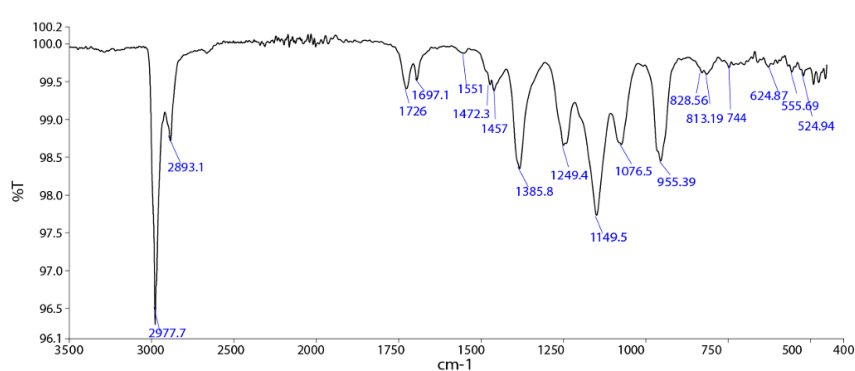


**Figure S6:** FT-IR spectrum of the CF7/PMMA co-assembly, showing the C=O stretching bands of the CF7 amide groups at  $1697.1\text{ cm}^{-1}$  and the PMMA ester groups at  $1726.0\text{ cm}^{-1}$ .

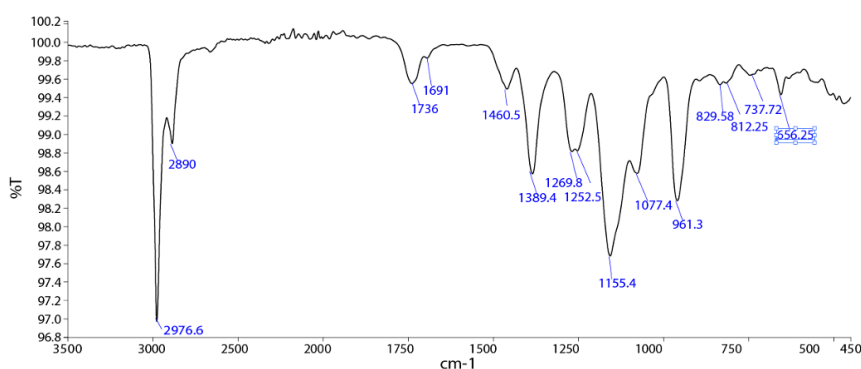


**Figure S7:** FT-IR spectrum of PTFEMA alone, showing the C=O stretching bands of the ester groups at  $1736.0\text{ cm}^{-1}$  and  $1691.0\text{ cm}^{-1}$ .

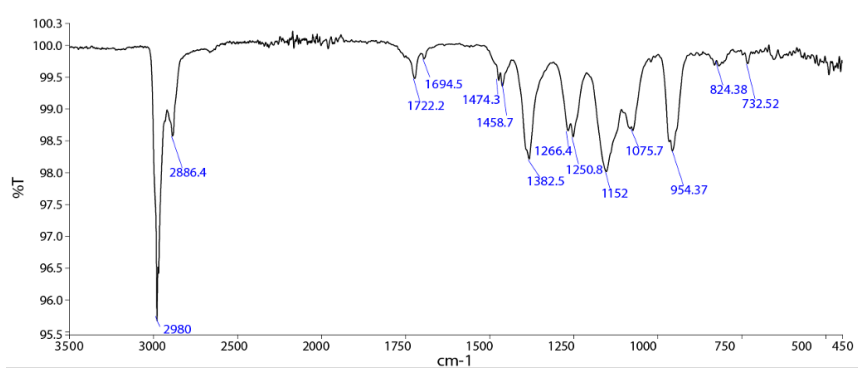


**Figure S8:** FT-IR spectrum of the CF7/PTFEMA co-assembly, showing a C=O stretching band of an ester group of PTFEMA at  $1722.2\text{ cm}^{-1}$ . The other C=O stretching bands corresponding to the other PTFEMA ester group and the CF7 amide groups are overlapped as a single broad band at  $1694.5\text{ cm}^{-1}$ .

### 3 SEM

The fibers of the **CF7/PMMA** co-assembly was observed with SEM using a higher magnification in order to show the nanostructures (Figure S9).

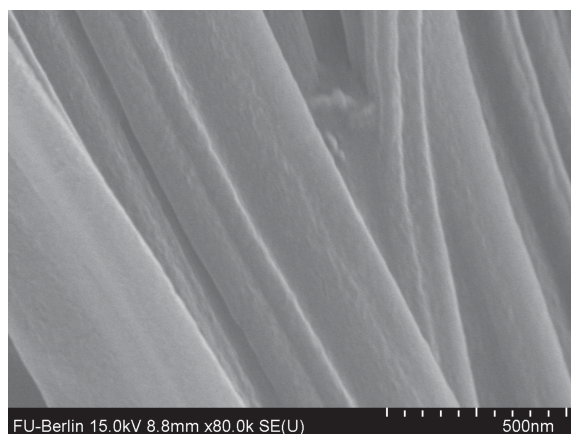


**Figure S9:** SEM image showing additional nanostructure observed on a **CF7/PMMA** coating.

### 4 Gravimetric Analysis

Gravimetric analysis of the coating stability was done on surfaces after they were freshly prepared and dried, and after each round of flushing. All rinsed surfaces were dried under ambient conditions overnight before they were measured. The degree of material loss of each examined surface was recorded. The presented mean values and standard deviations were calculated from three independent measurements on three different samples for each compound and given in wt%.

**Table S1:** Material loss in wt% after flushing as examined by gravimetry after multiple rounds of water flushing:

Coating	1 <sup>st</sup> flush	2 <sup>nd</sup> flush	3 <sup>rd</sup> flush	4 <sup>th</sup> flush	5 <sup>th</sup> flush
<b>CF7</b> <sup>[1]</sup>	6.0 ± 11	8.0 ± 13	12 ± 21	13 ± 21	13 ± 22
<b>CF7/PMMA</b>	0.52 ± 0.47	1.2 ± 0.86	2.1 ± 1.1	3.1 ± 1.3	3.7 ± 0.94
<b>CF7/PTFEMA</b>	0.65 ± 0.58	0.96 ± 0.13	2.4 ± 0.87	2.9 ± 0.59	3.5 ± 0.50

## 5 Elemental Analysis

Elemental analyses suggest the co-assemblies after the flushing cycles are analogous to the pristine ones. The obtained data revealed similar percentages of C, N and H in both pristine and flushed coatings.

**Table S2:** Elemental analysis data of the co-assemblies before and after 5 water flushing cycles:

Coating	C (%)	N (%)	H (%)
CF7/PMMA (pristine)	45.44	2.067	5.248
CF7/PMMA (flushed)	45.98	2.079	5.292
CF7/PTFEMA (pristine)	24.75	2.354	2.996
CF7/PTFEMA (flushed)	25.18	2.405	3.105

## 6 TGA

Thermogravimetric analyses were carried out in order to investigate the stability of the co-assemblies against high temperature. The degradation of CF7 (Figure S10a and b, green curve) starts at a similar temperature to that of the first degradation of the polymers (Figure S10a and b, black curve), so this step is overlapped in the co-assembled samples (Figure S10a and b, red curve). The thermostability of CF7, polymer and co-assemblies is analogous, showing a high thermal resistance. The stepwise degradation of the co-assemblies matches the degradation of CF7 and the respective polymer.

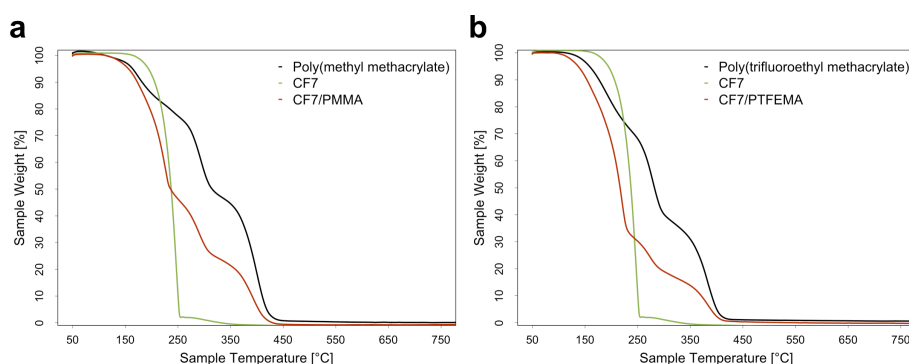


**Figure S10:** TGA curves of (a) CF7/PMMA and (b) CF7/PTFEMA with curves of CF7 and the respective polymer side by side. All samples show high thermostability (over 150 °C).



## 7 Scratch test

The scratch-resistance was tested using a sclerometer. The **CF7/PMMA** co-assembly is partially removed from the substrate with a constant scratch force of 2.5 N, and is almost fully removed when the force is increased to 2.7 N. As for the **CF7/PTFEMA** co-assembly, it is partially removed when scratching with the force of 0.6 N, and completely removed when the force is 0.7 N.

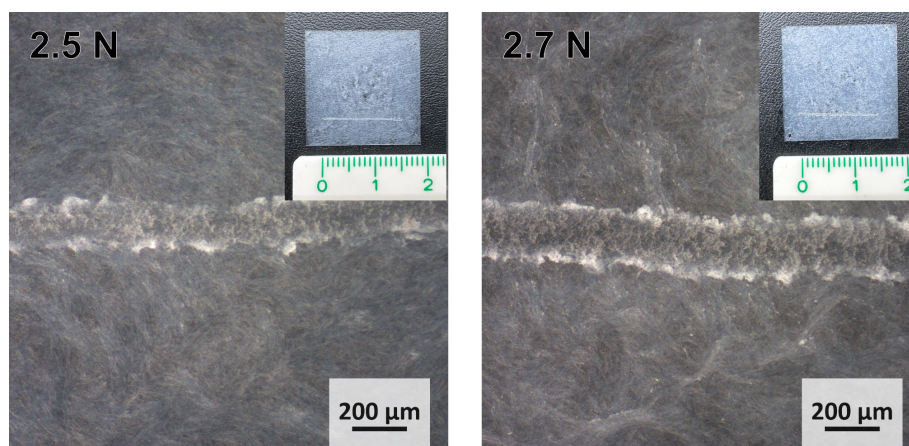


**Figure S11:** Optical micrographs showing the scratches on **CF7/PMMA** co-assembly with different preset scratching force. Photographs of the full length are shown in the insets.

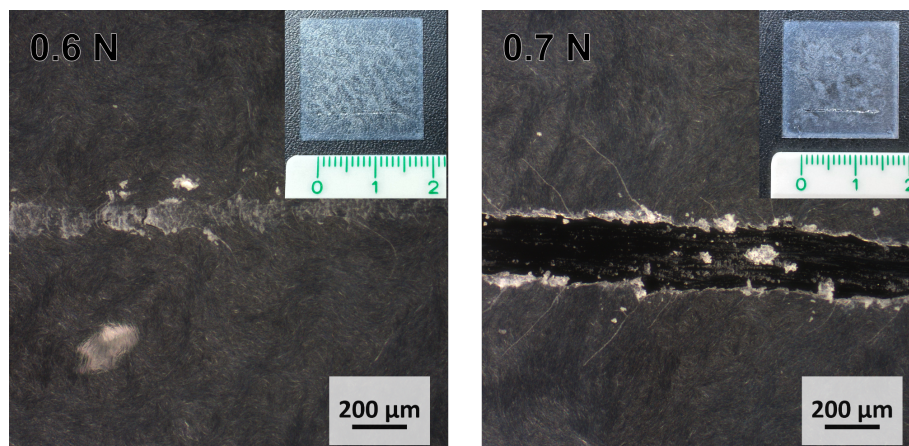


**Figure S12:** Optical micrographs showing the scratches on **CF7/PTFEMA** co-assembly with different preset scratching force. Photographs of the full length are shown in the insets.

## 8 Contact Angle Measurement

All CA measurements were performed under ambient conditions using 3  $\mu\text{L}$  of Milli-Q water or diiodomethane on horizontally placed samples. Laplace-Young fitting was used for all CA determinations.

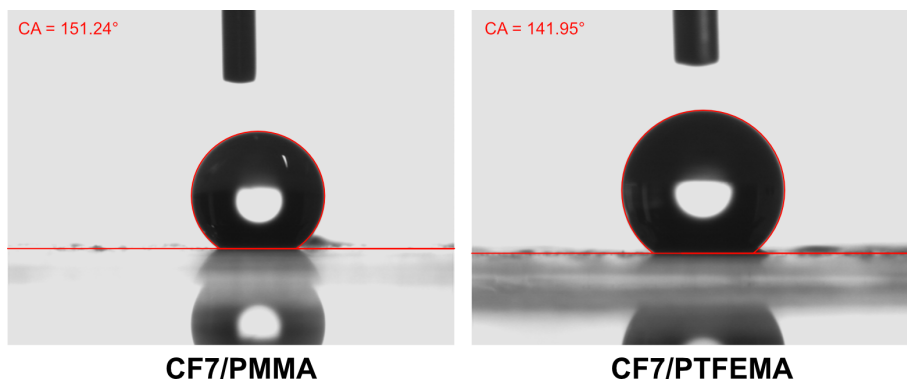


**Figure S13:** Representative digital photograph of the droplet profile used for determining the static contact angles.



## 9 XPS

The signal of fluorine in both co-assemblies suggests the presence of **CF7** molecules in the outer surface, which is consistent with the hydrophobic properties obtained.

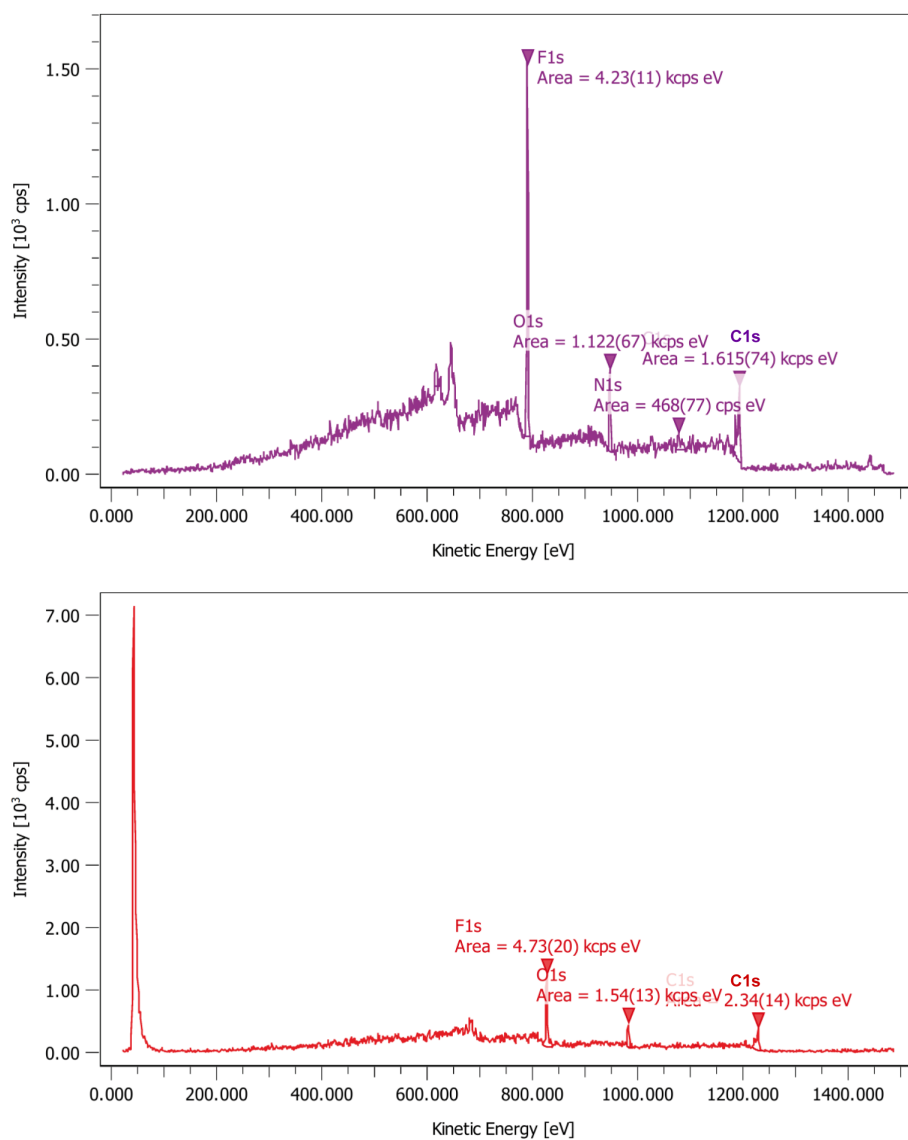


**Figure S14:** XPS surveys of **CF7/PMMA** (top) and **CF7/PTFEMA** (bottom) showing the presence of carbon, oxygen, nitrogen and fluorine.

## 10 References

- [1] P.-W. Lee, T. Kaynak, D. Al-Sabbagh, F. Emmerling, C. A. Schalley, Effect of Perfluorinated Side-Chain Length on the Morphology, Hydrophobicity, and Stability of Xerogel Coatings, *Langmuir*, **2021**, *37*, 14390–14397.